DEVELOPMENT OF A NEW METHOD FOR MODE I FRACTURE TOUGHNESS TEST ON DISC TYPE ROCK SPECIMENS

A THESIS SUBMITTED TO
THE GRADUATE SCHOOL OF NATURAL AND APPLIED SCIENCES
OF
MIDDLE EAST TECHNICAL UNIVERSITY

BY

ÇİĞDEM ALKILIÇGİL

IN PARTIAL FULFILLMENT OF THE REQUIREMENTS
FOR
THE DEGREE OF MASTER OF SCIENCE
IN
MINING ENGINEERING

SEPTEMBER 2006

Approval of the Graduate School of Natural and Applied Sciences

_____

Prof. Dr. Canan Özgen
Director

I certify that this thesis satisfies all the requirements as a thesis for the degree of Master of Science.

_____

Prof. Dr. Ümit Atalay
Head of Department

This is to certify that we have read this thesis and that in our opinion it is fully adequate, in scope and quality, as a thesis for the degree of Master of Science.

_____

Assoc. Prof. Dr. Levent Tutluoğlu
Supervisor

Examining Committee Members

Prof. Dr. Naci Bölükbaşı	(METU, MINE)	_____
Assoc. Prof. Dr. Levent Tutluoğlu	(METU, MINE)	_____
Prof. Dr. Celal Karpuz	(METU, MINE)	_____
Prof. Dr. Çetin Hoşten	(METU, MINE)	_____
Assoc. Prof. Dr. Sadık Bakır	(METU, CE)	_____

I hereby declare that all information in this document has been obtained and presented in accordance with academic rules and ethical conduct. I also declare that, as required by these rules and conduct, I have fully cited and referenced all material and results that are not original to this work.

Name, Last name: Çiğdem Alkılıçgil

Signature :

ABSTRACT

DEVELOPMENT OF A NEW METHOD FOR MODE I FRACTURE TOUGHNESS TEST ON DISC TYPE ROCK SPECIMENS

Alkılıçgil, Çiğdem

M.Sc., Department of Mining Engineering

Supervisor: Assoc. Prof. Dr. Levent Tutluoğlu

September 2006, 145 pages

A new testing method was introduced and developed to determine Mode I fracture toughness of disc type rock specimens. The new method was named as Straight Notched Disc Bending and it uses disc specimens under three-point bending. 3D Numerical modeling was carried out with a finite element program ABAQUS to find stress intensity factors for both well-known Semi-circular Bending specimen models and Straight Notched Disc Bending specimen models for varying disc geometries. Both specimen types included notches where a crack front is introduced at the tip of the notch to compute the stress intensity factors. For stress intensity analysis, crack front-upper loading point distance and span length between the two roller supports at the bottom boundary of the specimens were changed.

Fracture toughness testing was carried on Ankara Gölbaşı pink colored andesite for both specimen types; crack front-upper loading point distance and span length between the two roller supports at the bottom boundary of the specimens were changed during the tests. For both specimen geometries, notch lengths changing

from 5 mm to 20 mm were used. For each notch length, two different roller supports with span lengths 60 mm and 70 mm were used.

For both methods, fracture toughness values determined by using numerically computed stress intensity factors and failure loads obtained from the experiments were very close; the new method was verified by comparing the results. The new method had advantages of lower confining pressure at the crack front and lower stress intensities with a possible smaller crack tip plasticity region.

Keywords: Stress Intensity Factor, Mode I Fracture Toughness, Semi-Circular Bend Specimens, Fracture Testing on Rock Cores, Numerical Modeling

ÖZ

DİSK TİPİ KAYA NUMUNELERİNDE MOD I ÇATLAK TOKLUĞU TESTİ İÇİN YENİ BİR YÖNTEMİN GELİŞTİRİLMESİ

Alkılıçgil, Çiğdem

Yüksek Lisans, Maden Mühendisliği Bölümü

Tez Yöneticisi: Doç. Dr. Levent Tutluoğlu

Eylül 2006, 145 sayfa

Disk tipindeki kaya numunelerinin Mod I çatlak tokluğunu belirlemek için yeni bir test metodu ortaya koyulmuş ve geliştirilmiştir. Yeni yöntem Düz Çentikli Disk Eğilmesi olarak adlandırılmıştır ve bu yöntem disk numunelerini üç nokta eğilme tekniğiyle kullanır. Bir sonlu eleman programı olan ABAQUS kullanılarak hem çok iyi bilinen Yarım-dairesel Eğilme numune modellerinin hem de Düz Çentikli Disk Eğilmesi numune modellerinin değişik ölçüleri için 3 boyutlu sayısal modelleme yapılmıştır. Gerilme şiddet faktörlerinin bulunması için her iki numune tipi de uçta bir çatlak önü içermektedir. Gerilme şiddeti analizleri için, numunelerin çatlak önü ile üst yükleme noktası arasındaki mesafe ve alt sınırındaki iki yuvarlak çubuk destek arasındaki uzunluk değiştirilmiştir.

Her iki numune tipi için, Pembe renkli Ankara Gölbaşı Andeziti'nin çatlak tokluğu analizleri yapılmıştır; analizlerde çatlak önü ile üst yükleme noktası arasındaki mesafe ve numunelerin alt sınırındaki iki yuvarlak çubuk destek arasındaki

uzunluklar değiştirilmiştir. Her iki numune geometrisi için 5 mm'den 20 mm'ye kadar değişen çentik uzunlukları kullnılmıştır. Her çentik uzunluğu için 60 mm ve 70 mm lik iki farklı yuvarlak destek uzunluğu kullanılmıştır.

Her iki method için, sayısal yöntemle hesaplanan gerilme şiddet faktörleri ve deney sonuçlarından elde edilen kırılma yükü kullanılarak bulunan çatlak tokluğu değerleri birbirine çok yakın çıkmış; yeni yöntem sonuçlar karşılaştırılarak doğrulanmıştır. Yeni yöntemde, çatlak önünde daha düşük kuşatılmış basınç ve daha düşük gerilme şiddetleri ile çatlak ucundaki muhtemelen daha küçük plastisite bölgesinin oluşması, yeni yöntemin avantajlarındandır.

Anahtar Kelimeler: Gerilme Şiddet Faktörü, Mod I Çatlak Tokluğu, Yarım-dairesel Bükülme Numuneleri, Kaya Karotlarında Çatlak Deneyi, Sayısal Modelleme

TO MY FAMILY

ACKNOWLEDGEMENT

I would like to express my deep and sincere gratitude to my supervisor, Assoc. Prof. Dr. Levent Tutluoğlu for his technical advices and constructive comments throughout this thesis.

I want to acknowledge to the examining committee the members, Prof. Dr. Celal Karpuz, Prof. Dr. Naci Bölükbaşı, Prof. Dr. Çetin Hoşten and Assoc. Prof. Dr. Sadık Bakır for being interested in and reading this thesis.

I wish to express sincere appreciation to Mr. Ali Öge whom technical and project manager of A-Ztech Ltd., for his valuable comments and support on numerical modeling studies with ABAQUS program.

I would like to thank to Arman Koçal, Tahsin Işıksal, Hakan Uysal and İsmail Kaya for their help during laboratory work.

I want to thank my parents, my sister and my brother for their patience and encouragement, not only for my thesis, but in all dimensions of my life. I am also very grateful to my grandmothers Mucize Uyanusta and Elmas Alkılıçgil for their moral supports.

I would like to give my special thanks to Serhat Keleş for his enormous support and love. It would be impossible to finish this work without him.

Lastly, I would like to thank all whose direct and indirect support helped me completing my thesis in time.

TABLE OF CONTENTS

LIST OF TABLES

TABLES

LIST OF FIGURES

FIGURES

LIST OF SYMBOLS AND ABBREVIATIONS

a : Crack length

B : Specimen thickness

BDT : Uncracked Brazilian Disk Test

CB : Chevron Bend

CCBD : Central Cracked Brazilian Disc under diametral compression test

CCP : Centre Cracked Panel

CMOD : Crack Mouth Opening Displacement

$CMOD_f$: Crack Mouth Opening Displacement at failure

CNBD : Chevron-Notched Brazilian Disc

CNSCB : Chevron-Notched Semi-Circular Bend

CT : Compact Tension test

CTOD : Crack Tip Opening Displacement

D : Specimen diameter

E : Young's Modulus

EPFM : Elastic Plastic Fracture Mechanics

$\mathcal{G}$: Strain energy release rate

G_{max} : Maximum energy release rate criterion

ISRM : International Society for Rock Mechanics

J : J-integral

K : Stress intensity factor

K_c : Fracture toughness

K_I : Stress intensity factor in Mode I

K_{II} : Stress intensity factor in Mode II

L : Specimen length

L : Element size

LEFM : Linear Elastic Fracture Mechanics

LVDT : Linear Variable Differential Transformer

MR : Modified Ring test

P : Applied load

P_{cr} : Critical load

PTS : Punch Through Shear

R : Specimen Radius

r_y : Extent of a possible plastic or yield zone around the crack tip

S : Support Span

S_{min} : Minimum strain energy density criterion

SC3PB : Single edge straight through cracked rectangular plate in three-point bending test

SCB : Semi-Circular specimen under three-point Bending

SECB : Single Edge Cracked Beam under three-point bending

SECBD : Single edge cracked Brazilian disk in diametral compression

SECRBB : Single Edge Cracked Round Bar Bend

SENRBB : Single Edge Notched Round Bar in Bending

SNBD : Straight-Notched Brazilian Disc

SNDB : Straight-Notched Disc specimen under three-point Bending

SNSCB : Straight-Notched Semi-Circular Bend

SR : Short Rod

T_i : Traction vector

T_0 : Tensile strength

u_i : Crack tip displacement

UCS : Uniaxial Compressive Strength

w : Strain energy density

Y_I : Normalized stress intensity factor in Mode I

Y_{II} : Normalized stress intensity factor in Mode II

ε : Strain

δ : Crack Tip Opening Displacement

Γ : an arbitrary path around the crack tip

μ : Shear modulus

σ : Stress

σ_{max} : Maximum tangential stress criterion

υ : Poisson's Ratio

CHAPTER 1

INTRODUCTION

1.1 General

Fracture mechanics is the science of describing how a crack or a flaw occurs and propagates under applied loads in a structure. Cracks may occur in everywhere therefore application areas of fracture mechanics is extensive. Many sciences and engineering disciplines such as Materials and Medical Sciences, Aerospace Engineering, Mechanical Engineering, Civil Engineering, Geological Engineering, Petroleum Engineering and Mining Engineering have to consider fracture mechanics in their application fields.

As an example, adhesive joint applications are used in material sciences and although adhesive usage causes discontinuous interfaces in electronic packages, adhesive bonding is used in packaging technology for the integration of electronic devices. When the packages come across with different environmental loadings like thermal, mechanical, moisture, and electrical, several failures such as cracks will appear in the adhesive layer, causing the damage of solder joint and the loss of function and further leading to the failure of whole electronic device (Shi, 2006). In order to understand and to prevent that failure, fracture mechanics studies should be performed.

Fracture mechanics is also used in the medicine such as to determine fracture resistance of bones. In medical sciences, similar tests, which are used to determine fracture toughness of rocks and metals, are performed to determine fracture toughness of bones. As an example, disc-shaped compact specimens and three-point

bending specimens were used to determine fracture toughness of cancellous bone in the Ph.D. Thesis of Cook (2005).

Fracture mechanics has a survival importance in Aerospace engineering. There were many airplane accidents in the past because of the fracture and fatigue. For example, On April 28, 1988, an Aloha Airlines Boeing 737-200 aircraft lost part of its upper fuselage because of the multiple-fatigue cracks.

In civil engineering applications, the fracture studies are done in the analysis of the crack propagation in huge space concrete structures, such as arch Dams. Moreover, fracture mechanics is considered in asphalt pavement building. For instance, asphalt pavements in the northern US and Canada faced with low temperature cracking and in the paper of Li (2004), a standard method to characterize the resistance to cracking of asphalt mixtures was studied. Another research, fracture resistance of rubber-modified asphaltic mixtures exposed to high-temperature cyclic aging, was made by Othman (2006).

One of the fracture mechanics branches is rock fracture mechanics. Earth sciences like petroleum engineering, geological engineering and mining engineering cope with rock fracture mechanics. Finding wide application in the field of hydraulic fracturing, blasting, rock fragmentation and in many other practical problems, Mode I fracture toughness is an important property for rocks.

The explosion in rock fracture mechanics research has touched many diverse areas including blasting, hydraulic fracturing and in situ stress determination, mechanical fragmentation, rock slope analysis, earthquake mechanics, earthquake prediction, plate tectonics, magmatic intrusions, hot dry rock geothermal energy extraction, fluid transport properties of fracturing rock masses, propagating oceanic rifts, crevasse penetration and other glaciological problems, the development of steeply dipping extension fractures that are nearly ubiquitous at the earth's surface and are formed through folding, upwarping and rifting and the modeling of time-dependent rock failure (Atkinson, 1987; Whittaker et al., 1992).

1.2 Importance of Fracture Toughness in Rock Fracture Mechanics

Fracture toughness is an important parameter in Earth Sciences. It is used as:

A parameter: for classification of rock material.

Gunsallus and Kulhawy used fracture toughness in their research as a rock strength classification parameter.

In the study of Bearman (1996), fracture toughness was used as a rock strength classification parameter to predict comminution behavior.

An index: for fragmentation processes such as tunnel boring and model scale blasting.

Nelson and Fong (1986) found out that prediction of cutter forces and force penetration relationship are possible by using fracture toughness.

In the study of Momber (2006), fracture toughness was used in an index with strength parameter to verify the proposed transition-index. This index is used in the principal process for non-traditional drilling and cutting methods, such as hydrodemolition, hydrodynamic fragmentation, and cavitating drilling.

A material property: in the modeling of rock fragmentation like hydraulic fracturing, explosive simulation of gas wells, radial explosive fracturing, and crater blasting as well as in stability analysis.

Fracture toughness is widely accepted as the criteria for fracture propagation in the hydraulic fracturing simulation, that is the fracture is supposed to extend further when $K_I \geq K_{IC}$ (Chen and Chen, 1995).

The fracture toughness of the underground rock material at great depth is an important parameter in the numerical simulation of hydraulic fracturing treatments of reservoir pay-zones in petroleum industry (Chen and Zhang, 2002).

A sound knowledge of mechanical properties of rocks at high temperatures and pressures is essential for modeling volcanological problems such as fracture of lava flows and dike emplacement. In particular, fracture toughness is a scale-invariant material property of a rock that describes its resistance to tensile failure (Balme et.al, 2004).

1.3 Fracture Toughness Values of Some Rock Types

Since 1960s a large number of fracture mechanics tests were carried out on rocks by researchers. Variety of testing techniques and methods were used in these tests. Some of the relatively recent results were summarized in Table 1.1. In this table rock types were tried to be grouped according to the geological origin.

Table 1.1 Fracture toughness values of rocks with related testing method

Rock Type	Testing Method	K_{IC} $MPa\sqrt{m}$	Source
Johnstone (w =18%)	SECB	0.05	Harberfield & Johnstone, 1990
Johnstone (w =18%)	SCB	0.06	Lim, et. al., 1994
Fine grained sandstone	SCB	0.28	Singh & Sun, 1990
Coarse grained sandstone	SCB	0.35	Singh & Sun, 1990
Fine grained sandstone	SC3PB	0.56	Whittaker, 1992
Fine grained sandstone	CCBD	0.62	Fowell & Chen, 1990
Sandstone	BDT	0.67	Whittaker, 1992
Alvdalen sandstone	CB	0.73	Ouchterlony, 1987
Ruhr sandstone	CB	1.03	Müller & Rummel, 1984
Ryefield sandstone	SECBD	1.04	Whittaker, 1992
Flechtingen sandstone	CB	1.15	Backers, et al., 2003
Montcliffe sandstone	CB	1.18	Bearman, 1999
Grimsby sandstone	SR	1.47	Gunsallus & Kulhawy, 1984
Alvdalen sandstone	SR	1.91	Ouchterlony, 1987
Pennant sandstone	CB	2.10	Bearman, 1999
Pennant sandstone	SR	2.56	Meredith, 1983
Saudi Arabia limestone	SENRBB	0.39	Khan & Al-Shayea 2000
Middleton limestone	CB	0.73	Bearman, 1999
Harrycroft limestone	CB	0.82	Bearman, 1999
Welsh limestone	SCB	0.85	Singh & Sun, 1990
Indiana limestone	SECB	0.97	Ingraffea & Schmidt, 1979
Indiana limestone	CCP	0.97	Sun & Ouchterlony, 1986
Indiana limestone	SC3PB	0.99	Whittaker, 1992
Irondequoit limestone	SR	1.36	Gunsallus & Kulhawy, 1984
White limestone	BDT	1.38	Whittaker, 1992
Shelly limestone	SR	1.44	Meredith, 1983
Grey limestone	BDT	1.58	Whittaker, 1992

Table 1.1 (Continued) Fracture toughness values of rocks with related testing method

Rock Type	Testing Method	K_{IC} $MPa\sqrt{m}$	Source
Wredon limestone	CB	1.70	Bearman, 1999
Klinthagen limestone	SR	1.87	Ouchterlony, 1987
Reynales limestone	SR	2.06	Gunsallus & Kulhawy, 1984
Siltstone	SECBD	0.80	Whittaker, 1992
Fine grained marble	BDT	1.00	Whittaker, 1992
Coarse grained marble	BDT	1.12	Whittaker, 1992
Carrara marble	CB	1.38	Müller & Rummel, 1984
Treuchtlingen marble	CB	1.70	Müller & Rummel, 1984
Ekeberg marble	CB	1.76	Ouchterlony, 1987
Ekeberg marble	SR	2.25	Ouchterlony, 1987
Colorado oil shale	SCB	1.02	Chong,et al., 1987
Utinga granite (Rift plane)	CNBD	0.60	Almeida, et al., 2006
Falkenberg granite	CB	0.65	Müller & Rummel, 1984
Utinga granite (Grain plane)	CNBD	0.73	Almeida, et al., 2006
Utinga granite (Hardway plane)	CNBD	0.82	Almeida, et al., 2006
Favela granite (Grain plane)	CNBD	0.90	Almeida, et al., 2006
Favela granite (Rift plane)	CNBD	0.97	Almeida, et al., 2006
Iidate granite	SR	1.12	Takahashi et al, 1986
Favela granite (Hardway plane)	CNBD	1.16	Almeida, et al., 2006
Daejeon granite	BDT	1.18	Yoon & Jeon, 2004
Cornwall granite	CB	1.32	Müller & Rummel, 1984
Bohus granite	CB	1.42	Ouchterlony, 1987
Falkenberg granite	CB	1.52	Müller & Rummel, 1984
Granite	SECBD	1.65	Whittaker, 1992
Newhurst granite	SCB	1.72	Whittaker, 1992
Iidate granite	CB	1.73	Müller & Rummel, 1984
Epprechtstein granite	CB	1.74	Müller & Rummel, 1984
Stripa granite	SECRBB	1.74	Sun & Ouchterlony, 1986
Merrivale granite	SR	1.80	Meredith, 1983
Westerly granite	SR	1.82	Meredith, 1983
Penryn granite	CB	1.83	Bearman, 1999
Pink granite	SR	2.03	Meredith, 1983
TGP granite	SENRBB	2.08	Yu,2001
Krakemala granite	CB	2.16	Ouchterlony, 1987
Straht Halladale granite	SR	2.19	Meredith, 1983
Krakemala granite	SR	2.22	Ouchterlony, 1987
Iidate granite	CB	2.26	Takahashi et al, 1986
Westerly granite	SR	2.27	Ouchterlony, 1987
Stripa granite	SR	2.36	Sun & Ouchterlony, 1986
Bohus granite	SR	2.40	Ouchterlony, 1987
Stripa granite	SR	2.70	Ouchterlony, 1987
Westerly granite	CT	2.70	Schmidt & Lutz, 1979
Westerly granite	CT	2.70	Sun & Ouchterlony, 1986
Rasjö granite	SR	2.80	Ouchterlony, 1987
Ogino tuff	SR	1.06	Matsuki et al, 1987
Ogino tuff	CB	1.08	Matsuki et al, 1987
Göynük tuff	SR	1.29	Şantay, 1990
Falkirk dolostone	SR	1.66	Gunsallus & Kulhawy, 1984
Kankakee dolostone	SR	1.66	Gunsallus & Kulhawy, 1984
Oatka dolostone	SR	1.78	Gunsallus & Kulhawy, 1984
Markgraf dolostone	SR	1.80	Gunsallus & Kulhawy, 1984
Romeo dolostone	SR	2.47	Gunsallus & Kulhawy, 1984

Table 1.1 (Continued) Fracture toughness values of rocks with related testing method

Rock Type	Testing Method	K_{IC} $MPa\sqrt{m}$	Source
Tampomas andesite	CB	1.26	Abrahamsson, et al, 1987
Ankara andesite	MR	1.59	Şener, 2002
Tampomas andesite	CB	1.68	Abrahamsson, et al, 1987
Whitwick andesite	CB	2.17	Bearman, 1999
Bolton hill diorite	CB	2.22	Bearman, 1999
Cliffe hill diorite	CB	2.77	Bearman, 1999
Äspö diorite	SENRBB	3.21	Nordlund, et al., 1999
Finnsjön granodiorite	SR	3.35	Ouchterlony, 1987
Basalt	SECBD	1.80	Whittaker, 1992
Basalt	SC3PB	2.27	Whittaker, 1992
Basalt	BDT	3.01	Whittaker, 1992
Ingleton greywacke	CB	2.38	Bearman, 1999
Cornish greywacke	CB	3.15	Bearman, 1999
Kallax gabbro	SR	2.58	Yi, 1987
Kallax gabbro	SR	3.23	Yi, 1987
Grey norite	SR	2.69	Meredith, 1983
Whin Sill dolerite	SR	3.26	Meredith, 1983

BDT : Uncracked Brazilian Disk Test
CB : Chevron Bend
CCBD : Central Cracked Brazilian Disc under diametral compression test
CCP : Centre Cracked Panel
CNBD : Chevron-Notched Brazilian Disc
CT : Compact Tension
MR : Modified Ring test
SC3PB : Single edge straight through cracked rectangular plate in three-point bending test
SCB : Semi-Circular Bend test
SECB : Single Edge Cracked Beam under three-point bending test
SECBD : Single edge cracked Brazilian disk in diametral compression
SECRBB : Single Edge Cracked Round Bar Bend
SENRBB : Single Edge Notched Round Bar in Bending
SNBD : Straight-Notched Brazilian Disc
SR : Short Rod

1.4 Statement of the Problem and the Thesis Objective

In previous studies of rock fracture testing, generally disc type specimens were used due to the simplicity of coring. A lot of testing techniques such as the Semicircular specimen under three-point bending (SCB) technique for fracture testing of rocks were developed for conducting fracture toughness tests on disc type rock core specimens, since rock cores are readily available from drilling work and that is why the specimen preparation is easy for them.

As a loading configuration, diametrical compression or three-point bending were used to gain fracture toughness of the rock cores. During tests, researchers investigated the effects of the sample geometry in terms of sample thickness and diameter, notch length, angle and type, and span ratio (for three-point bending), testing method, loading rate and temperature.

This study aims to make improvements in the testing techniques and to develop a new testing technique for fracture testing of rock cores.

In this study, to determine fracture toughness, experiments were performed on half discs and discs. Three-point bending was used as a loading method for both sample types. The effects of the sample geometries were studied by changing the notch and the span length of the samples. Disc with three-point bending that is Straight Notched Disc specimen under three-point Bending (SNDB) method, which is a new method, was introduced to determine the Mode I fracture toughness of the pink colored Ankara Gölbaşı andesite. Half disc under three-point bending, namely Semi-Circular specimen under three-point Bending (SCB) was studied by other researchers before. Therefore, in this study, tests with SCB type specimens were performed for comparison purposes.

To determine stress intensity factors, generally ABAQUS, ANSYS, CRACK3D, FRAC3D, FRACTRAN, FRANC2D/L, FRANC3D, LS-DYNA, NASGRO, NASTRAN and TDLCR programs are used in the world. On the other hand, ABAQUS, ANSYS, FRANC2D/L and FRANC3D software are available in Middle East Technical University. In numerical modeling of the SCB and SNDB techniques to find the stress intensity factors, ABAQUS program which is a finite element program was used here. All the numerical studies were conducted with 3D models.

1.5 Sign Convention

Although stresses are positive in compression and negative in tension by sign convention in rock mechanics, compressive stresses are negative and tensile stresses are positive throughout this study as in general solid mechanics, since the work here

involves the use of general linear elastic fracture mechanics principals and numerical modeling with a general purpose finite element package ABAQUS.

1.6 Outline of the Thesis

After a brief introduction in Chapter 1, historical overview of the fracture mechanics, loading modes, fracture criteria and some fracture parameters are mentioned in Chapter 2. Rock fracture test techniques with previous studies are reviewed in Chapter 3. Numerical modeling of the SCB and SNDB for estimation of stress intensity factor is presented in Chapter 4. Laboratory work with experimental setup is devoted in Chapter 5. Finally, conclusions and recommendations for further studies are given in Chapter 6.

CHAPTER 2

FRACTURE MECHANICS

2.1 Historical Overview

The earliest works considering fracture mechanics belonged to Griffith. He began his studies around 1920s. In those days, it was postulated that the theoretical uniaxial strength of a material was equal to 0.1 times Young's Modulus of the particular material. However, it was not the truth. It was examined that the exact values of critical strength were as much as 1000 times less than that predicted value, and Griffith wished to investigate that contradiction. He discovered that in each material there were many microscopic cracks and these small cracks in fact reduced the overall strength of the material since when a load was applied to these cracks, stress concentration was experienced. Stress concentration means the stress is concentrated around the crack tips or flaws and these cracks will grow much more rapidly, therefore causing the material to fracture long before it ever reaches its theoretical strength. According to Griffith's Theory, while the value of stress actually reached the theoretical maximum, the overall average of the stress was lower. Furthermore, not only the microscopic cracks but also any void like holes that have been drilled out in the material, corners, or hollow areas in the internal area of the material could cause stress concentration and fracture will begin in one of these areas due to the stress concentration. During his studies, Griffith found that there was a relation between crack length and surface energy connected traction-free crack surfaces and applied stress and he formed Equation 2.1.

$$\sigma = \sqrt{\frac{2\gamma E}{\pi a}} \tag{2.1}$$

where,

a = crack length

2γ = surface energy

E = Young's modulus

σ = applied stress

Although Griffith's Theory was so significant, there were some limitations on Griffith's Theory. He was only considering elastic, brittle materials, in which no plastic deformation took place.

Since Griffith's theory was developed only for brittle materials as mentioned above, Irwin extended the theory for ductile materials in the 1940s. He hypothesized that for ductile materials, there was also a definite energy from plastic deformation and that energy had to be added to the strain energy which was originally considered by Griffith.

Irwin noticed that for ductile materials, the surface energy term is so small when it is compared to the energy associated with plastic deformation thus it can be omitted. Additionally, he described a quantity which is called the strain energy release rate or "crack driving force," and it is symbolized as $\mathcal{G}$. Irwin postulated that the strain energy release rate is the total energy absorbed during cracking per unit increase in crack length and per unit thickness. In the mid-1950s, he concluded that the local stresses near the crack tip are almost equivalent to Equation 2.2 as a general form.

$$\sigma_{ij} = \frac{K_I}{\sqrt{2\pi r}} f_{ij}(\theta) + \ldots \tag{2.2}$$

where

r , θ = cylindrical coordinates of a point with respect to the crack tip

K = stress intensity factor

Moreover, Irwin explained that the energy approach ($\mathcal{G}$) is equal to the stress intensity approach (K). According to him, when a critical strain energy release rate ($\mathcal{G}$) or critical stress intensity (K_c) is accomplished, crack propagation occurs.

In 1960s, scientists began to focus on the plasticity of the crack tips and in 1968, the plastic deformation as nonlinear elastic behavior was modeled by Rice. In addition, he extended the energy approach to nonlinear materials. He pointed out that the energy release rate can be expressed as a path-independent line integral, called the J integral. Rice's theory has provided the development of fracture mechanics in United States. In the meantime, Wells (1961) intended a parameter called crack tip opening displacement (CTOD), which led the fracture mechanics research in Europe.

2.2 Linear Elastic Fracture Mechanics

Linear Elastic Fracture Mechanics (LEFM) assumes that the material is isotropic and linear elastic. Isotropic and linear elastic (Figure 2.1) means the material properties are independent of direction and these materials have only two independent elastic constants which are Young's Modulus (E) and Poisson's ratio (υ). Derived from the LEFM assumption, the stress field near the crack tip is calculated by considering the theory of elasticity. Moreover, it is applicable to brittle fracture situations where the load-deflection response of the cracked body is essentially linear up to the point of fracture.

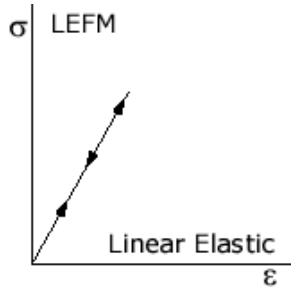

Figure 2.1 Stress - Strain curve of the LEFM

LEFM is valid only when the inelastic deformation is smaller than the size of the crack. If large zones of plastic deformation develop before the crack propagations, Elastic Plastic Fracture Mechanics (EPFM) should be used instead of LEFM.

LEFM equation is expressed generally as in Equation 2.2. By considering linear elasticity theories, the stress field near a crack tip depends on the location, the loading conditions, and geometry of the specimen (Equation 2.3).

$$\sigma_{ij}^{Crack\ tip} \equiv \sigma_{ij}^{Crack\ tip}\left(Location, Loading, Geometry\right) \equiv \sigma_{ij}^{Crack\ tip}\left(r, \theta, K\right) \tag{2.3}$$

where,

Location = polar coordinates, r and θ

Loading and *Geometry* = stress intensity factor, K

2.3 Loading Modes

Fracture classification is based on the fracture mode terminology of classical fracture mechanics. Three basic failure modes are possible in fracture mechanics. These are mode I, mode II and mode III (Figure 2.2).

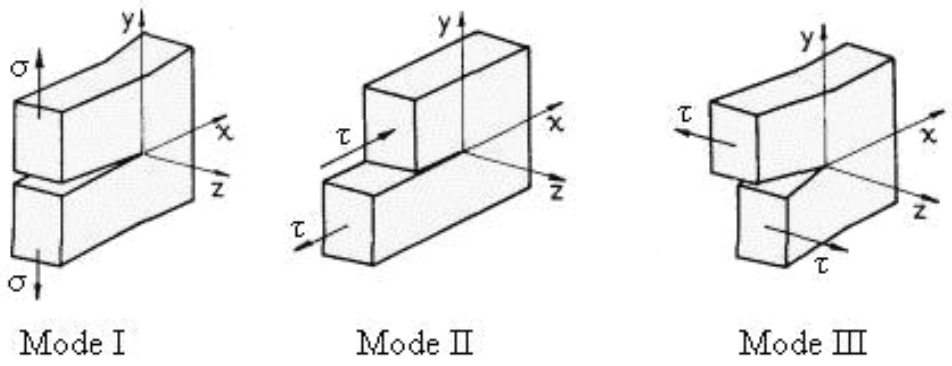

Figure 2.2 Fracture modes

Mode I: it is also called the tensile opening mode. In Mode I, the crack faces separate in a direction normal to the plane of the crack.

Mode II: the crack faces are mutually in the direction normal to the crack front in Mode II and it is termed as in-plane sliding or shear mode,

Mode III: the tearing or out of plane mode is Mode III. Namely, the crack faces are sheared parallel to the crack front in Mode III.

These crack deformations can occur separately or in any combinations. Combinations of the modes are called as mixed mode.

In LEFM, most formulas are derived considering these modes by assuming either plane stress or plane strain conditions (Figure 2.3).

Plane Stress Condition: In a thin plate, the stress through the thickness (σ_{zz}) cannot change noticeably owing to the thin section and it is equal to zero ($\sigma_{zz} = 0$). This is termed as plane stress condition.

Plane Strain Condition: In a thick body, the material is constrained through the thickness and strain in z-direction is equal to zero ($\varepsilon_{zz} = 0$). This condition is called as plane strain condition.

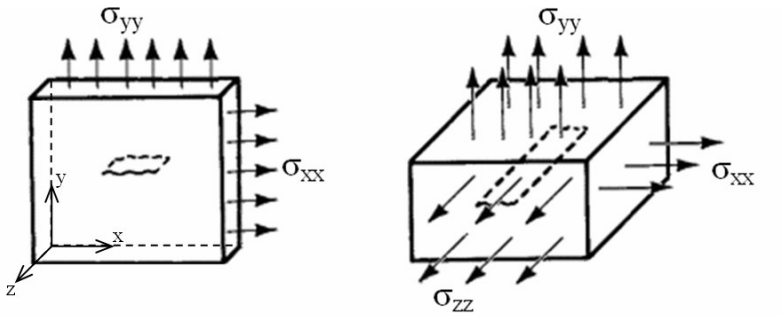

Figure 2.3 Plane Stress and Plane Strain Conditions for plates under biaxial positive tensile stresses

2.4 Crack Tip Stress and Displacement Components

The crack tip stress and displacement components of a linear elastic isotropic material can be expressed separately for all three modes by considering Equation 2.2 as follows (Figure 2.4).

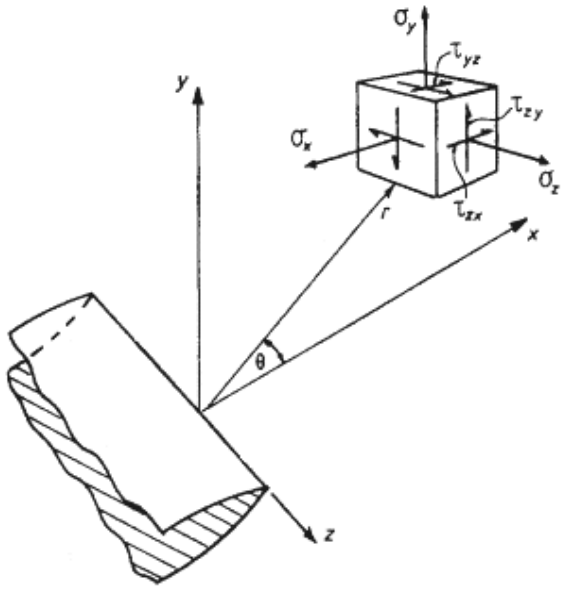

Figure 2.4 Location of local stresses near a crack tip

The small differences in formulas for plane stress and plane strain are handled by κ, where

$$\kappa = \begin{cases} \dfrac{3-\nu}{1+\nu} & (\text{Plane Stress}) \\ 3-4\nu & (\text{Plane Strain}) \end{cases} \tag{2.4}$$

Crack Tip Stress Components of Mode I:

$$\begin{aligned}
\sigma_{xx} &= \frac{K_I}{\sqrt{2\pi r}}\cos\left(\frac{\theta}{2}\right)\left[1-\sin\left(\frac{\theta}{2}\right)\sin\left(\frac{3\theta}{2}\right)\right] \\
\sigma_{yy} &= \frac{K_I}{\sqrt{2\pi r}}\cos\left(\frac{\theta}{2}\right)\left[1+\sin\left(\frac{\theta}{2}\right)\sin\left(\frac{3\theta}{2}\right)\right] \\
\sigma_{zz} &= \begin{cases} 0 & (\text{Plane Stress}) \\ \nu\left(\sigma_{xx}+\sigma_{yy}\right) & (\text{Plane Strain}) \end{cases} \\
\tau_{xy} &= \frac{K_I}{\sqrt{2\pi r}}\cos\left(\frac{\theta}{2}\right)\sin\left(\frac{\theta}{2}\right)\cos\left(\frac{3\theta}{2}\right),\ \tau_{yz}=0,\ \tau_{zx}=0
\end{aligned} \tag{2.5}$$

Crack Tip Displacement Components of Mode I:

$$\begin{aligned}
u_x &= \frac{K_I}{2G}\sqrt{\frac{r}{2\pi}}\cos\left(\frac{\theta}{2}\right)\left[\kappa-1+2\sin^2\left(\frac{\theta}{2}\right)\right] \\
u_y &= \frac{K_I}{2G}\sqrt{\frac{r}{2\pi}}\sin\left(\frac{\theta}{2}\right)\left[\kappa+1-2\cos^2\left(\frac{\theta}{2}\right)\right] \\
u_z &= 0
\end{aligned} \tag{2.6}$$

Crack Tip Stress Components of Mode II:

$$\begin{aligned}
\sigma_{xx} &= -\frac{K_{II}}{\sqrt{2\pi r}}\sin\left(\frac{\theta}{2}\right)\left[2+\cos\left(\frac{\theta}{2}\right)\cos\left(\frac{3\theta}{2}\right)\right] \\
\sigma_{yy} &= \frac{K_{II}}{\sqrt{2\pi r}}\sin\left(\frac{\theta}{2}\right)\cos\left(\frac{\theta}{2}\right)\cos\left(\frac{3\theta}{2}\right) \\
\sigma_{zz} &= \begin{cases} 0 & (\text{Plane Stress}) \\ \nu\left(\sigma_{\mathrm{xx}}+\sigma_{yy}\right) & (\text{Plane Strain}) \end{cases} \\
\tau_{xy} &= \frac{K_{II}}{\sqrt{2\pi r}}\cos\left(\frac{\theta}{2}\right)\left[1-\sin\left(\frac{\theta}{2}\right)\sin\left(\frac{3\theta}{2}\right)\right],\ \tau_{yz}=0,\ \tau_{zx}=0
\end{aligned} \tag{2.7}$$

Crack Tip Displacement Components of Mode II:

$$\begin{aligned}
u_x &= \frac{K_{II}}{2G}\sqrt{\frac{r}{2\pi}}\sin\left(\frac{\theta}{2}\right)\left[\kappa+1+2\cos^2\left(\frac{\theta}{2}\right)\right] \\
u_y &= -\frac{K_{II}}{2G}\sqrt{\frac{r}{2\pi}}\cos\left(\frac{\theta}{2}\right)\left[\kappa-1-2\sin^2\left(\frac{\theta}{2}\right)\right] \\
u_z &= 0
\end{aligned} \tag{2.8}$$

Crack Tip Stress Components of Mode III:

$$\begin{aligned}
&\sigma_{xx} = 0 \\
&\sigma_{yy} = 0 \\
&\sigma_{zz} = 0 \\
&\tau_{xy} = 0\,,\ \tau_{yz} = \frac{K_{III}}{\sqrt{2\pi r}}\cos\left(\frac{\theta}{2}\right),\ \tau_{zx} = -\frac{K_{III}}{\sqrt{2\pi r}}\sin\left(\frac{\theta}{2}\right)
\end{aligned} \tag{2.9}$$

Crack Tip Displacement Components of Mode III:

$$\begin{aligned}
&u_x = 0 \\
&u_y = 0 \\
&u_z = \frac{K_{III}}{G}\sqrt{\frac{r}{2\pi}\sin\left(\frac{\theta}{2}\right)}
\end{aligned} \tag{2.10}$$

In order to compute mixed mode stress field, Equation 2.5, 2.7 and 2.9 are added.

$$\sigma_{ij}^{(Total)} = \sigma_{ij}^{(I)} + \sigma_{ij}^{(II)} + \sigma_{ij}^{(III)} \tag{2.11}$$

Furthermore, to calculate mixed mode displacement around the crack, Equation 2.6, 2.8 and 2.10 are summed.

$$u_i^{(Total)} = u_i^{(I)} + u_i^{(II)} + u_i^{(III)} \tag{2.12}$$

2.5 Fracture Criteria

In order to predict fracture direction and evaluate fracture loadings of cracked materials various fracture criteria are available. The widely used ones are maximum tangential stress criterion, minimum strain energy density criterion and maximum energy release rate criterion.

2.5.1 Maximum Tangential Stress Criterion, σ_{max}

Maximum tangential stress criterion, which is also called maximum circumferential stress criterion, was proposed by Erdogan and Sih in 1963.According to maximum

tangential stress criterion, fracture occurs in the direction where the circumferential stress surrounding the crack tip is the maximum. To compute crack propagation angle, θ, Equation 2.13 is considered.

$$\tan\left(\frac{\theta}{2}\right) = \frac{-2K_{II}}{K_I + \sqrt{(K_I)^2 + 8(K_{II})^2}} \tag{2.13}$$

As seen from the Equation 2.13 crack propagation angle with maximum tangential stress criterion could be determined by knowing stress intensity factors, K_I and K_{II}.

2.5.2 Maximum Energy Release Rate Criterion, G_{max}

Maximum energy release rate criterion was suggested by Griffith. In maximum energy release rate criterion, fracture propagation direction depends on the maximum energy release rate around the crack tip. Equation 2.14 shows the corresponding crack propagation angle depends on the stress intensity factors, K_I and K_{II} as mentioned in the maximum tangential stress criterion.

$$\theta = \arctan\left(\frac{2K_I K_{II}}{K_I^2 + K_{II}^2}\right) \tag{2.14}$$

2.5.3 Minimum Strain Energy Density Criterion, S_{min}

In 1974, Sih postulated that the critical value of the local strain energy could affect the crack instability and could be a criterion to determine crack propagation direction. The minimum of strain energy density around the crack tip states crack propagation direction. By solving Equation 2.15 and 2.16, angle of crack propagation can be calculated.

$$[2\cos\theta - (\kappa - 1)]\sin\theta K_I^2 + 2[2\cos 2\theta - (\kappa - 1)\cos\theta]K_I K_{II} + [(\kappa - 1 - 6\cos\theta)\sin\theta]K_{II}^2 = 0 \tag{2.15}$$

and

$$[2\cos 2\theta - (\kappa - 1)\cos\theta]K_I^2 + 2[(\kappa - 1)\sin\theta - 4\sin 2\theta]K_I K_{II} + [(\kappa - 1)\cos\theta - 6\cos 2\theta]K_{II}^2 > 0 \tag{2.16}$$

2.6 Fracture Toughness

Fracture Toughness is the resistance to fracture and it is also termed as the critical value of stress intensity factor. In general, fracture toughness depends on temperature, environment, loading rate, the composition of the material and its microstructure, together with geometric effects. Fracture toughness is denoted as K_c. The dimension of K_c is:

$$Dim[K_c] = \frac{F}{L^2}\sqrt{L} = FL^{-3/2} = Stress \cdot \sqrt{Length} = Pa\sqrt{m} \tag{2.17}$$

Fracture toughness can be established from a single fracture toughness specimen in terms of stress intensity factor (K), crack-tip opening displacement ($CTOD$ or δ) and the J-integral (J). These are the some typical fracture parameters.

2.6.1 Stress Intensity Factor

The stress intensity factor, K, which was introduced in Equation 2.2, defines the magnitude of the local stresses around the crack tip. This factor depends on loading, crack size, crack shape, and geometric boundaries. Engineers mostly pay attention to the maximum stress near the crack tip and whether it surpasses the fracture toughness. Therefore, the stress intensity factor is generally expressed in terms of the remote stress applied to component, σ at $r \to 0$ and $\theta = 0$. Stress intensity factor is a stress-based measure and it is calculated mainly from the Equation 2.18:

$$K = \sigma\sqrt{\pi \times a} \times f\left(\frac{a}{w}\right) \tag{2.18}$$

where:

σ = remote stress applied to component (not to be confused with the local stresses, σ_{ij}, in Equation 2.2)

a = crack length

$f(a/w)$ = correction factor that depends on specimen and crack geometry

Figure 2.5 shows the stress intensity relationships for a few of the more common loading conditions.

The dimension of K is same as the fracture toughness:

$$Dim[K] = \frac{F}{L^2}\sqrt{L} = FL^{-3/2} = Stress \cdot \sqrt{Length} = Pa\sqrt{m} \tag{2.19}$$

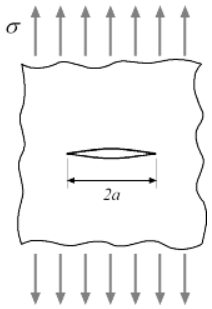

$$K_I = \sigma\sqrt{\pi a}$$

(a) Infinite Plate with a Center Through Crack under Tension

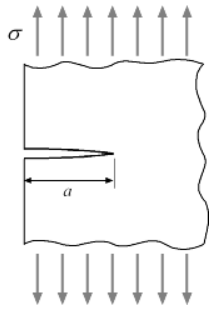

$$K_I = 1.12\sigma\sqrt{\pi a}$$

(b) Semi-infinite Plate with an Edge Through Crack under Tension

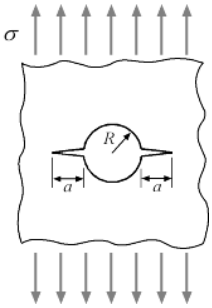

$$K_I = \sigma\sqrt{\pi a}\left[1 + 2.365\left(\frac{R}{R+a}\right)^{2.4}\right]$$

(c) Infinite Plate with a Hole and Symmetric Double Through Cracks under Tension

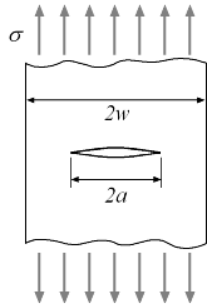

$$K_I = \sigma\sqrt{\pi a}\left[\frac{2w}{\pi a}\tan\left(\frac{a}{2w}\right)\right]^{1/2}$$

(d) Semi-infinite Plate with an Edge Through Crack under Tension

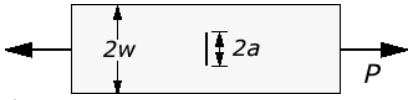

$$K_I = \frac{P}{B\sqrt{w}}\left\{\sqrt{\frac{\pi a}{2w}\sec\left(\frac{\pi a}{2w}\right)}\left[1 - 0.025\left(\frac{a}{w}\right)^2 + 0.06\left(\frac{a}{w}\right)^4\right]\right\}$$

(e) Center Cracked Specimen Under Tension

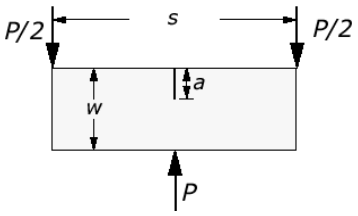

$$K_I = \frac{P}{B\sqrt{w}}\left\{\frac{3\frac{s}{w}\sqrt{\frac{a}{w}}}{2\left(1+2\frac{a}{w}\right)\left(1-\frac{a}{w}\right)^{\frac{3}{2}}}\left\{1.99 - \frac{a}{w}\left(1-\frac{a}{w}\right)\left[2.15 - 3.93\frac{a}{w} + 2.7\left(\frac{a}{w}\right)^2\right]\right\}\right\}$$

(f) Single Edge Notched Specimen Under Bending

Figure 2.5 K_I calculations for a few of more common loading conditions (www.efunda.com)

2.6.2 Crack-tip Opening Displacement

There are two types of description for Crack-tip opening displacement (*CTOD* or δ): one of them is the opening displacement of the original crack tip (Figure 2.6) and the other is the displacement at the intersection of a 90° vertex with the crack edges (Figure 2.7).

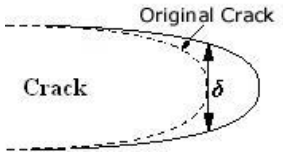

Figure 2.6 CTOD of the original Crack (www.efunda.com)

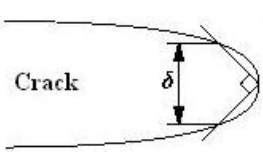

Figure 2.7 CTOD at the intersection of a 90° vertex with the edges (www.efunda.com)

CTOD is a strain-based measure, and it is separated into two components which are elastic and plastic (Equation 2.20). While the elastic part of CTOD is obtained from the stress intensity factor, K considering LEFM, the plastic component is derived from the crack mouth opening displacement which is measured by the help of a clip gauge (Figure 2.8).

$$\delta = \delta_{elastic} + \delta_{plastic} \tag{2.20}$$

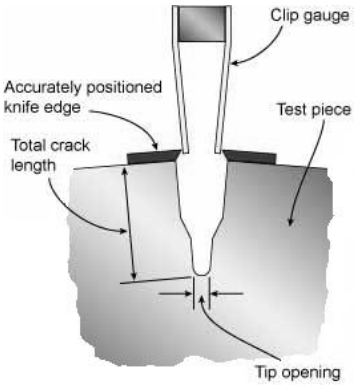

Figure 2.8 Clip gauge at the crack opening

2.6.3 Computation of Stress Intensity Factors

As stated before there are a number of closed form solutions available to determine the stress intensity factors for relatively simple geometries and loading conditions. Complicated problems need to be handled by numerical modeling. In the numerical modeling work for the computation of stress intensity factor there are three fracture techniques which are Displacement Correlation Technique, Modified Crack Closure Technique and J-Integral Technique.

2.6.3.1 Displacement Correlation Technique

To obtain stress intensity factors, this method correlates the nodal displacements from a finite element analysis, at specific locations, with the analytical solutions (Anderson, 1991).

Equation 2.21 shows the crack opening displacement δ(r) at a distance *r* from the crack tip along the crack face.

$$\delta(r) = K_I \left(\frac{\kappa + 1}{\mu} \right) \sqrt{\frac{r}{2\pi}} \tag{2.21}$$

where

μ = shear modulus

κ = 3 - 4υ for plane strain and κ = (3 – υ)/(1+ υ) for plane stress

The crack opening displacement is also calculated by a displacement expansion where the higher order terms are neglected. The Equation 2.22 shows the expression.

$$\delta(r) = \left(4v_{j-1} - v_{j-2} \right) \sqrt{\frac{r}{L}} \tag{2.22}$$

where

v_{j-1} and v_{j-2} = relative displacements in y-direction, at *j*-1 and *j*-2 nodes

L = element size (Figure 2.9)

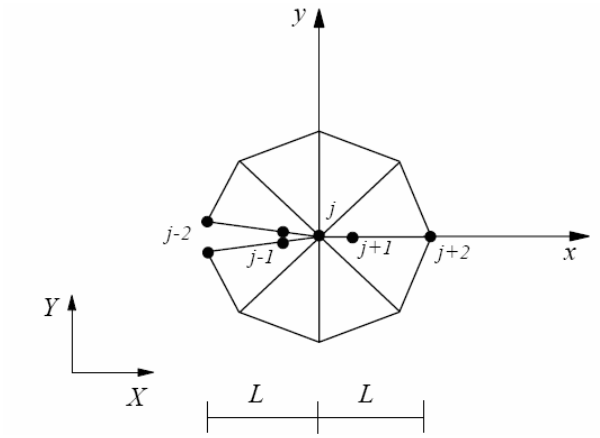

Figure 2.9 Quarter point elements at the crack tip (Denyse de Araújo, et al., 2000)

From the Equations (2.21) and (2.22) stress intensity factor is calculated as in Equation 2.23 (Denyse de Araújo, et al., 2000).

$$K_I = \left(\frac{\mu}{\kappa+1}\right)\sqrt{\frac{2\pi}{L}}\left(4v_{j-1} - v_{j-2}\right) \tag{2.23}$$

2.6.3.2 Modified Crack Closure Technique

This method is based on the preliminary work of Irwin. According to the method, the same work is done to close the crack from "a + δa" to "a" and to extend it from "a" to "a + δa" (Figure 2.10). In this case, strain-energy release rate is obtained for Mode I is in Equation 2.24.

$$G_I = \lim_{\delta a \to 0} \frac{1}{2\delta a}\int_0^{\delta a} v(r)\sigma_y(r)dr \tag{2.24}$$

where

δa = virtual crack extension

σ_y = normal stress distribution ahead of the crack tip

$v(r)$ = crack opening displacement at a distance r behind the new crack tip

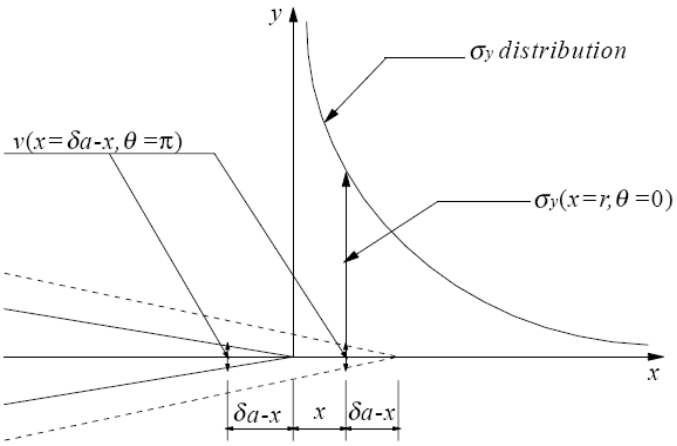

Figure 2.10 Irwin's concept of crack-closure integral (Denyse de Araújo, et al., 2000)

In the linear elastic analysis, stress intensity factor is related to the strain-energy release rates through the Equation 2.25 (Denyse de Araújo, et al., 2000).

$$G_I = \frac{\kappa + 1}{8\mu} K_I^2 \tag{2.25}$$

2.6.3.3 J-Integral Technique

J-integral, *J* is defined as a path-independent line integral (Figure 2.11) that measures the strength of the singular stresses and strains near a crack tip was introduced by Rice (1968). *J* is calculated on nonlinear elastic materials with crack.

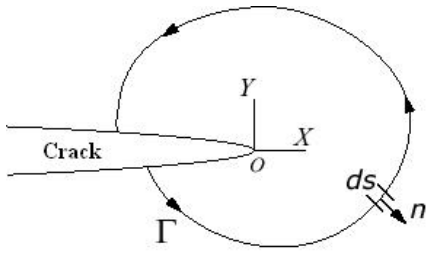

Figure 2.11 J-integral contour path surrounding a crack-tip (www.efunda.com)

J is derived from the Equation 2.26:

$$J = \int_{\Gamma} w dy - T_i \frac{\partial u_i}{\partial x} ds \tag{2.26}$$

where,

w = the strain energy density, i.e. strain energy per unit volume, ($w = \int_0^{\varepsilon_{ij}} \sigma_{ij} d\varepsilon_{ij}$)

T_i = traction vector, ($T_i = \sigma_{ij} n_j$)

Γ = an arbitrary path around the crack tip

n = unit outer normal vector to path Γ

σ = stress component

ε = strain

u = displacement vector

s = distance along the path Γ

Stress intensity factor in Mode I is calculated with the Equation 2.27. (Denyse de Araújo, et al., 2000)

$$K_I = 0.5\sqrt{\frac{8\mu}{\kappa+1}}\left(\sqrt{J_1 - J_2} + \sqrt{J_1 + J_2}\right) \tag{2.27}$$

where

μ = shear modulus

$\kappa = 3 - 4\upsilon$ for plane strain and $\kappa = (3 - \upsilon)/(1+ \upsilon)$ for plane stress

For linear elastic problems, all three numerical techniques mentioned here for calculation of conditions the stress intensity factors gave consistent results. The results from the Modified Crack Closure Technique and J-Integral methods can be considered exact, indicating that the use of simplified formulae and associated fields, respectively, are reliable. The Displacement Correlation Technique, considered by many authors a method of low precision, presented satisfactory percentage error (below 5% for the stress intensity factor in the dominant mode and below 10% for the non-dominant mode).(Denyse de Araújo et. al., 2000).

CHAPTER 3

ROCK FRACTURE TESTING ON DISC TYPE SPECIMENS

In the rock engineering field, crack deformations occur in opening mode (Mode I) for parts under tension, however since the structures are generally under compression crack deformations occur in shear mode (Mode II) or in mixed modes (Mode I-II).

In order to assess the stress intensity factor under Mode I conditions, International Society for Rock Mechanics (ISRM) suggests three methods which use following specimen types:

- Short Rod (SR) Specimens
- Chevron Bend (CB) Specimens
- Chevron-Notched Brazilian Disc (CNBD) Specimens

To evaluate the fracture toughness of rocks there is not any standard method suggested by ISRM, however various methods were used to evaluate fracture toughness of rocks.

Some of the additional testing methods used in the previous work to find fracture toughness use the following specimen types for which stress intensity evaluations are given in the related literature:

- Straight-Notched Brazilian Disc (SNBD) Specimens
- Straight-Notched Semi-Circular Bend (SNSCB) Specimens
- Punch Through Shear (PTS) Tests

3.1 SR Specimens

Short Rod specimen was developed by Barker (1977). In SR specimen, a chevron notch is cut in cylindrical specimen and fracture toughness computation is done by an analytical method which is achieved by ISRM (1988) and a correction factor for the nonlinear behavior of the material is calculated with another equation depending on the Load-CMOD curve of the fracture experiments. SR method is only used to determine Mode I fracture toughness.

3.1.1 Specimen Preparation and Testing Equipment

In the beginning, cores are taken from rock blocks. Then, cylindrical samples are obtained from these blocks. In order to provide loading surface in tension, a rectangular grip groove is machined in one end of the short rod specimen (Figure 3.1 and Figure 3.2).

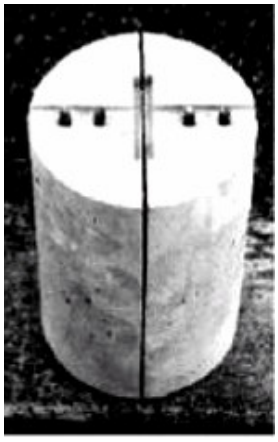

Figure 3.1 Short Rod Specimen
(Sousa & Bittencourt, 2001)

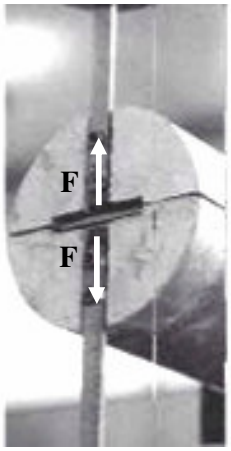

Figure 3.2 Loading surface
(Sousa & Bittencourt, 2001)

After grip groove is opened, two slots are cut at opposing angles. Moreover, these slots must form a triangular ligament which is called as chevron. The specimen dimensions for Short Rod are given in Figure 3.3 and in Table 3.1.

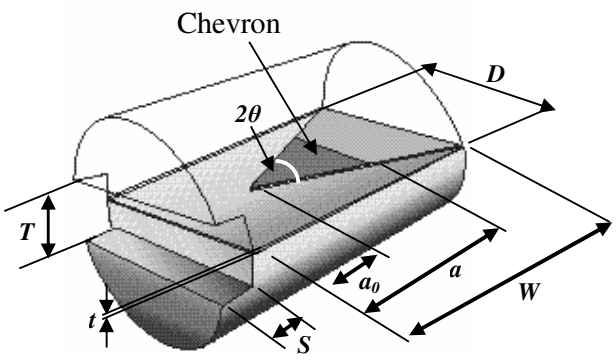

Figure 3.3 Short-Rod Specimen Dimensions

Table 3.1 Specimen dimensions for Short Rod (Ouchterlony, 1988)

Symbol	Definition	Value	Tolerance
D	Specimen diameter	D	>10 x grain size
W	Specimen length	1.45D	± 0.02
θ	Subtended chevron angle	54.6°	±1.0°
a_0	Distance to Chevron notch tip	0.48D	± 0.02D
W-a_0	Chevron length	0.97D	±0.02D
t	Notch width	≤0.03D or 1mm*	

* whichever is greater

In order to perform Short Rod Fracture Testing, Tensile Loading Machine and Displacement measuring system are used (Figure 3.2). There are two levels of testing in SR method. In Level 1 testing, maximum load during bending is recorded and in Level 2 testing, load and displacement measurements are taken into account.

3.1.2 Fracture Toughness Determination

For Level 1 testing, according to the ISRM (1988), fracture toughness of the SR specimen is accomplished by Equation 3.1.

$$K_{SR} = C_K 24.0 F_{\max} / D^{1.5} \tag{3.1}$$

where

F_{max}= failure load

D = specimen diameter

C_K = correction factor to account for the size variation of the specimen;

$$C_K = \left(1 - \frac{0.6\Delta W}{D} + \frac{1.4\Delta a_0}{D} - 0.01\Delta\theta\right) \tag{3.2}$$

where

ΔW = variation in specimen height

Δa_0 = initial position of chevron notch apex

$\Delta\theta$ = chevron notch angle

For Level 2 testing, fracture toughness evaluation of the SR specimen start with Equation 3.1 and Equation 3.2. Afterward a nonlinearity correction factor is calculated and corrected fracture toughness of SR specimen is evaluated as in Equation 3.3 by using Load-CMOD curves (Figure 3.4).

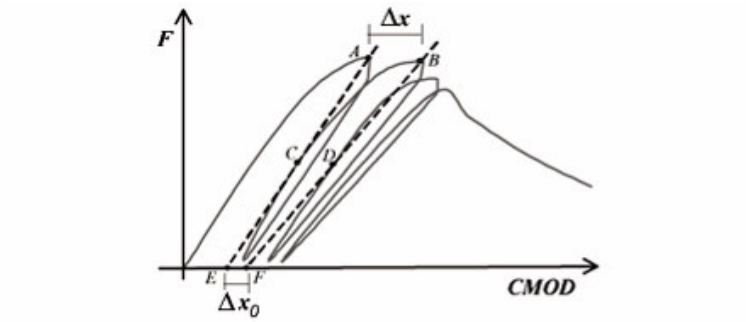

Figure 3.4 Definitions for computation of correction factor based on Load-CMOD plot (Sousa & Bittencourt, 2001)

$$K_{SR}^{c} = \sqrt{\frac{1+p}{1-p}} K_{SR} \tag{3.3}$$

where $p = \Delta x_0 / \Delta x$ (Figure 3.4)

3.1.3 Related Studies

Short rod specimens were used to analyze experimentally fracture processes in concrete by Sousa and Bittencourt in 2001. By using short rod samples, fracture toughness tests of concrete were performed. In experiments, crack mouth opening displacement (*CMOD*) was measured with a MTS Model 632.03C.20 clip on gauge. Furthermore, MTS Model 810 closed-loop testing machine was used to apply load at a rate between 2 and 3 N/s and that load application was controlled by the *CMOD*.

During the test, *CMOD* versus applied load graph was drawn. Dependent on that plot, the system was unloaded down to 10-20% of the maximum observed load and reloaded subsequently (Figure 3.5). In order to calculate nonlinearity of the concrete behavior, correction factor was computed from unloading-reloading cycles. That correction factor should be applied to the fracture toughness calculation to acquire the actual fracture toughness of the concrete.

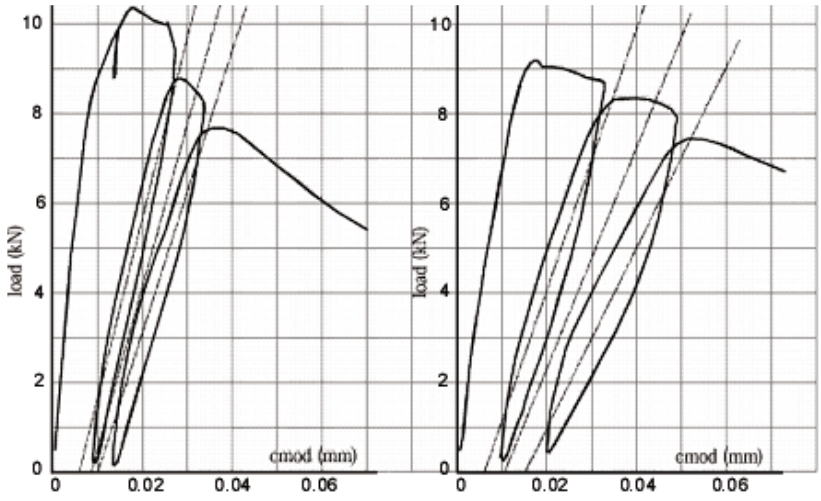

Figure 3.5 Plots of load versus *CMOD* obtained from tests (Sousa & Bittencourt, 2001)

3.2 CB Specimens

CB specimen was proposed by Ouchterlony (1988). In chevron bend specimen, v-shaped notch is sawed in cylindrical specimen and loaded under three-point bending. Fracture toughness of the CB specimen is evaluated like fracture toughness of the SR specimen. . CB method is only used to determine fracture toughness in Mode I.

3.2.1 Specimen Preparation and Testing Equipment

Cylindrical samples are obtained from bored rocks. Cores are cut into needed lengths. Then, by the help of rotary saw, two notches which are formed a v-shape ligament are achieved in opposite angles. This v-shape ligament which is termed as a chevron shaped notch is in the middle of the core perpendicular to its axis. After preparation of the sample, the ready specimen is subjected to a three-point bending load. The loading and resulting fracture propagation is servo-controlled by a clip gauge that measures the chevron notch opening (Figure 3.6).

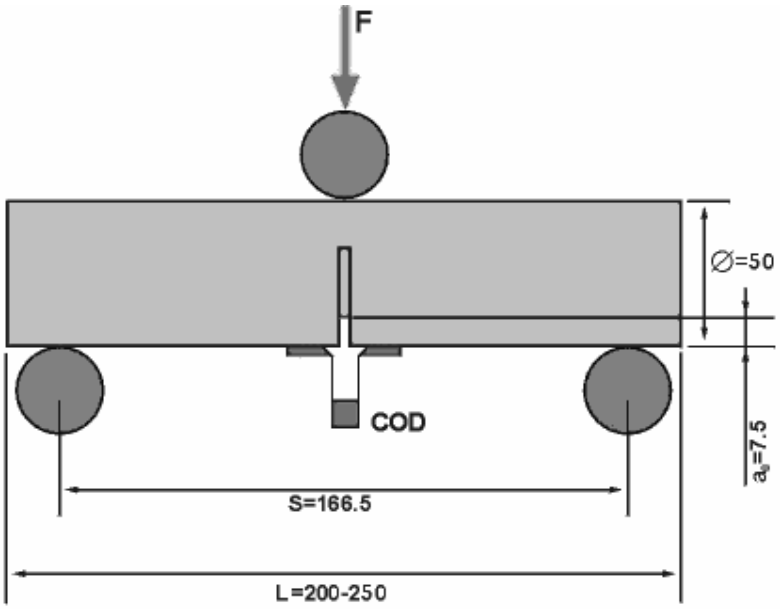

Figure 3.6 Dimensions of the Chevron Bend Specimen (Ouchterlony, 1988)

3.2.2 Fracture Toughness Determination

Equations 3.1-3.3 are used to calculate fracture toughness of CB. In equations K_{CB} is calculated instead of K_{SR}.

3.2.3 Related Studies

In order to determine mode I fracture toughness of Äspödiorite, Backers (2003) studied on CB method, Level 2 testing. Sample preparation was achieved by considering Ouchterlony, 1988. Typical sizes of the specimens used in the experiments are shown in Table 3.2 (Figure 3.6).

Table 3.2 Dimensions of the CB specimen for K_{IC} determination

Geometrical parameter	Value	In Backers' study
Specimen diameter	D	~ 51 mm
Specimen length, L	> 3.5 D	200–250 mm
Support span, S	(3.33 ± 0.02) D	169.5 mm
Chevron angle, θ	90.0° ± 1.0°	90°
Chevron tip position, a_o	(0.15 ± 0.01) D	7.50 ± 0.06 mm
Notch width, t	0.03 D	1.5 mm

A stiff, servo-controlled MTS (Material Test Systems Corporation, Minneapolis, MI, USA) loading machine was used in experiments. The maximum force capacity of the MTS is 4600 kN.

3.3 CNBD Specimens

To measure the fracture toughness of ceramics, Shetty et al. (1985) used CNBD specimen firstly. In CNBD specimen, circular cuts are opened to the centers of both sides of the disc shape specimen. Fracture toughness is calculated by an equation which depends on normalized stress intensity factor. Stress intensity factor is computed with numerical methods and an equation can be derived by fitting the numerical results. CNBD specimen is used not only achieved fracture toughness in Mode I but also fracture toughness in Mode II and mixed modes.

3.3.1 Specimen Preparation and Testing Equipment

The chevron notches are made using a slow speed circular saw. The rock disks are first marked on both sides along the diameter of the disc to show the two extreme points up to which the saw can cut. The marked Brazilian disc is pressed against the rotating circular saw until the saw reached the two marked extreme points. The disc is removed and turned. Then the same procedure is repeated from the other side of the disc. This makes a central opening, $2a_0$ (Figure 3.7). During the notch-making process, the discs are held manually against the saw, making it difficult to obtain precise dimensions and crack geometry.

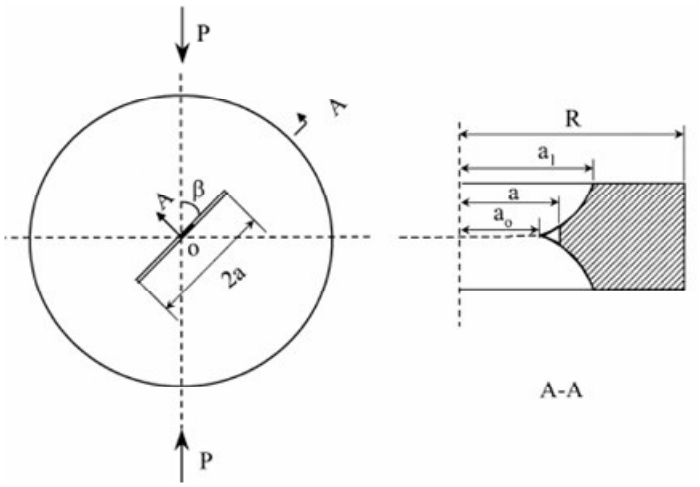

Figure 3.7 CNBD under diametrical compression (Khan and Al-Shayea, 2000)

A strain-controlled loading frame is used for the load application. The applied load and load point displacement are obtained using a computerized data logger (Figure 3.8).

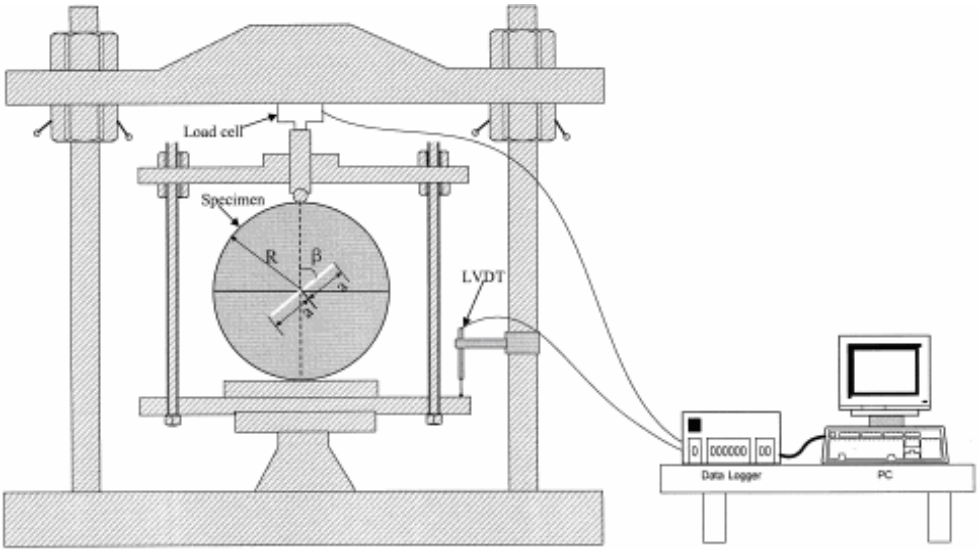

Figure 3.8 Loading setup for fracture testing on CNBD specimen (Khan and Al-Shayea, 2000)

3.3.2 Fracture Toughness Determination

Fracture toughness is calculated by using expression suggested by ISRM (1995). The expression is in Equation 3.4.

$$K_{IC} = \frac{P_{\max}}{B\sqrt{D}} Y^*_{\min} \tag{3.4}$$

where

D = diameter of the Brazilian disc

B = thickness of the specimen

P_{max} = compressive load at failure

$Y^*_{\min}$ = critical dimensionless stress intensity factor

$Y^*_{\min} = ue^{v\alpha}$

where

u and v = constants determined by a_0/R and B/R

Dimensionless stress intensity factor is derived from by fitting the numerical results of various geometries of CNBD specimens.

3.3.3 Related Studies

In the study of Khan and Al-Shayea (2000), slow speed circular saw with a disk of 80 mm diameter and 1.8 mm thickness was used. The length of the extreme point on each side from the center along the diameter of the disc was 30 mm. Moreover, central opening, $2a_0$, was about 29 mm.

Chang et al. (2002) used Keochang Granite and Yeosan Marble produced in Korea for testing. CNBD specimens 75 and 54 mm in diameter and 15-35 mm in thickness were used to investigate effects of specimen size on fracture toughness values. The cutting machine for preparing a chevron notch for the CNBD specimen was manufactured to satisfy the ISRM suggested geometrical conditions for the CNBD disk specimen (Table 3.3). The diameter and thickness of the diamond saw were 50 and 0.8 mm, respectively.

Table 3.3 Standard geometrical dimensions of the CNBD specimen

Description	Values	Dimensionless expression
D (mm)	75.0	
B (mm)	30.0	$\alpha_B = B/R = 0.80$
a_0 (mm)	9.89	$\alpha_0 = a_0/R = 0.2637$
a_1 (mm)	24.37	$\alpha_1 = a_1/R = 0.65$
D_s (mm)	52.0	$\alpha_s = D/D_s = 0.6933$
h_c (mm)	16.95	
Y^*_{min} (dimensionless)	0.84	
Notch width (mm)	≤ 1.5	
a_m (mm)	19.31	$\alpha_m = a_m/R = 0.5149$

3.4 SNBD Specimens

SNDB specimen was developed by Chong and Kuruppu (1984). In SNBD specimen, straight notch is opened to circular disc with drill bit and wire saw. Fracture toughness is calculated by a mathematical expression. The expression

includes normalized stress intensity factor, which is determined by using numerical methods.

Mode I, Mode II and mixed mode fracture toughness determination is possible by using SNBD method.

3.4.1 Specimen Preparation and Testing Equipment

Firstly, cores are obtained from the rock blocks. They are cut into circular discs, using a high speed diamond plated rotary saw. The sliced discs are sanded to ensure uniform thickness. Then a hole is initially drilled at the center of the discs using a drilling bit in a lathe. The bit is made to penetrate the rotating disc to the mid-thickness of the specimen, afterward the disk is reversed and the hole is completed. The wire of the saw is passed through the drilled hole and a notch of any length is machined in the disk. The depth of the cut is precisely controlled by a moving platform on which specimen is mounted (Figure 3.9). Testing equipment and setup are similar to that of CNBD specimen test (Figure 3.8).

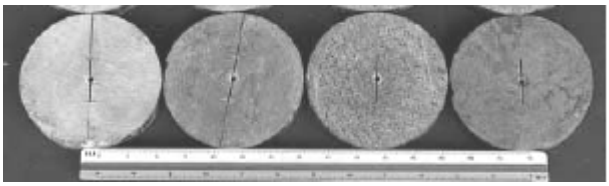

Figure 3.9 SNBD Specimens (Al-Shayea, 2002)

3.4.2 Fracture Toughness Determination

For fracture toughness computation, Equation 3.5 was proposed by Atkinson et al. (1982).

$$K_I = \frac{P\sqrt{a}}{\sqrt{\pi RB}} N_I \tag{3.5}$$

where

K_I = stress intensity factor in Mode I

R = radius of the Brazilian disc

B = thickness of the specimen

P = compressive load at failure

N_I = non-dimensional coefficients which depend on a/R

For N_I, Equation 3.6 was derived by Shetty and Rosenfield (1985) by fitting the numerical results of Atkinson et al. (1982).

$$N_I = 0.99 + 0.141\left(\frac{a}{R}\right) + 0.863\left(\frac{a}{R}\right)^2 + 0.886\left(\frac{a}{R}\right)^3 \tag{3.6}$$

3.4.3 Related Studies

In the testing program of Khrishnan (1998), cylindrical soft sandstone samples of size 7.19 cm were cored by a specially designed. The cores that obtained were sliced at 2.54 cm thickness and they were leveled to 2.11 cm size. To have straight edge notch, a special technique was developed since the specimens are soft. Two thin square cardboard pieces with 0.1 cm thickness, 7.24 cm widths were prepared and each piece has a slot at the center with a 1.05 cm length. The specimen was sandwiched between these pieces firmly by the help of elastic bands. The notch was cut from both sides by using a triangular shaped steel blade of 0.05 cm thick.

In the study of Khan and Al-Shayea (2000), rock blocks were collected from a limestone rock formation outcropping in the Central Province of Saudi Arabia. In the experiments of SNBD, cores were 84 mm and 98 mm in diameter, core thickness was 22 mm, and drill bit diameter and wire saw thickness used in the experiments had a value of 3 mm and 0.25 mm, respectively. The Brazilian disks were tested with crack orientations ranging between 0 to 75˚ and were tested under diametrical compression.. The crack to radius (a/R) ratio and thickness to diameter (B/D) ratio were chosen as 0.3 and 0.23, respectively (Figure 3.10).

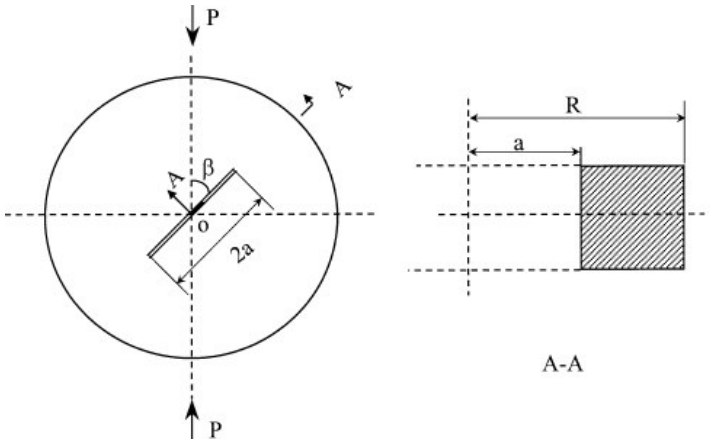

Figure 3.10 SNBD under diametrical compression (Khan and Al-Shayea, 2000)

SNBD were also used to study the effect of crack size on mixed Mode I-II fracture toughness. The diameter and thickness (*D* and *B*) of the disks were 84 and 19 mm, respectively. The two normalized crack sizes (i.e., *a/R*) used in this investigation were 0.3 and 0.4.

3.5 SNSCB Specimens

SNSCB technique was advocated by Lim et al. (1994). SNSCB specimen is obtained from a half disc. A straight notch is cut into half disc. Fracture toughness is determined from an equation which depends on a numerical constant, normalized stress intensity factor. SNSCB specimen is used for Mode I, Mode II and mixed mode studies.

3.5.1 Specimen Preparation and Testing Equipment

Cores are obtained from the rock blocks and they are sliced into circular disks, using a high-speed diamond plated rotary saw. The sliced disks are polished to ensure uniform thickness. Then the disks are cut along the diameter into two equal halves. A radial line is marked at the required orientation with respect to the loading direction.

A notch of any required length is then made along this marked line by using a wire saw. It was difficult to machine a crack at an angle greater than 60˚ (Figure 3.11).

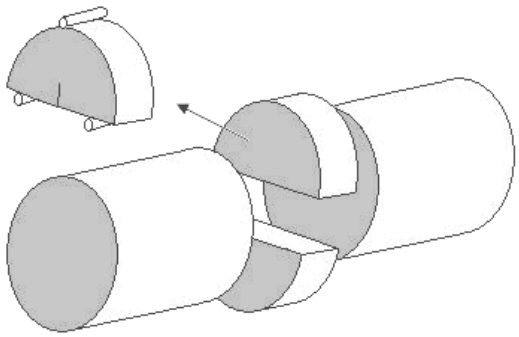

Figure 3.11 SNSCB Specimens

A strain-controlled loading frame is used for the load application. The applied load, load point displacement, and crack opening are acquired using a computerized data logger (Figure 3.12).

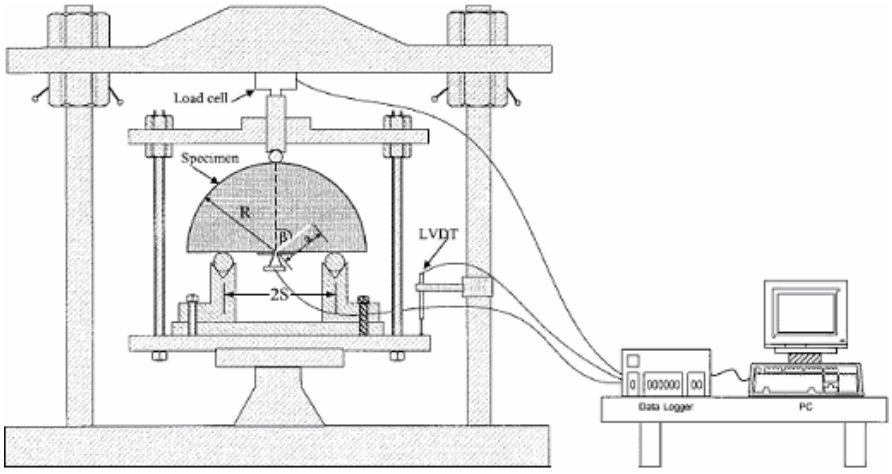

Figure 3.12 Loading setup for fracture testing on SNSCB specimen (Khan and Al-Shayea, 2000)

3.5.2 Fracture Toughness Determination

To estimate fracture toughness in Mode I, firstly, normalized stress intensity factor is calculated with Equation 3.7. The stress intensity factor in the equation is achieved by using numerical methods.

$$Y_I = \frac{K_I}{\sigma_0 \sqrt{\pi a}} \tag{3.7}$$

where,

Y_I = normalized stress intensity factor

K_I = stress intensity factor

a = notch or crack length

$\sigma_0 = \frac{P}{2RB}$

P = failure load

R = specimen radius

B = specimen thickness

By using same equation fracture toughness is calculated with experimental data and normalized stress intensity factor calculated by numerical results.

3.5.3 Related Studies

In the study of Khan and Al-Shayea (2000), rock blocks were collected from a limestone rock formation outcropping in the Central Province of Saudi Arabia. In the experiments of SNSCB, core diameter was 98 mm, core thickness was 22 mm, and wire saw used in the experiment had a thickness of 0.25 mm. The semi-circular specimens were tested with notch orientations between 0 to 60˚ and tested under a three point bend loading configuration with a span to radius ratio (S/R) of 0.8 (Figure 3.13). The notch to radius ratio (*a*/*R*) of 0.3 was used.

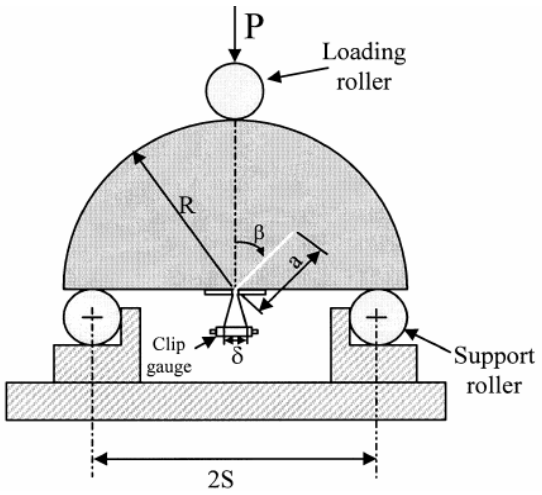

Figure 3.13 A semi-circular specimen containing an angled edge crack under three-point-bending (Khan and Al-Shayea, 2000)

3.6 PTS Tests

PTS method was proposed by Backers et al. (2002) to compute fracture toughness in Mode II. In PTS test, circular notches are cut in both and of the specimen. Fracture toughness is calculated by using a mathematical expression. The displacement gradient at the notch tip in the equation is determined from FEM analysis.

3.6.1 Specimen Preparation and Testing Equipment

Cylindrical samples are cut to length equal to diameter. End surfaces are polished perpendicular to the lateral surface. Circular notches are drilled at both ends leaving an intact portion in the centre of the core. The inner part is punched down while a confining pressure acts perpendicular on the sample surface (Figure 3.14).

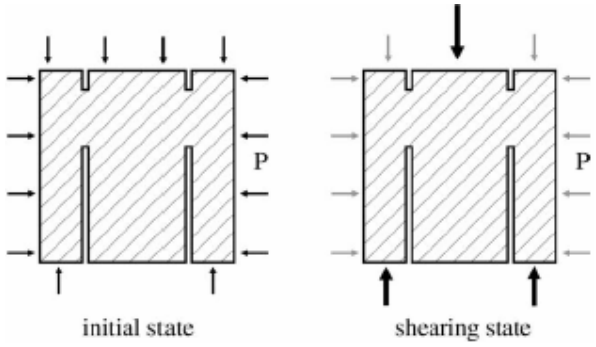

Figure 3.14 Axial stress and confining pressure applied in PTS test (Backers et al., 2002)

3.6.2 Fracture Toughness Determination

Fracture toughness in Mode II is calculated from Equation 3.8.

$$K_{IIC} = \frac{1}{2}\left(\frac{dv}{dy} + \frac{du}{dx}\right)\frac{E}{2(1+\upsilon)}\sqrt{\pi c} \tag{3.8}$$

where

K_{IIC} = fracture toughness in Mode II

c = initial crack length (is assumed to be equal to the notch width, *t*)

$\frac{dv}{dy}, \frac{du}{dx}$ = gradients of the displacements *v* and *u* in *x* and *y* directions (Figure 3.15)

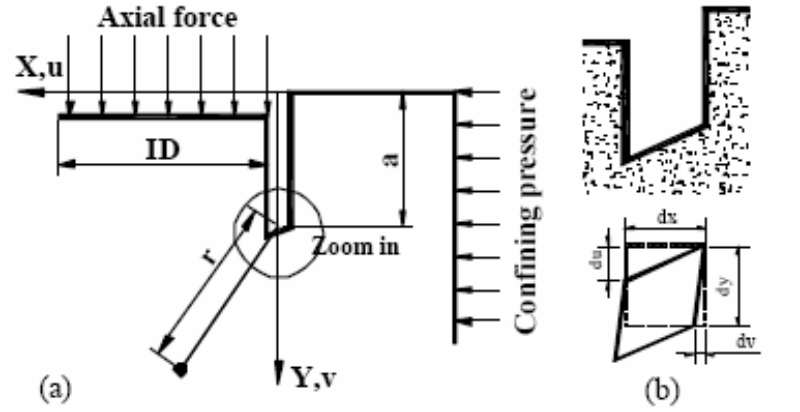

Figure 3.15 (a) Geometry and nomenclatures around the notch tip (b) when deformed

3.6.3 Related Studies

Yoon and Jeon (2004) applied PTS test to Daejeon granite. A rock core of 52 mm in diameter was cut into pieces with length equal to the diameter. The depth of upper notch was 5 mm. The bottom notch depth of 7, 17, and 27 mm was drilled. Typical specimen geometry for the test and its dimensions are shown in Figure 3.16.

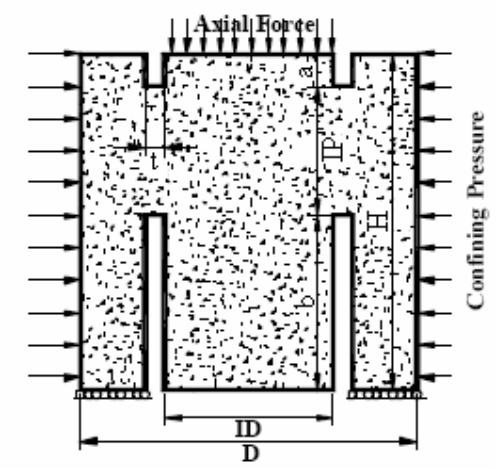

Figure 3.16 PTS Sample Dimensions (Yoon and Jeon, 2004)

Table 3.4 PTS Specimen dimensions

Description	Value (mm)
Height, H	52
Diameter, D	52
Upper notch depth, a	5
Bottom notch depth, b	7, 17, 27
Notch width, t	3
Inner diameter, ID	26
Intact portion, IP	20, 30, 40

Rüdersdof limestone, Carrara marble and Aue granite were used in the study of Backers et al. (2002). The sample geometry, the principle loading and its dimension were given in Figure 3.17.

Six rock types with different mineral content and grain sizes were used in the Backers et al. (2004). The rock types are briefly characterized in Table 3.5. The sample geometry, the principle loading and its dimension were given in Figure 3.17.

Table 3.5 Compilation of selected rock properties of the six rock types

Rock Type	σ_c MPa	σ_T MPa	E GPa	υ
Äspö diorite	219±15	15±1	68±8	0.24
Aue granite	134±7	8±1	48±8	0.19
Mizunami granite	166±35	9±2	50±8	0.37
Carrara marble	101±6	~7	49	0.23
Flectingen sst.	96±13	6±1	21±5	0.12
Rüdersdorf lim.	40	5±1	22	0.22

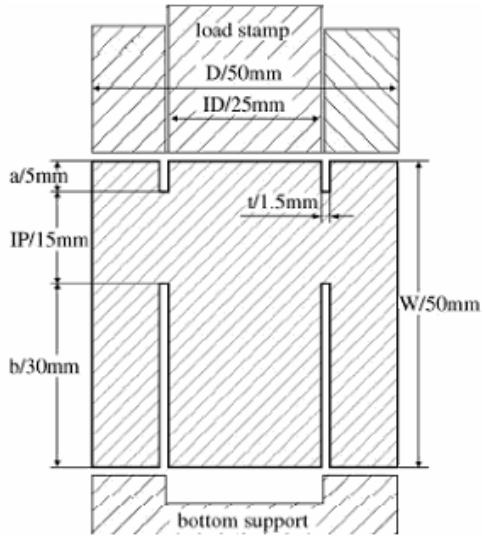

Figure 3.17 Sample geometry and loading set-up for the PTS-Test (Backers et al., 2002 and 2004)

3.7 Conclusions on the Related Studies

Sousa and Bittencourt (2001) concluded that fracture toughness of SR specimens was influenced by the increase in the water/cement ratio and by the increase in the aggregate size in inversely.

Backers (2003) drew a conclusion with his studies on CB specimens that the influence of the loading rate on Mode I fracture toughness of the sandstone was negligible.

Khan and Al-Shayea (2000) used SCB specimens under three-point-bending and Brazilian disk specimens under diametrical compression in their mixed mode I-II study to investigate the effect of testing method and specimen geometry such as diameter, thickness, and crack length and type on measured fracture toughness. The results show that specimen diameter and crack type have a substantial influence on the measured fracture toughness; however, loading rate, crack size, and specimen thickness seem to have a negligible effect on the fracture toughness. Mode I fracture toughness is significantly influenced by specimen diameter and crack type, while their effects on Mode II fracture toughness are generally negligible. The different specimens (Brazilian disc, and semicircular) can give comparable results only when

the proper span to diameter ratio is used. The Brazilian disc with a straight notch was found to be the most convenient geometry to use for fracture toughness determination.

In the study of Chang et al. (2002), rock fracture toughness under mixed-mode conditions was measured by using the straight through crack assumption (STCA) applied to the CNBD specimen and SCB specimen. Size effects, in terms of specimen thickness, diameter and notch length on fracture toughness, were investigated.

The CNBD specimen can be used to measure mixed-mode and mode II fracture toughness values by the STCA method. It is also unnecessary to perform precracking for the CNBD specimen because it uses a chevron notch which induces self-precracking during testing and leads to a stable crack propagation. As a result, it is concluded that the CNBD specimen is the most preferable and versatile among disc-type specimens used in this study.

Krishnan et al. (1997) pointed out the SNBD specimen is the most convenient configuration when the soft sand stone is considered since the SNBD specimen configuration permits the use of the same setup and conditions for mode I, mode II and mixed mode I-II testing with fewer preparations than other type of tests. Also the effect of anisotropy and bedding planes in fracture toughness can be evaluated easily by orienting the notch with respect to the area of interest (e.g. bedding planes).

According to Yoon and Jeon (2004), and Backers et al. (2004), PTS test is the most promising method for determination of Mode II fracture toughness. In the study of Yoon and Jeon (2004), relation between the Mode II fracture toughness and confining pressure was found to be proportional; Mode II fracture toughness increases with the increasing confining pressure. Moreover, numerical analyses revealed that maximum shear stress is concentrated at the upper inner notch tip and bottom outer notch tip. Crack occurred in this region of high shear stress are predominantly occurred in Mode II.

CHAPTER 4

NUMERICAL MODELING FOR ESTIMATION OF STRESS INTENSITY FACTORS

In order to calculate stress intensity factors of the samples with different geometries, numerical computations were carried out. The package programs used in this study were ABAQUS, ANSYS, FRANC2D/L and FRANC3D. Disc type specimens require 3D modeling for stress analysis and stress intensity factor computations. For 3D modeling a choice had to be done among ABAQUS, ANSYS and FRANC3D. In the verification trials, among these the most user friendly package was found to be ABAQUS due to the ease in learning and running applications with the program. To decide if this program produces accurate results for stress intensity factor calculations comparable to the result of other packages, simple models with known analytical results for model verification were first employed. After verification studies, the program was decided to be appropriate for further stress intensity factor computations.

4.1 Package Programs

4.1.1 ABAQUS

ABAQUS is a finite element (FE) program used for stress, heat transfer, and other types of analysis in structural, mechanical, civil, biomedical, and related engineering applications. It was developed by Habbitt, Karlson and Sorensen, Inc. (HKS) in 1978. ABAQUS Version 6.5 was leased by METU is used in modeling work here.

Two dimensional and three dimensional fracture analyses can be performed with ABAQUS. ABAQUS uses J-Integral method to compute stress intensity factors.

4.1.2 ANSYS

ANSYS is a FE software used to model problems in structures, thermal flow, fluid flow and electromagnetic. ANSYS was developed and is supported by ANSYS, Inc. Licensed ANSYS Version 9.2 was used in modeling verification example here.

Although two dimensional and three dimensional fracture modeling can be conducted with ANSYS, three dimensional modeling is difficult due to the structure of the programming part of the ANSYS package. To compute stress intensity factors, J-Integral method and displacement correlation technique are available in ANSYS.

4.1.3 FRANC2D/L

FRANC2D/L (FRacture ANalysis Code for 2D), which is finite element program, is a two dimensional crack propagation simulator. It was originally developed by Paul Wawrzynek at Cornell University and also the recent additions and expansions of the program were conducted at Cornell University. FRANC2D Version 3.1 is available for free downloading in Cornell Fracture Groups websites.

FRANC2D/L is used with CASCA program. CASCA is used to build initial mesh of the model. After building initial mesh with CASCA, crack is defined in FRANC2D/L program and this program computes the stress intensity factors. There are three techniques for estimating stress intensity factors in the program which are displacement correlation technique, J-integral technique and modified crack closure integral technique.

4.1.4 FRANC3D

FRANC3D (FRacture ANalysis Code for 3D) developed by Cornell Fracture Group since 1987 is a hybrid software that combine solid modeling, mesh generation and

fracture mechanics for nucleating and propagating cracks in the model geometry. In this program, Stress intensity factors are computed using the displacement correlation technique for all cases (Chan et al., 1970).

FRANC3D is neither a boundary nor a finite element analysis code, although it is capable of writing input files for a variety of commercial BEM (boundary element method) and FEM (finite element method) codes like ANSYS and ABAQUS. FRANC3D Version 3.0 is available for free downloading in Cornell Fracture Groups websites.

Before using FRANC3D, in order to form solid model firstly OSM (Object Solid Modeler) program was used. In this study, BES analysis part of the program was used for stress analysis and to compute stress intensity factors.

4.2 Verification Example

In order to compute stress intensity factor of a model, plate with a single, flat, part-through edge crack was selected as an example. The dimensions and geometry of the model were given in Figure 4.1 and Table 4.1. The example was taken from ANSYS Tutorial.

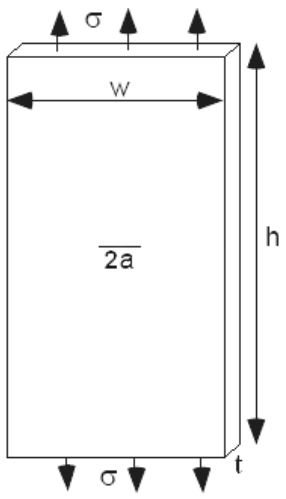

Figure 4.1 Single edge crack model under tension

Table 4.1 Dimensions and mechanical properties of the single edge crack model

Dimensions and Properties	Values
Width of the plate, *w*	0.2 m
Height of the plate, *h*	0.2 m
Thickness of the plate, *t*	0.003 m
Crack length of the plate, *a*	0.02 m
Load on the plate in tension, σ	100 MPa
Young's modulus, *E*	200 GPa
Poisson's ratio, υ	0.3

4.2.1 Analytical Calculation of Stress Intensity Factor

Analytical solution for stress intensity factor in mode I for this example is given in Equation 4.1.The Equation 4.1 was driven by Pilkey (1994).

$$K_I = \sigma\sqrt{\pi a} \times F_I(\alpha) \tag{4.1}$$

The correction factor is:

$$\alpha = \frac{a}{w}$$

$$F_I(\alpha) = \left(1 - 0.1\alpha^2 + 0.96\alpha^4\right)\sqrt{1/\cos(\pi\alpha)}$$

For the example above, by using Equation 4.1, K_I was found as $25.680\,\text{MPa}\sqrt{\text{m}}$.

4.2.2 Numerical Calculations of Stress Intensity Factor

For this verification example in order to simplify the model by taking advantage of the symmetry conditions, the analyses were performed on one half of the model in ABAQUS (for 2D and 3D applications), ANSYS (for 2D application), FRANC2D/L and FRANC3D programs, and one quarter of the model in ANSYS (for 3D application) program. For half models because of the symmetry on x-direction, model was fixed there on x-direction. In order to prevent body motion, the model was fixed also in y-direction from the right edge center of the model. Moreover, since the analytical equation is valid for plane strain condition, the three-dimensional model boundaries perpendicular to z-direction were fixed to generate an equivalent model to the plane strain models (Figure 4.2). For quarter model, in

addition to boundary conditions above, bottom boundary of the quarter part was fixed in y-direction except crack front to allow movements along the crack. For comparison all models are shown together in Figure 4.3.

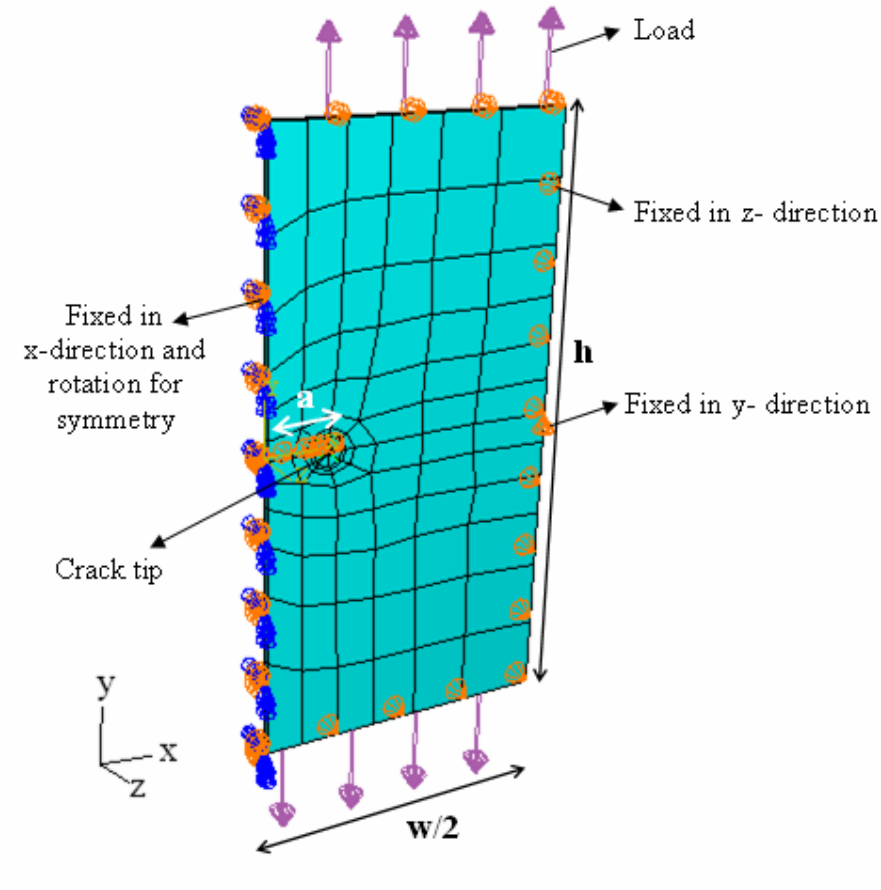

Figure 4.2 Boundary conditions and mesh of an example model

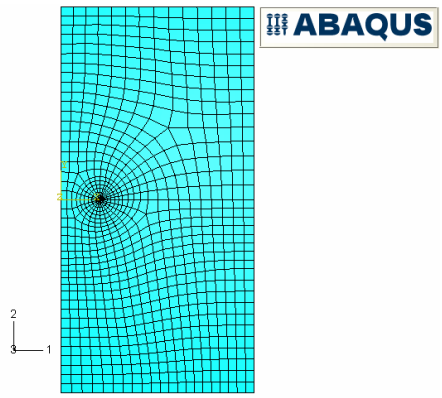

2D model in ABAQUS program

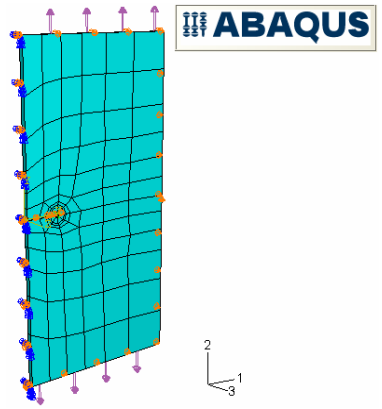

3D model in ABAQUS program

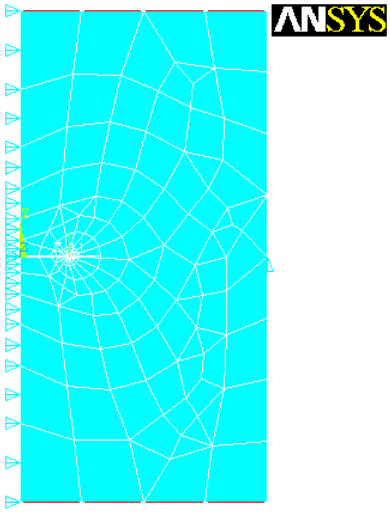

2D model in ANSYS program

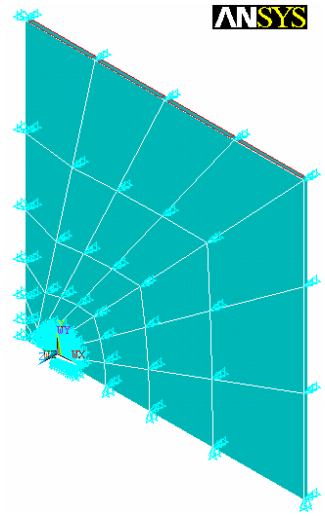

3D model in ANSYS program

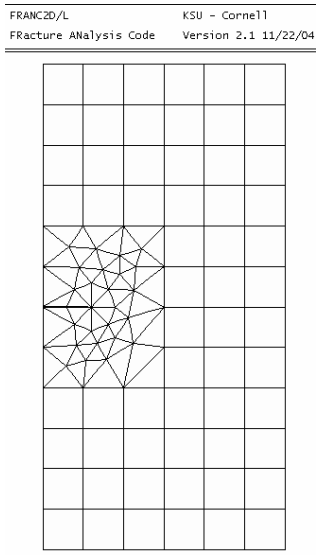

2D model in FRANC2D/L program

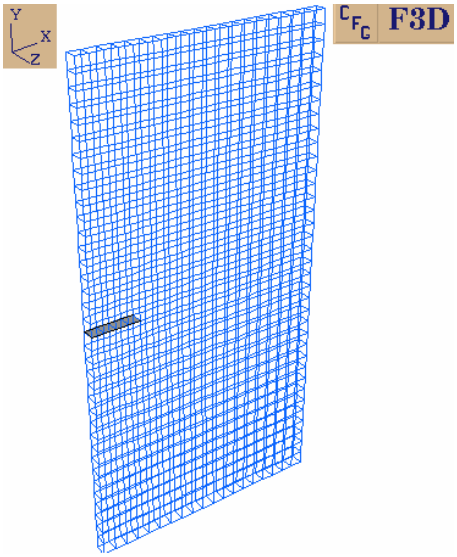

3D model in FRANC3D program

Figure 4.3 Central crack plate model with different programs

To compute the stress intensity factor of the verification example, ABAQUS, ANSYS, FRANC2D/L and FRANC3D programs were used. Computed K_I values at the crack tips were compared in Table 4.2. In the table, percentage error was calculated from Equation 4.2.

$$\text{Error}\ (\%) = \frac{K_{comp} - K_{anal}}{K_{anal}} \times 100\% \tag{4.2}$$

where,

K_{anal} = analytical solution for the stress intensity factor

K_{comp} = computed stress intensity factor

Since the mesh densities and number of nodes are different for the model plate of each program, it is not possible to reach an exact conclusion about accuracy of a single program. As seen from the Table 4.2 all programs produced almost the same results. ABAQUS produced a value with a little error of 2.282% although the mesh intensity used was not as intensive as the ANSYS 3D quarter model.

Table 4.2 Comparison of the K_I results

	K_I (MPa$\sqrt{\text{m}}$)	Error (%)
Pilkey's Solution	25.6800	
Numerical Results		
ABAQUS (2D)	26.4542	3.015
ABAQUS (3D)	25.0939	2.282
ANSYS (2D)	26.5770	3.493
ANSYS (3D)	25.3580	1.254
FRANC2D/L	26.6800	3.894
FRANC3D	24.9586	2.809

3D modeling was necessary for the disc type specimens used in the experimental studies, therefore, in numerical modeling two-dimensional plane strain programs like ABAQUS, ANSYS2D and FRANC2D/L.

In ANSYS program, a macro has to be written to model crack opening and to find the stress intensity factor at the crack tip. Because of the difficulties in writing macros, ANSYS program was not preferred in 3D analysis.

Although FRANC3D is more user friendly than ANSYS and produced a reasonably accurate result, the input procedure for this program is time consuming and takes more effort in generating different specimen geometries with varying notch and span lengths. In addition, displacement correlation technique used by FRANC3D to compute stress intensity factors usually generate less accurate results as mentioned before in Chapter 2.

In consequence, ABAQUS software was preferred to use for stress and fracture analysis of the disc type specimens used in the experiments.

4.3 ABAQUS Software

ABAQUS program was written and maintained by Hibbitt, Karlsson and Sorensen, Inc (HKS). The company was established in 1978, and today has several hundred employees with offices around the world. In Turkey ABAQUS office is in Istanbul and the company name is 'A to Z Advanced Engineering Technologies' (A-Ztech Ltd.).

4.3.1 ABAQUS Capabilities

ABAQUS, as mentioned before, is a highly sophisticated, general purpose finite element program. ABAQUS includes:

- Capabilities for both static and dynamic problems,

- The ability to model very large shape changes in solids, in both two and three dimensions,

- A very extensive element library, including a full set of continuum elements, beam elements, shell and plate elements, among others.

- A sophisticated capability to model contact between solids

- An advanced material library, including the usual elastic and elastic – plastic solids; models for foams, concrete, soils, piezoelectric materials, and many others.

- Capabilities to model a number of phenomena of interest, including vibrations, coupled fluid/structure interactions, acoustics, buckling problems, and so on (Brown University, 2001).

4.3.2 ABAQUS Modules

ABAQUS is a very user friendly program. In order to define the geometry and other physical properties of the model and then to submit the model for analysis, several different modules are used step by step in the program as following.

4.3.2.1 Part Module

Part module is used to create, edit, and manage the parts in the current model. Part module has ability to create deformable, discrete rigid or analytical rigid parts. Solids, shells, wires, cuts, and rounds can be drawn by part module.

4.3.2.2 Property Module

Property module is briefly used to define material properties of the model and assign this property to model.

4.3.2.3 Assembly Module

Assembly module is basically used to create part instances and position them relative to each other in a global coordinate system.

4.3.2.4 Step Module

Step module is used to perform a sequence of one or more analysis steps. The sequence of steps provides a convenient way to capture changes in the loading and boundary conditions of the model. Step module also has an ability to specify output

requests. For instance, in fracture mechanics applications, to obtain stress intensity factor data at the end of the analysis, a history output request is defined in step module.

Under the menu options of step module J-Integral and stress intensity factor computation options are available. Maximum tangential stress criterion, maximum strain energy release rate criterion or $K_{II} = 0$ criterion can be selected to calculate the crack propagation direction at initiation. Calculation of contour integrals for the evaluation of the J-integral and the stress intensity factors is carried out in a region surrounded by a number of contours specified by the user. Stress intensity factors are computed for the elements in the chosen contour region around the notch tip. Then user can request an averaging of the stress intensity factors in the chosen region to end up one single accurate value for the particular notch tip.

4.3.2.5 Interaction Module

Interaction module is used to satisfy mechanical and thermal interactions between regions of a model, connections between two points of a model or between a point of a model and ground. Moreover, springs and dashpots between two points of a model or between a point of a model and ground are applied by interaction module. Furthermore, to define a crack in a region interaction module is used. Crack can be defined in two ways one is sharp crack that is also called seam and the other is blunted crack.

4.3.2.6 Load Module

Loads and boundary conditions are defined by considering step module in Load module.

4.3.2.7 Mesh Module

The Mesh module is used to generate meshes on parts and assemblies of the model. Mesh attributes such as seeds, mesh techniques, and element types are determined in mesh module. In fracture tests, crack tips cause stress concentrations and stress

and strain gradients are large as a crack tip is approached. Therefore, to get accurate stresses and strains, the finite element mesh must be refined in the vicinity of the crack tip.

4.3.2.8 Job Module

Job module is used to submit the analysis for processing. During process, job module can monitor progress of the process. Job module starts the Visualization module.

4.3.2.9 Visualization Module

Visualization module finally shows the results of the analysis in terms of deformed shapes, contours, symbols, animations, and graphs.

4.4 Stress Intensity Factor Computation for SCB

Semi-circular bend specimen with a straight edge notch was modeled by using ABAQUS program. Specimen geometry was changed by using different notch sizes (a/R) and span lengths (S/R). Mesh refinement studies were carried out to obtain a better accuracy for the estimation of stress intensity factor. Stress intensity factors for different specimen geometries were computed and compared to the work of other researchers.

4.4.1 Geometry, Boundary Conditions and Crack Modeling

The radius and thickness of all SCB specimens modeled were 50 mm. Various notch lengths (5, 10, 15, 20, 25, 30.5, 33.5 and 40 mm) and different span lengths (25, 30, 35 and 40 mm) were studied to study the effects of normalized notch length (a/R) and normalized span length (S/R) on stress intensity factor, respectively. Model geometry is in Figure 4.4.

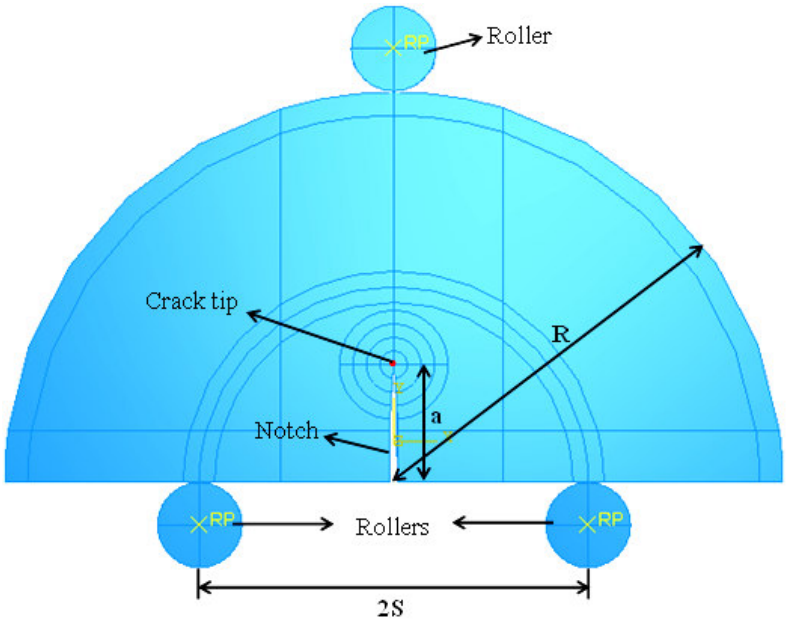

Figure 4.4 SCB Geometry

Two boundary condition options were tried in the models for the application of vertical load: (i) a unit negative vertical load (F_y = -1 N) is applied on the top roller where bottom roller supports and their rotations (R_x, R_y and R_z) are kept fixed in all directions which means that the contact points of the bottom boundary of the specimen model is fixed in vertical y-direction, (Figure 4.5-a). (ii) half of the unit load P/2 (F_y = +0.5 N) is applied to each of the bottom roller supports and the top roller support and its rotations are fixed in all directions which means that upper contact point of the specimen model remains fixed in y-direction (Figure 4.5-b). For all cases roller support material is modeled as analytical rigid.

Application of the boundary conditions and 3D ABAQUS model appearance are presented in Figure 4.6. In the figure fixed directions were indicated with orange triangles, fixed rotations were symbolized with blue triangles and load was represented with yellow arrow.

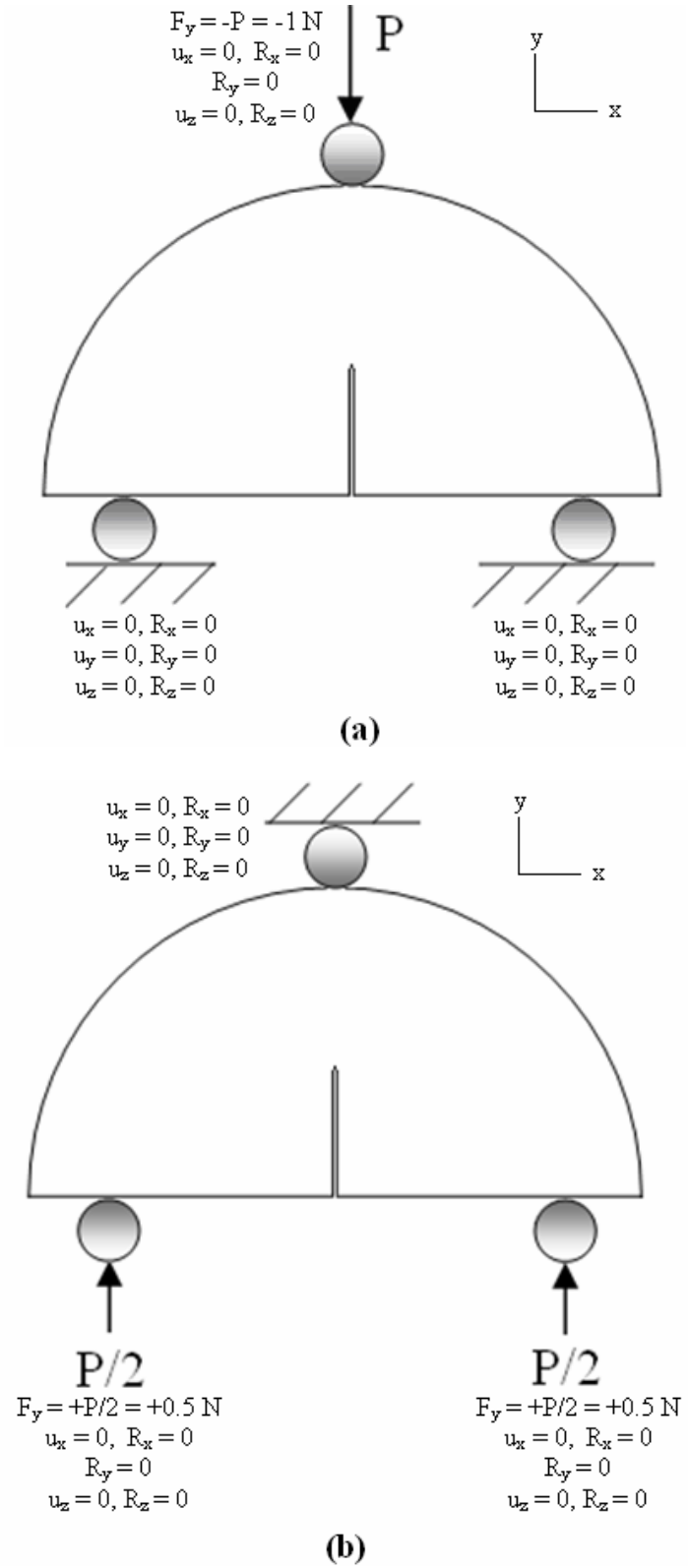

Figure 4.5 Boundary conditions of two loading options

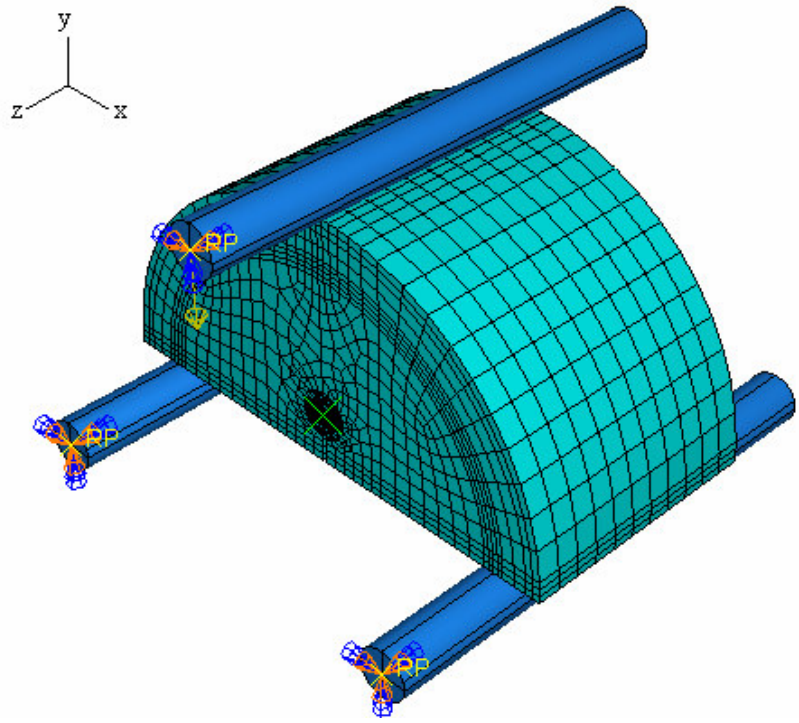

Figure 4.6 Boundary Conditions on the 3D ABAQUS model of SCB specimen

For one typical semi-circular specimen model, stress analysis was done and stress intensity factor was computed for two boundary condition options. The details of comparisons and results are illustrated in "4.4.2 Confirmation of Stress Analysis Results" part in Figure 4.8-Figure 4.12. Results showed that stress analysis results and stress intensity factor (found as 160.819 for SCB model) for both boundary loading options were equal to each other. Similar results were obtained for SNDB model trials. This is due to the same external work done on the boundaries for both loading conditions. Although the model with two load application points at the bottom boundary was similar to the experimental loading conditions, the loading option with a load at the top was used in further modeling work. The reason for this was that with this option, it was possible to make comparisons with previous studies; previous studies such as by Lim et al. (1993), Ayatollahi and Aliha (2004 and 2006), Ayatollahi et al (2006), were always performed by using loading option with a single load application point at the top.

The crack was defined in interaction module. Stress intensity factor can be computed by using contour integral estimates. To perform a contour integral analysis, the crack front and the crack extension direction were selected (Figure 4.7-a). Different crack extension directions can be selected in the module which will yield different combinations of stress intensity factors K_I and K_{II}. In our case crack extends in the vertical direction parallel to the applied load or in the direction of the maximum principle stress. Crack tip loading is supposed to be pure Mode I loading for our specimens. Therefore crack extension direction is attached in the vertical direction to the front of the initial vertical notch.

To construct the FE mesh around the crack front and to control the singularity at the crack tip, a ring of wedge shape elements was assigned to the crack front and surrounding this ring hexahedral elements were used for the remainder of the contour integral region. The ring of wedge shape elements was achieved by using swept meshing technique. In Figure 4.7-a, b, the crack tip is marked with a green "X".

To compute the stress intensity factor, stress intensity factors of contour integral region marked in Figure 4.7-b were calculated and averaged by using history output request menu at the step module.

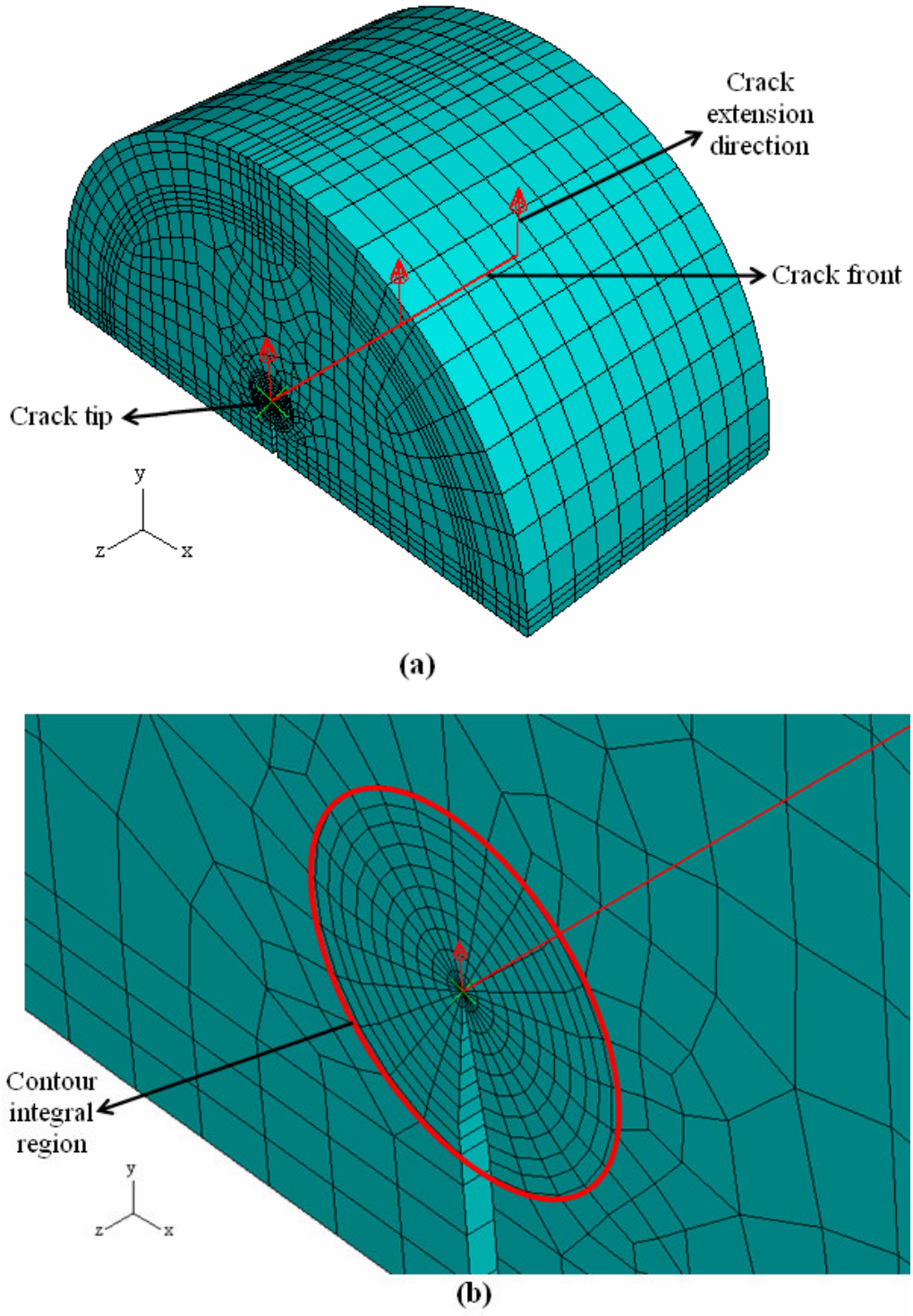

Figure 4.7 Crack front and contour integral region of the SCB model

4.4.2 Confirmation of Stress Analysis Results

Before starting to model different geometries with various notch and span lengths, stress analysis were done for one model with two boundary condition options mentioned above to see the model was working properly or not.

Stress analyses were performed for SCB specimen geometry with normalized notch length (a/R) was equal to 0.2 and normalized span length (S/R) was equal to 0.8. The results after analysis, stresses (σ_{xx} and σ_{yy}) and displacements (u_x and u_y) were obtained for both options. Stress and displacement magnitudes seem to be small because all the modeling work here was conducted by a unit load application of 1 N in order to carry out stress intensity factor analysis in a normalized way. Once stress intensity factors for different specimen geometries are obtained in a normalized way for unit loads, failure load magnitudes obtained from the experiments can be applied easily to these normalized stress intensity factors for the fracture toughness computation in a particular test.

Compression is negative and tension is positive in the program. S11 equals to stress in x-direction (σ_{xx}), S22 shows the stress in y-direction (σ_{yy}), and U1 and U2 represents the horizontal and vertical displacements respectively.

The typical results presented in "(a)" figures are obtained for a boundary load application of 1N to the top roller support whereas the results presented in "(b)" figures are obtained for a boundary load application of 1/2 N to each of the roller supports at the bottom boundary of the specimen.

Figure 4.8 shows the stress distributions in x-direction. As seen from the Figure 4.9, tensile stresses rapidly increase around the crack front.

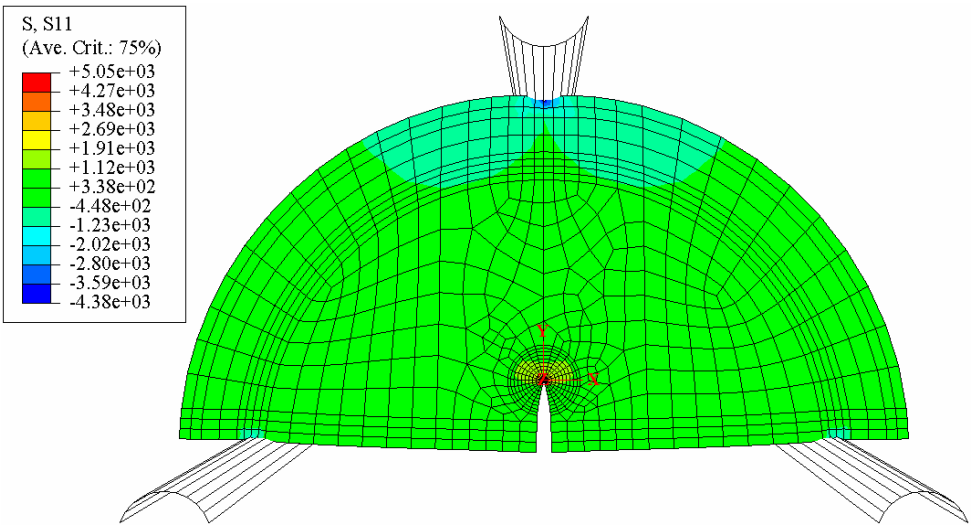

(a) Load application of 1N to the top roller support

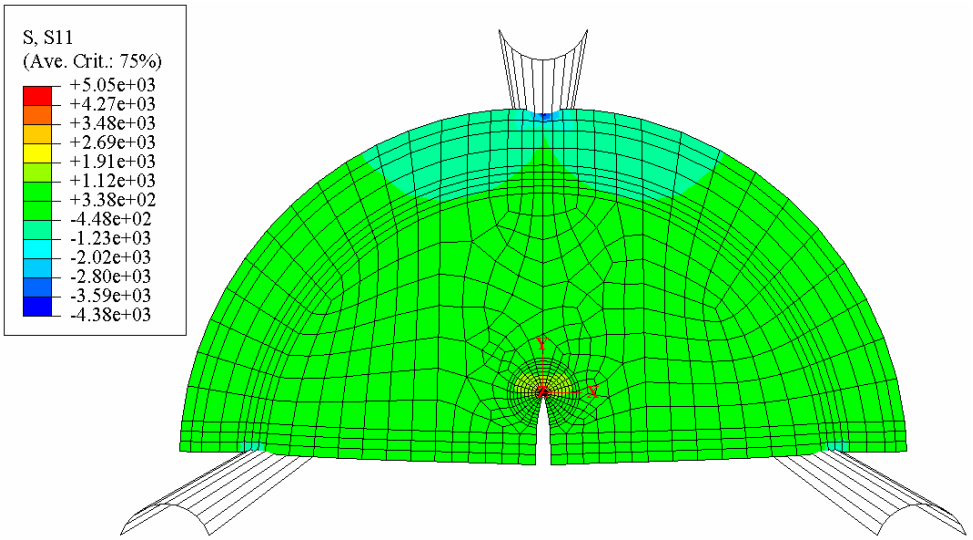

(b) Load application of 1/2 N to the bottom roller supports

Figure 4.8 σ_{xx} contours

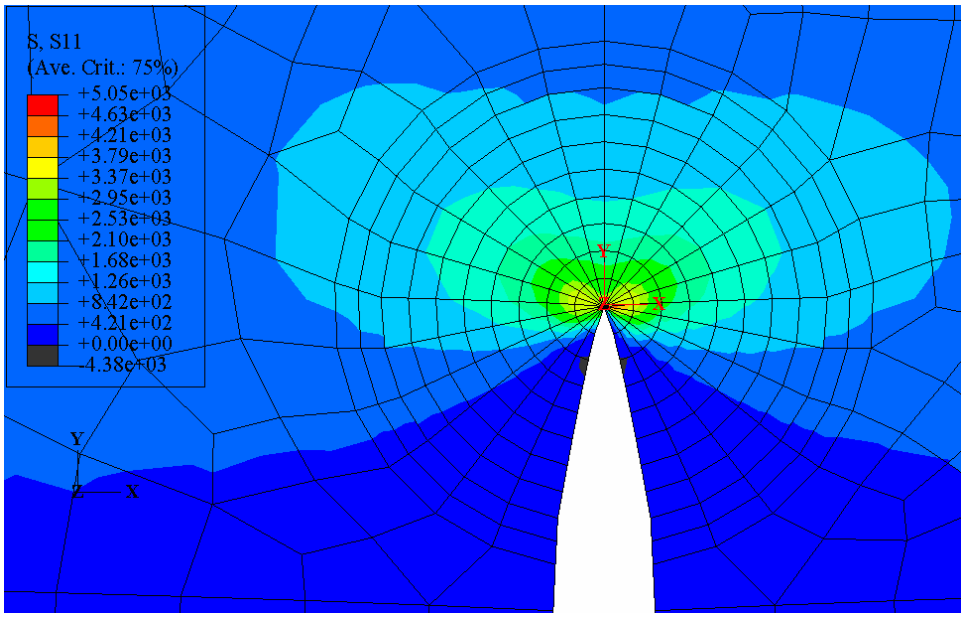

(a) Load application of 1N to the top roller support

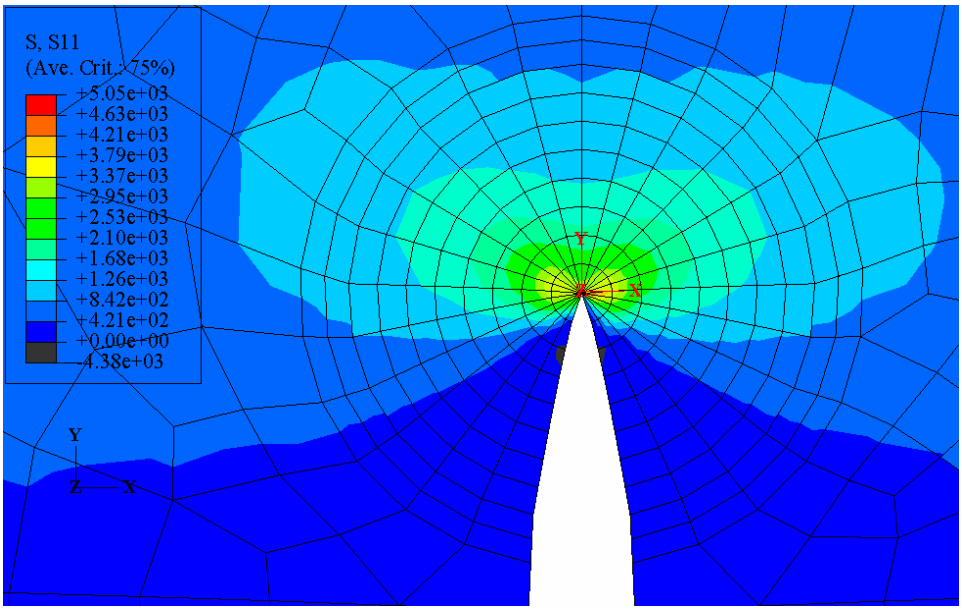

(b) Load application of 1/2 N to the bottom roller supports

Figure 4.9 σ_{xx} contours around the crack tip

Figure 4.10 shows the stress contours in y-direction (σ_{yy}), which was denoted as S22 in the program. As seen from the figure compressive stresses in the specimen model were highly concentrated on at the contact regions of the roller supports.

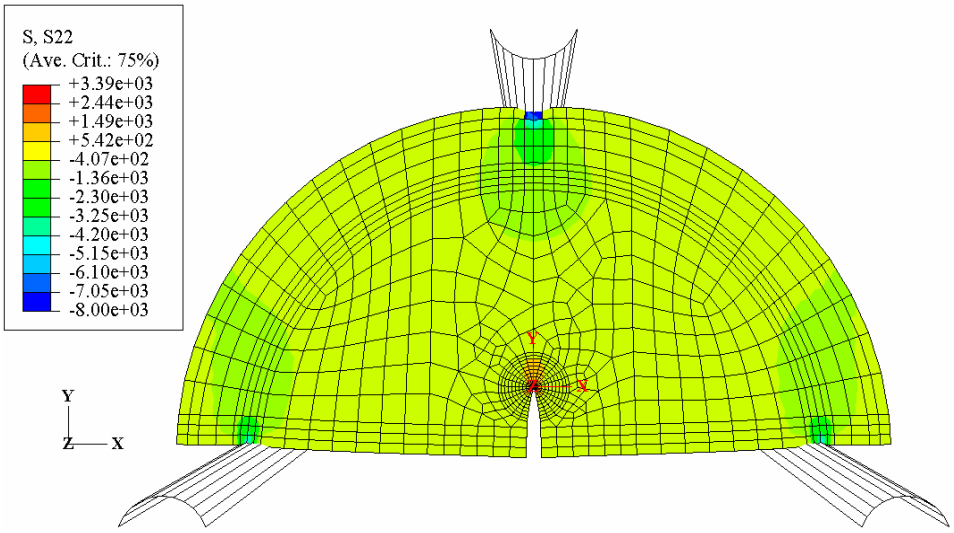

(a) Load application of 1N to the top roller support

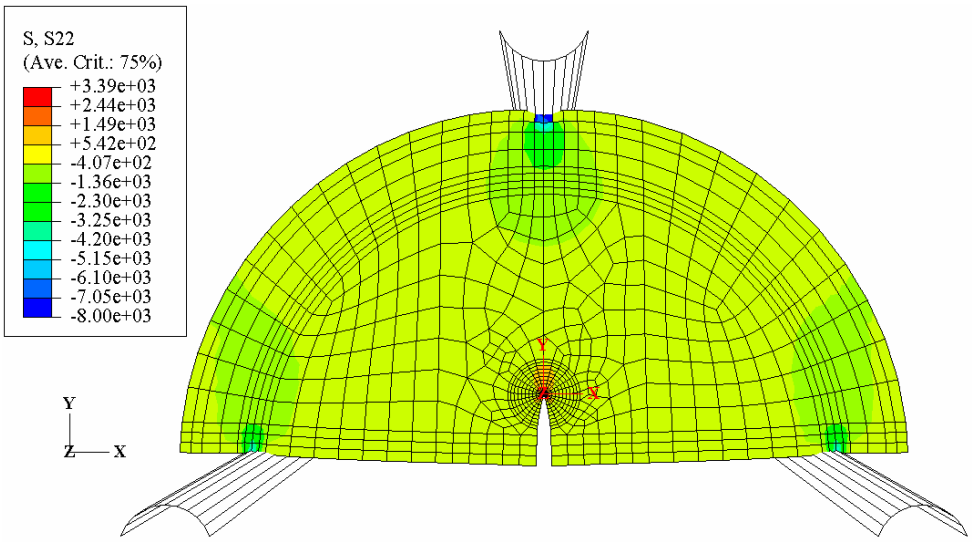

(b) Load application of 1/2 N to the bottom roller supports

Figure 4.10 σ_{yy} contours

In Figure 4.11, x-displacements were illustrated. Deformation in opening mode was seen in x-displacement contours. Figure 4.12 shows y-displacement contours (u_y). It was clearly seen in Figure 4.12-a that the model was loaded by top roller supports and fixed around the two roller supports at the bottom, whereas in Figure 4.12-b, the model was loaded by the two rollers at the bottom and fixed around the top roller support.

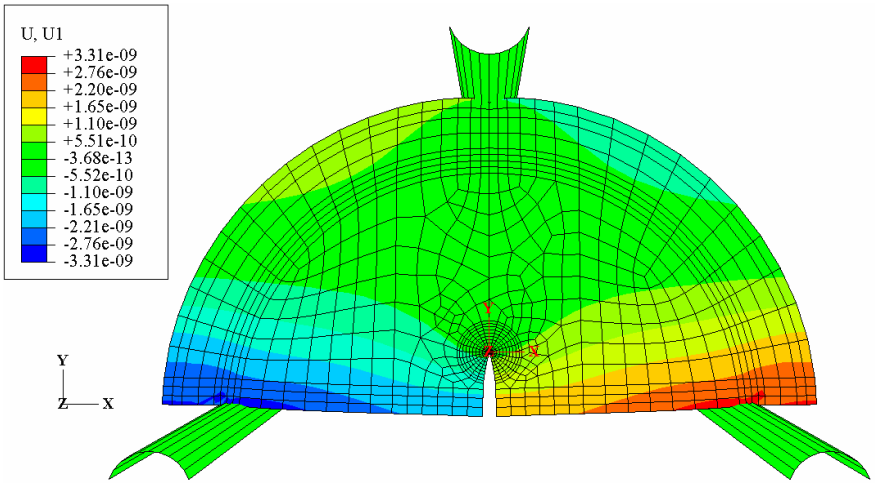

(a) Load application of 1N to the top roller support

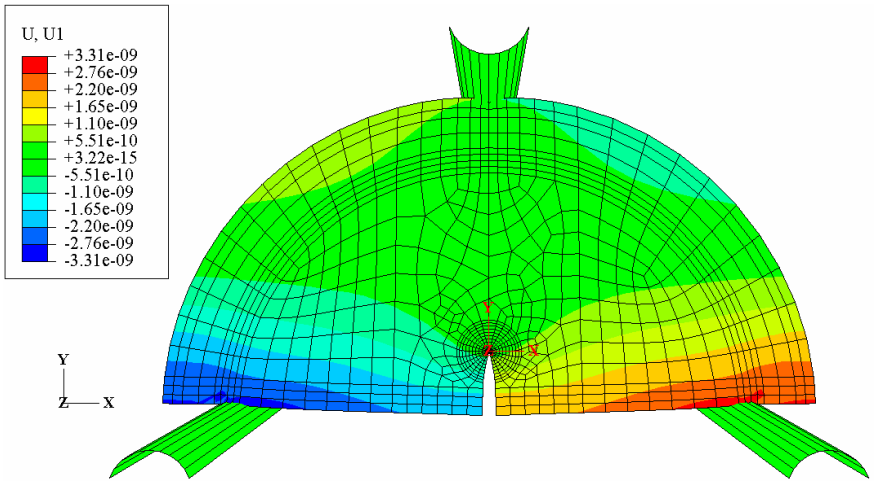

(b) Load application of 1/2 N to the bottom roller supports

Figure 4.11 u_{xx} contours

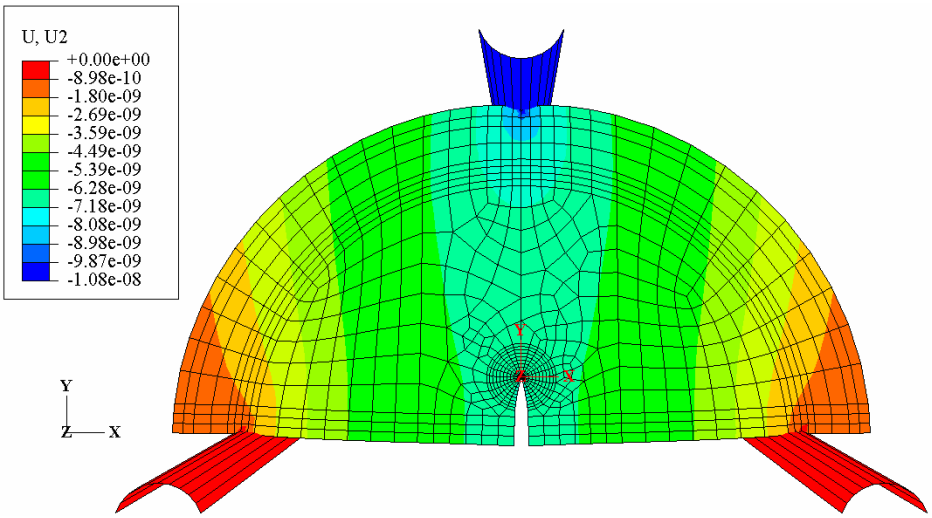

(a) Load application of 1N to the top roller support

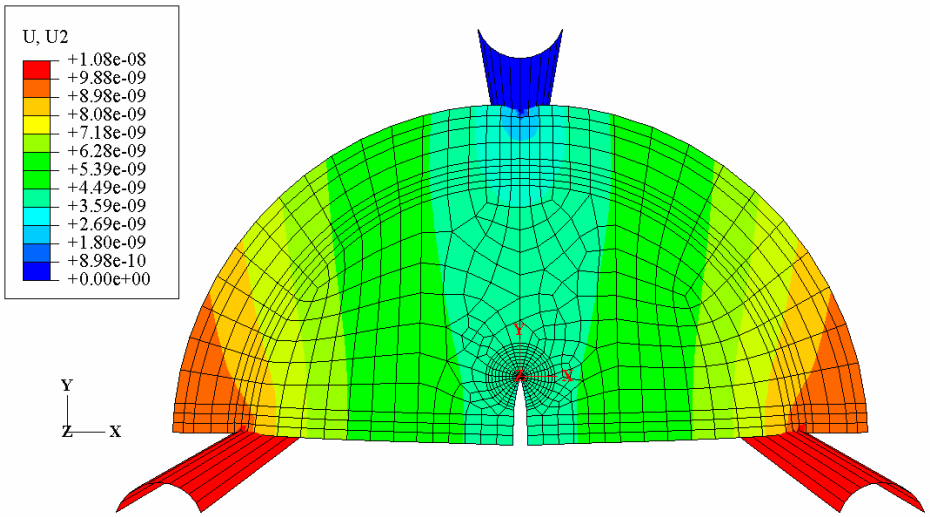

(b) Load application of 1/2 N to the bottom roller supports

Figure 4.12 u_{yy} contours

According to the stress analysis, the results showed that as mentioned above, the both load application condition models were working properly.

4.4.3 Convergence Studies

To figure out the optimum mesh intensity for the SCB technique with a/R = 0.2 and S/R = 0.8, a numerical convergence study was performed. Four mesh densities were examined (Figure 4.13). Mesh intensity around the crack tip was increased instead of increasing other parts to see the mesh intensity effect on stress intensity factor.

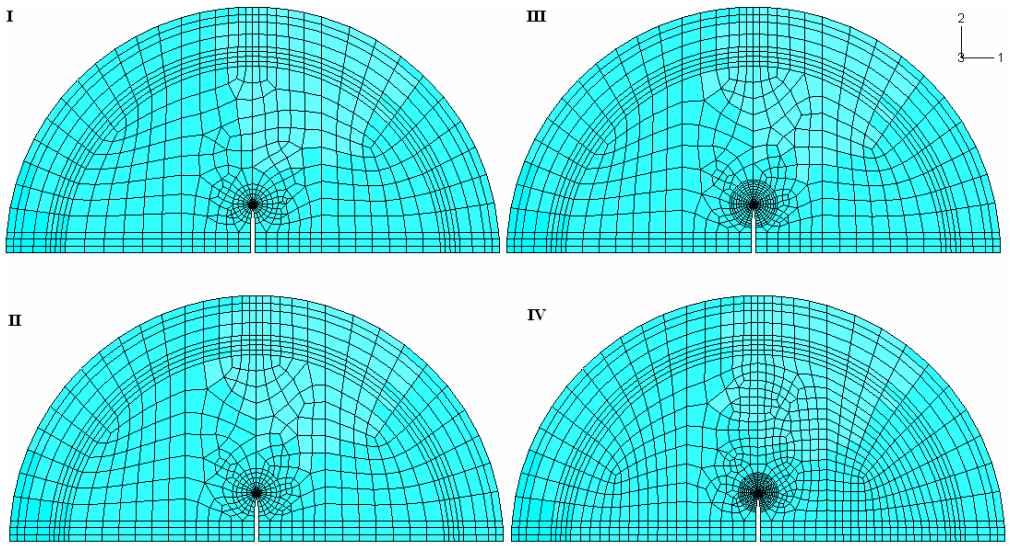

Figure 4.13 SCB finite element meshes
(I) Coarse mesh, (II) Medium mesh, (III) Fine mesh, (IV) Very fine mesh

The results of the analyses were plotted considering normalized stress intensity factor (Y_I) and mesh intensity (Figure 4.14). Normalizing the stress intensity factor, Y_I is carried out according to the other researchers' works (Lim et al., 1994).

$$Y_I = \frac{K_I}{\sigma_0 \sqrt{\pi a}} \tag{4.3}$$

where

K_I = mode I stress intensity factor

$$\sigma_0 = \frac{P}{2RB}$$

P = applied load

R = specimen radius

B = specimen thickness

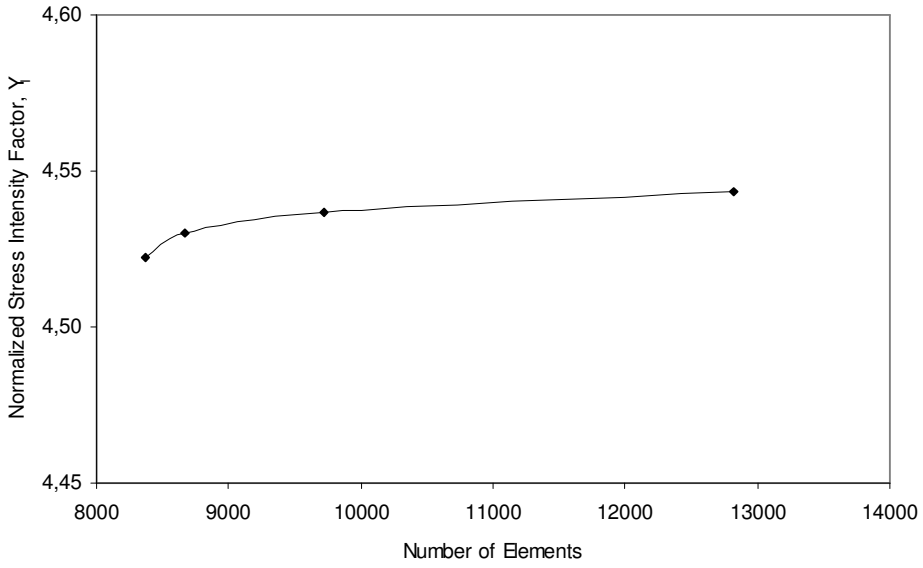

Figure 4.14 Convergence in Y_I with increasing mesh intensity at SCB

The difference in Y_I between the fine and very fine mesh is less than 1.6% therefore fine mesh was employed for the remaining study. Fine mesh was formed with eight rings of elements around the crack front to form the contour integral region in order to compute stress intensity factor.

4.4.4 Comparison with Previous Studies

The numerical results obtained for the Mode I loading with S/R = 0.5, 0.6, 0.7 and 0.8 were depicted in Figure 4.15. The results of Lim et al. (1993) for S/R = 0.5 and 0.8 were found to be in excellent agreement.

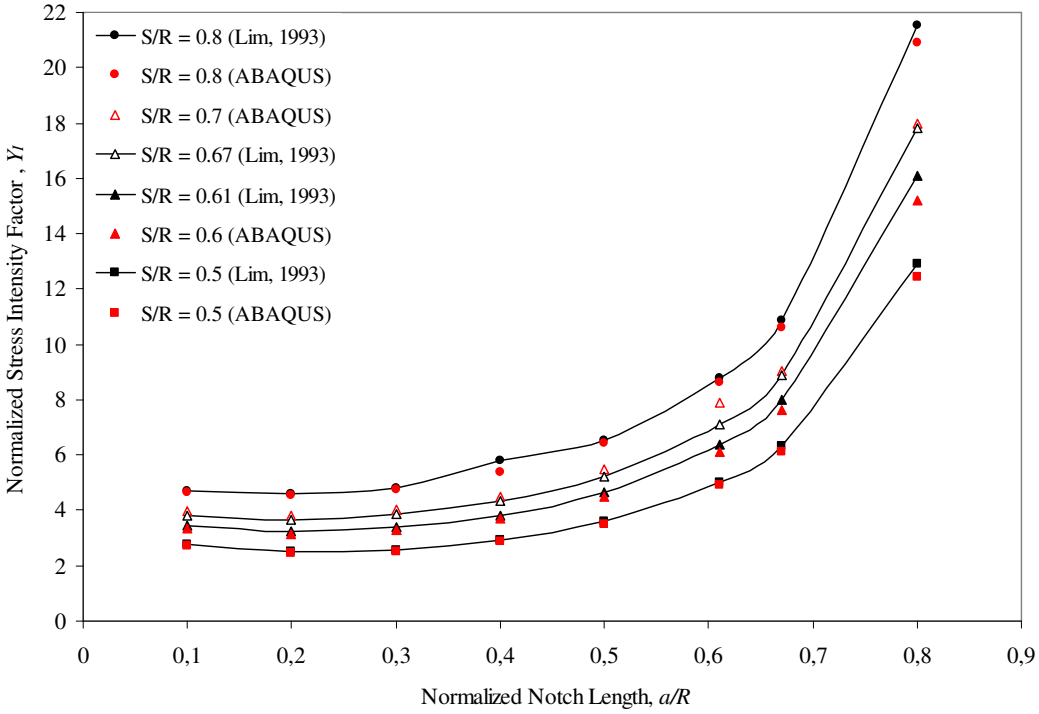

Figure 4.15 Computed normalized mode I stress intensity factor Y_I for SCB

4.4.5 Results

In order to cover a wide range of SCB geometry, a total of 32 different geometries were analyzed for mode I loading. The results according to normalized stress intensity factors (Y_I) were tabulated in Table 4.3.

Table 4.3 Normalized mode I stress intensity factors for the SCB method for various geometries

S/R	a/R							
	0.1	0.2	0.3	0.4	0.5	0.61	0.67	0.8
0.5	2.7233	2.4818	2.5277	2.8513	3.5233	4.8908	6.1372	12.4588
0.6	3.3281	3.3281	3.2688	3.6879	4.4842	6.1119	7.6173	15.2201
0.7	3.9699	3.8314	4.0021	4.5014	5.4707	7.9061	9.0236	17.9979
0.8	4.6284	4.5366	4.7440	5.3696	6.4340	8.6106	10.6175	20.9190

Consequently, as seen from the Table 4.3 the rate of Y_I variation increases as the notch length increases. Moreover, the span length also affects the Y_I. Y_I increases with increasing span length.

By considering Table 4.3, it is possible plot a 3-D graph of Y_I variation depending on a/R and S/R (Figure 4.16).

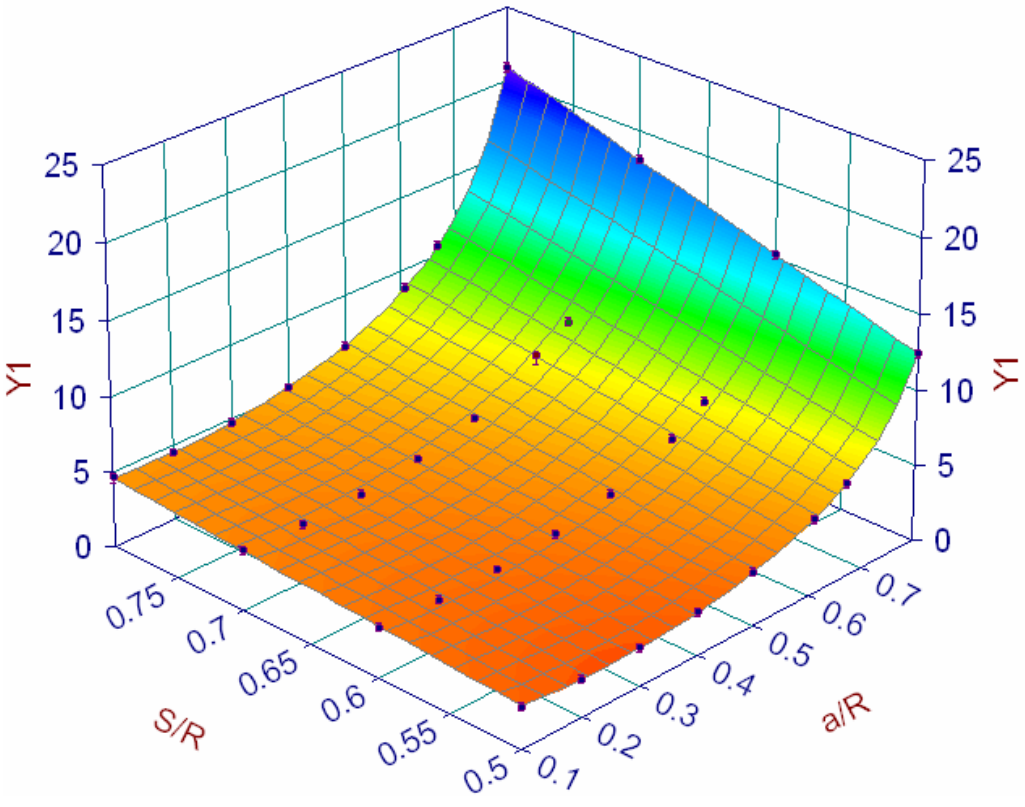

Figure 4.16 3-D Graph of Y_I for different a/R and S/R for SCB technique

With the help of Figure 4.16 and Table 4.3, Y_I values for different notch lengths and span lengths could be calculated. In this study, an equation was achieved to calculate Y_I; the equation developed included the effect of various a/R and S/R ratios together different from Lim's equations where different equations were given for specific span lengths as below.

$$
\begin{aligned}
Y_{I\{0.8\}} &= 4.782 - 1.219\left(\frac{a}{R}\right) + 0.063\exp\left(7.045\left(\frac{a}{R}\right)\right) \quad \text{for } \frac{S_0}{R} = 0.8 \\
Y_{I\{0.67\}} &= 3.638 - 0.139\left(\frac{a}{R}\right) + 0.039\exp\left(7.387\left(\frac{a}{R}\right)\right) \quad \text{for } \frac{S_0}{R} = 0.6 \\
Y_{I\{0.61\}} &= 3.286 - 0.432\left(\frac{a}{R}\right) + 0.039\exp\left(7.282\left(\frac{a}{R}\right)\right) \quad \text{for } \frac{S_0}{R} = 0.6 \\
Y_{I\{0.5\}} &= 2.959 - 2.716\left(\frac{a}{R}\right) + 0.076\exp\left(6.305\left(\frac{a}{R}\right)\right) \quad \text{for } \frac{S_0}{R} = 0.5
\end{aligned}
\tag{4.4}
$$

within the range $0.03 \le a \le 0.8$. For span lengths, that is S_0/R ratios different from the ones above another equation is suggested as below:

$$
\frac{K_I}{\sigma_0\sqrt{(\pi a)}} = Y_{I\{S_0/R\}} + \frac{\Delta S_0}{R}B, \quad 0.5 \le \frac{S_a}{R} \le 0.8 \tag{4.5}
$$

where, according to Lim's notation

S_a/R = actual span ratio employed

S_0/R = the nearest span ratio analyzed in Lim's paper to S_a/R, i.e. S_0/R = 0.5, 0.61, 0.67 or 0.8

$\Delta S_0/R$ = deviation from S_0/R, i.e. $(S_a - S_0)/R$

$Y_{I\{S_0/R\}}$ = normalized stress intensity at a given span ratio S_0/R

B=6.557+16.640$(a/R)^{2.5}$+27.970$(a/R)^{6.5}$+215.084$(a/R)^{16}$, for $0.03 \le a/R \le 0.8$

Instead of using separate expressions a compact formula was derived here. By using TableCurve 3D program and surface fit options, the regression analyses were performed to fit an analytical function to Y_I. As a result the following single equation including the a/R and S/R ratios together was obtained.

$$Y_I = \frac{0.615 - 9.676\left(\frac{a}{R}\right) + 18.904\left(\frac{a}{R}\right)^2 - 9.987\left(\frac{a}{R}\right)^3 + 5.235\left(\frac{S}{R}\right)}{1 - 1.136\left(\frac{a}{R}\right) + 0.876\left(\frac{a}{R}\right)^2 - 0.866\left(\frac{a}{R}\right)^3 - 0.019\left(\frac{S}{R}\right)} \quad (4.6)$$

within the range $0.1<a/R<0.8$ and $0.5<S/R<0.8$ with $R^2 = 0.99955$.

4.5 Stress Intensity Factor Computation for SNDB

After performing SCB technique, the SNDB method was achieved to calculate normalized stress intensity factor for SNDB geometry. Disc bend specimen with a straight notch was modeled by using ABAQUS program. Specimen geometry was changed by using different notch sizes (a/B) and span lengths (S/R). Mesh refinement studies were carried out to obtain a better accuracy for the estimation of stress intensity factor.

4.5.1 Geometry and Boundary Conditions

The radius and thicknesses were 50 mm for all SNDB specimen models as SCB model geometries. Different notch lengths (5, 10, 15, 20, 25, 30, 35, 40 and 45 mm) and various span lengths (25, 30, 35 and 40 mm) were performed to figure out the effect of a/B and S/R on stress intensity factor, respectively. Model geometry is in Figure 4.17.

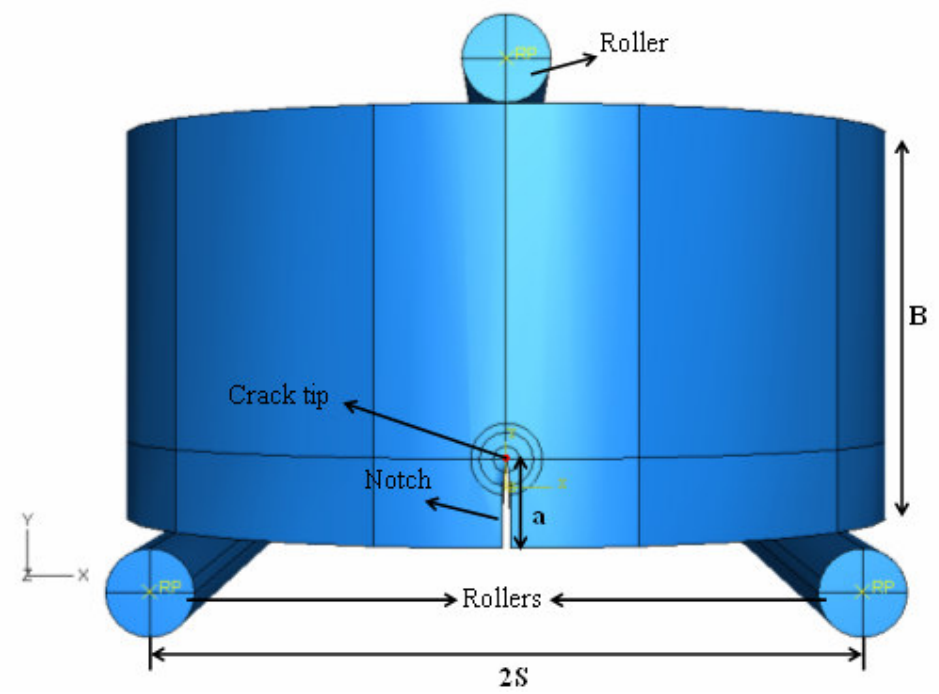

Figure 4.17 SNDB Geometry

Since the study of stress analysis of SCB specimen geometries showed there is no difference between the two boundary condition options for the failure load application, only one boundary condition option was tried in the SNDB models for the application of vertical load. A unit negative vertical load (F_y = -1 N) is applied on the top roller where bottom roller supports and their rotations (R_x, R_y and R_z) are kept fixed in all directions which means that the contact points of the bottom boundary of the specimen model is fixed in vertical y-direction (Figure 4.18). For all cases roller support material is modeled as analytical rigid.

Boundary conditions application and 3D ABAQUS model appearance are illustrated in Figure 4.19. Fixed directions were symbolized with orange triangles, fixed rotations were represented with blue triangles and load was indicated with yellow arrow in the figure.

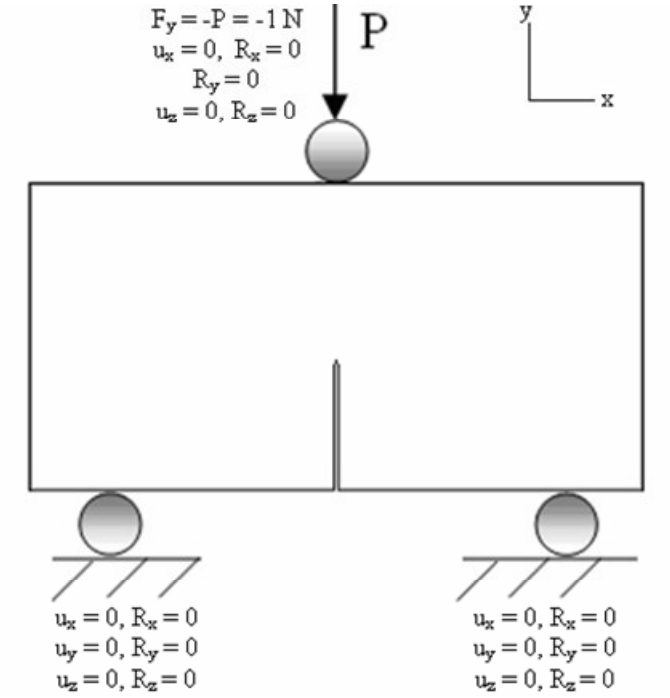

Figure 4.18 Boundary conditions of loading option

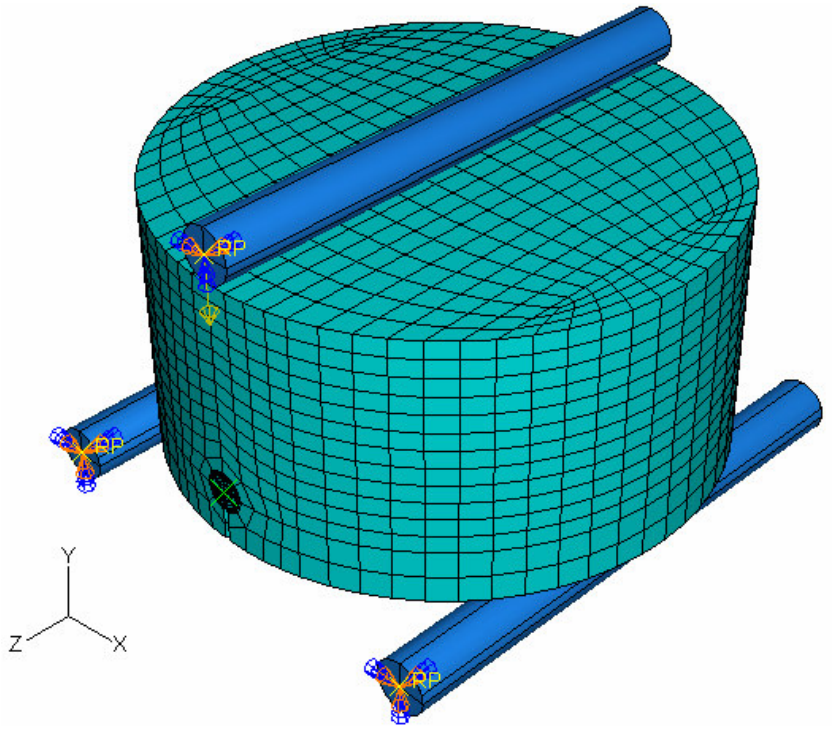

Figure 4.19 Boundary Conditions on the 3D ABAQUS model of SNDB specimen

The crack was introduced in interaction module. To accomplish contour integral analysis, the crack front and the crack extension direction were selected (Figure 4.20-a). Crack tip loading is supposed to be pure Mode I loading for SNDB specimens like SCB specimens thus crack extension direction is attached in the vertical direction to the front of the initial vertical notch (Figure 4.20-b).

In the SNDB specimen geometry, a ring of wedge shape elements could not be assigned to the crack front because the swept meshing could not be used due to the curved nature of the surface of the SNDB specimen model. As a result, wedge elements can not be created here, and the crack tip singularity is not included for the contour integral estimates. However, according to the ABAQUS manuals in most cases the singularity at the crack line can be ignored if the mesh is sufficiently refined to model the deformation around the crack tip or crack line and the resulting high strain gradients. Moreover, the singularity can be ignored if the contour integral output is considered only. As seen from the Figure 4.20, mesh was refined around the crack front. To compute stress intensity factors, contour integral region was defined and the stress intensity value found by an averaging process in this region was used as the stress intensity factor of this model.

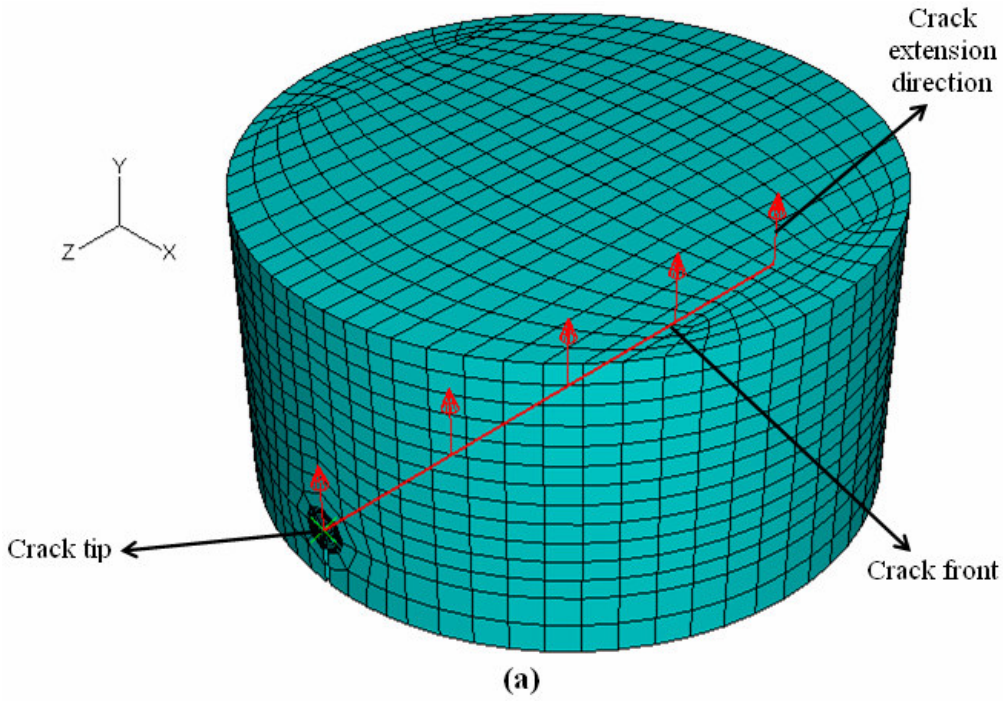

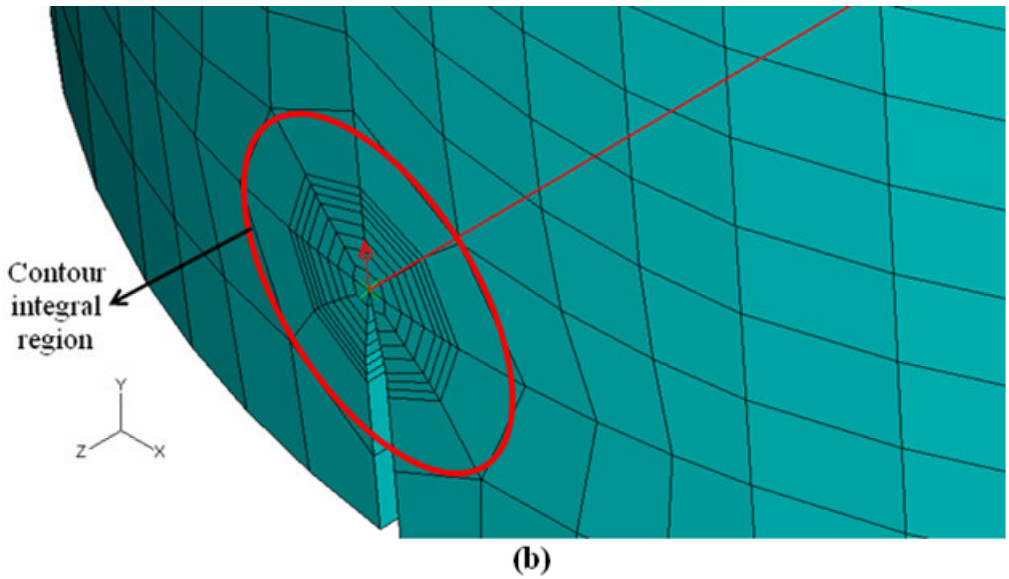

Figure 4.20 Crack front and contour integral region of the SNDB model

4.5.2 Convergence Studies

For SNDB method, to perform convergence study, a/B = 0.2 and S/R = 0.8 was selected. Four mesh densities were studied (Figure 4.21). Crack tip mesh density was increased to see the effect on stress intensity factor.

For SNDB technique, Y_I is calculated from Equation 4.7.

$$Y_I = \frac{K_I}{\sigma_0 \sqrt{\pi a}} \tag{4.7}$$

where

K_I = Mode I stress intensity factor

$\sigma_0 = \frac{P}{\pi R^2}$

P = applied load

R = specimen radius

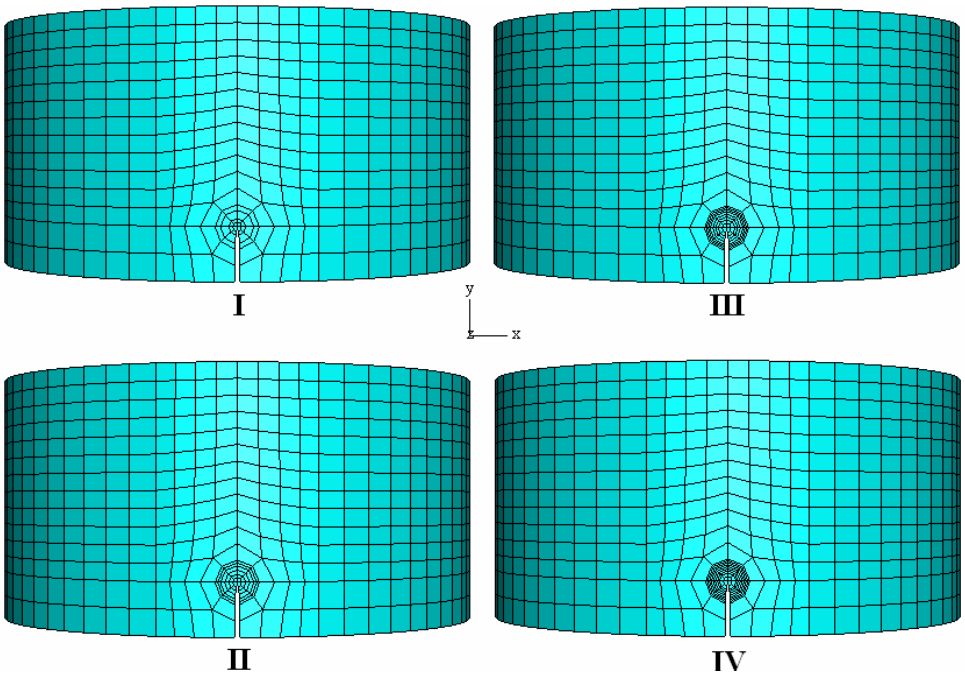

Figure 4.21 SNDB finite element meshes
(I) Coarse mesh, (II) Medium mesh, (III) Fine mesh, (IV) Very fine mesh

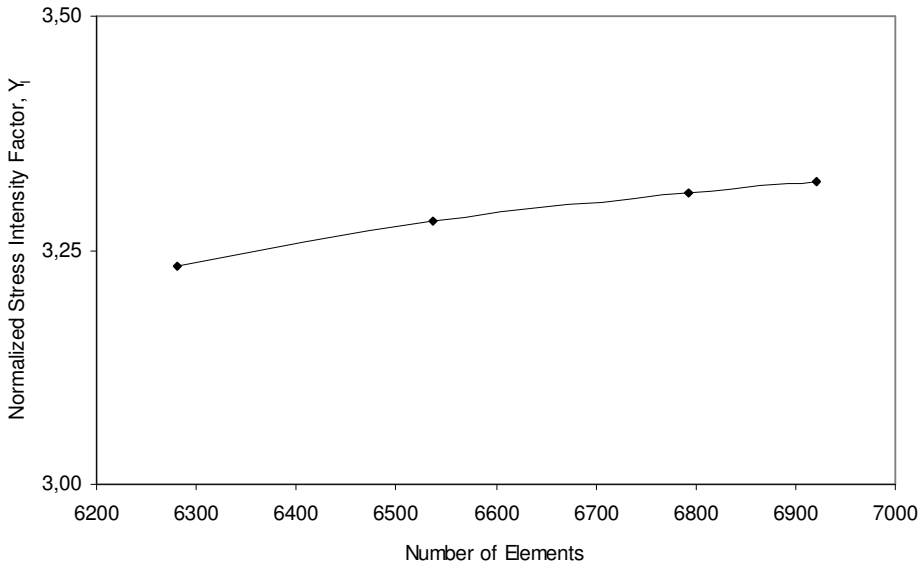

Figure 4.22 Convergence in Y_I with increasing mesh intensity at SNDB

As seen from the Figure 4.22 the distinction in Y_I between the fine and very fine mesh is approximately 0.3%. Hence, fine mesh was enough for remaining studies related to SNDB specimens. Fine mesh was defined with nine rings of elements around the crack front. These rings were also used to form the contour integral region to compute stress intensity factor.

4.5.3 Results

A total of 36 various geometries were studied for mode I loading, to perform wide range of SNDB geometry. The results were shown in Table 4.4.

Table 4.4 Normalized mode I stress intensity factors for the SNDB method for various geometries

S/R	a/B								
	0.1	0.2	0.3	0.4	0.5	0.6	0.7	0.8	0.9
0.5	2.0577	1.9428	1.9373	2.1849	2.6417	3.4666	5.1731	8.9616	22.9699
0.6	2.4981	2.4319	2.4912	2.7867	3.3788	4.4303	6.4567	11.2892	28.2386
0.7	2.9063	2.8580	2.9743	3.3621	4.0263	5.2108	7.6138	13.0023	32.7873
0.8	3.3143	3.3079	3.4656	3.9345	4.6991	6.0983	8.7321	14.9568	38.0640

The variations in the Y_I were similar to SCB technique results. Namely, the rate of Y_I variation increases with increasing notch length. Similarly, the Y_I increases with increasing span length (Figure 4.23).

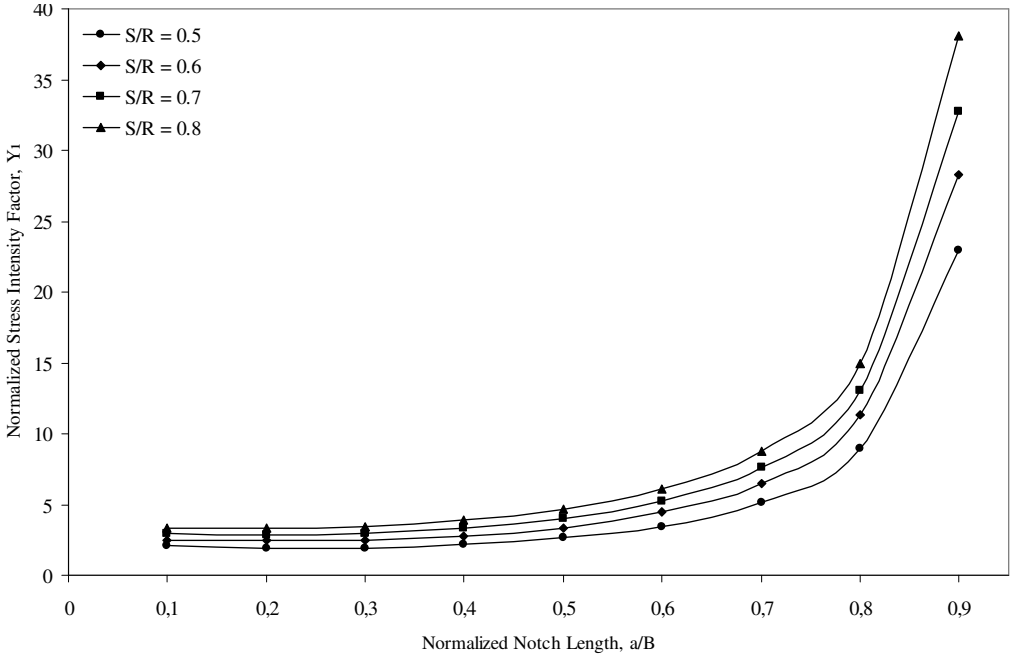

Figure 4.23 Computed normalized mode I stress intensity factor Y_I for SNDB

By considering Table 4.4, it is also possible to plot a 3-D graph of Y_I variation depending on a/B and S/R (Figure 4.24). Furthermore, by using TableCurve3D program and surface fit options, the regression analyses were performed to fit an analytical function to Y_I. Consequently, the following single equation depending on the a/R and S/R ratios together was achieved.

$$Y_I = \frac{-3.940-3.212\left(\frac{a}{B}\right)+3.791\left(\frac{a}{B}\right)^2+23.057\left(\frac{S}{R}\right)-28.540\left(\frac{S}{R}\right)^2+13.918\left(\frac{S}{R}\right)^3}{1-0.295\left(\frac{a}{B}\right)-1.273\left(\frac{a}{B}\right)^2-0.571\left(\frac{a}{B}\right)^3-0.033\left(\frac{S}{R}\right)} \quad (4.8)$$

within the range $0.1<a/B<0.9$ and $0.5<S/R<0.8$ with $R^2 = 0.99998$.

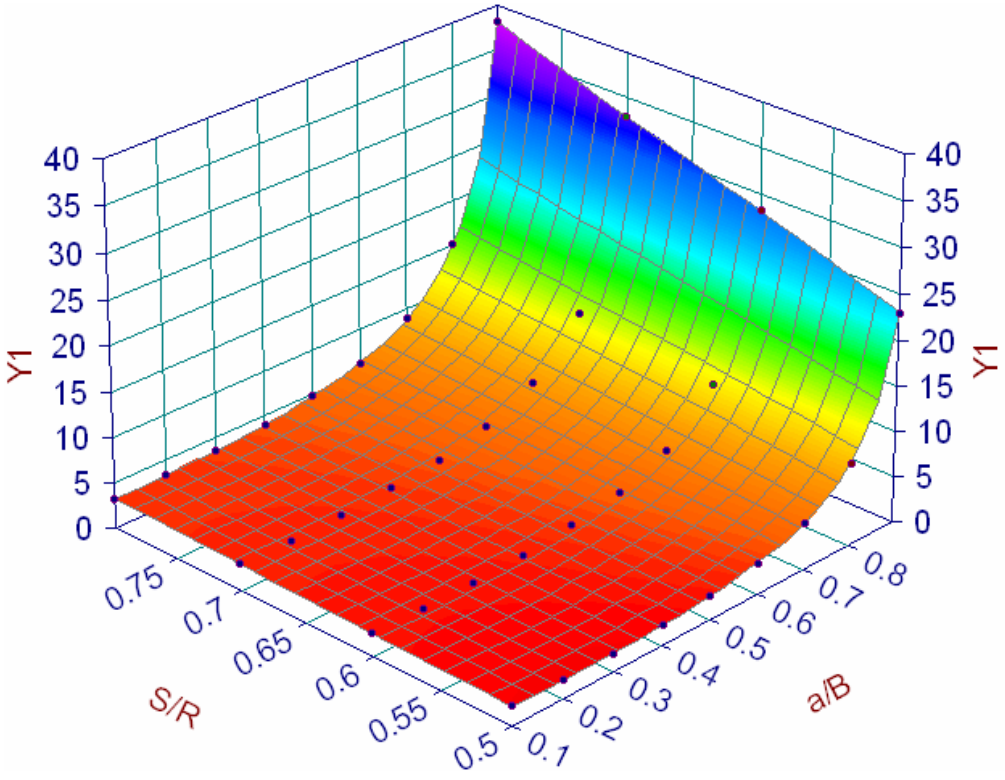

Figure 4.24 3-D Graph of Y_I for different a/B and S/R for SNDB method

4.6 Comparison of the SCB Method with the SNDB Method

For comparison purposes, distribution of horizontal stresses (σ_{xx}) and out of plane stresses (σ_{zz}) were considered first. In the previous models for the determination of the stress intensity factors unit loads had been used for the normalization procedure to generalize the results. However, to reach the actual order of stress magnitudes that existed in the tested specimens boundary loads with a comparable order of magnitude were applied to the SCB and SNDB stress analysis models. For both SCB and SNDB model geometries, load levels at failure obtained from the experiments were applied to the models with the same proportional geometrical properties, that is the same load application point-notch front distance (a/R = 0.2 for SCB specimen and a/B = 0.2 for SNDB specimen) and the same span length (S/R =

0.7 for both). Applied loads were 6.85 kN for SCB specimen and 14.76 kN for SNDB specimen.

Horizontal stress contours (σ_{xx}) in the models were plotted as seen in the example Figure 4.25. Then the notch front stress field was studied in detail as in Figure 4.26-a for SCB specimen and in Figure 4.26-b for SNDB specimen. Notch front horizontal stresses for both models were highly tensile increasing rapidly as the notch front was approached. Notch front tensile stresses for SCB model were seen to be higher in Figure 4.26. Variation of notch front stresses with the distance from the notch front was plotted in Figure 4.27 for both SCB and SNDB specimens. The stress values forming the distribution curves were obtained from the nodal point data following a specified path parallel to the notch plane in to the specimen. Then, considering the possible computation errors due to the mesh intensity the nodal point data were fitted to obtain smooth stress distribution curves in Figure 4.27.

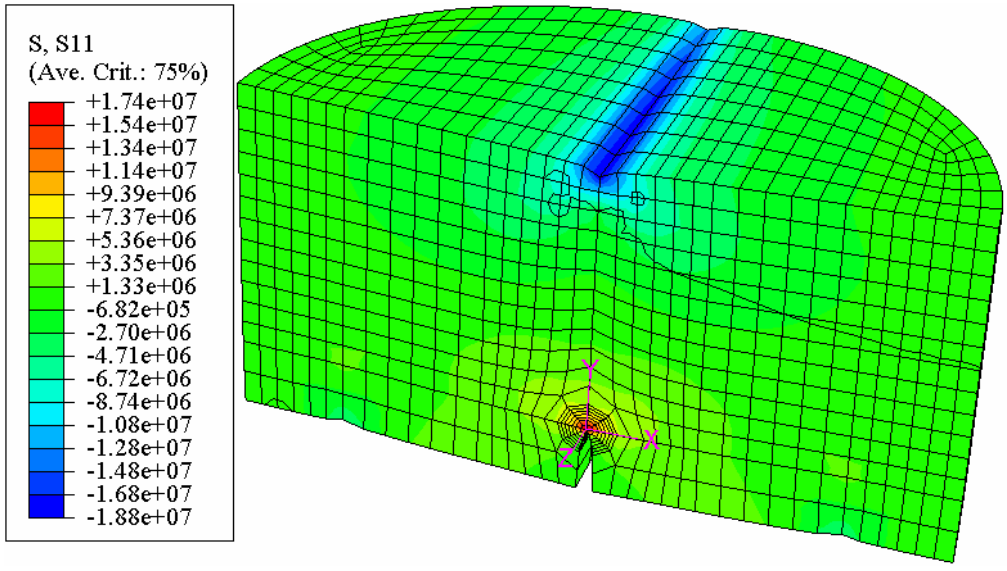

Figure 4.25 An example to horizontal stress contours (σ_{xx}) (in SNDB model)

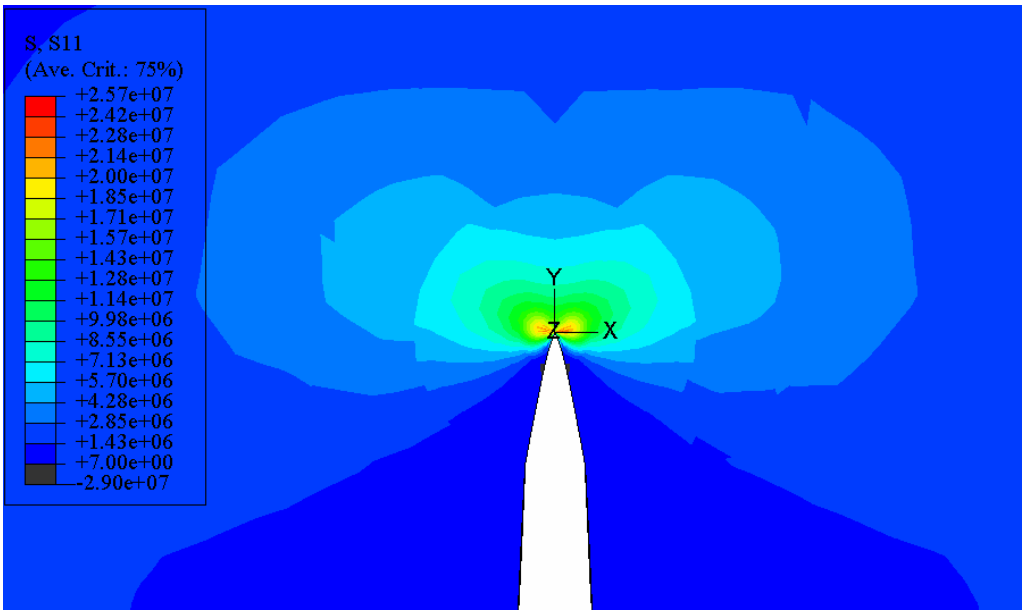

(a) Applied load was 6.85 kN for SCB specimen

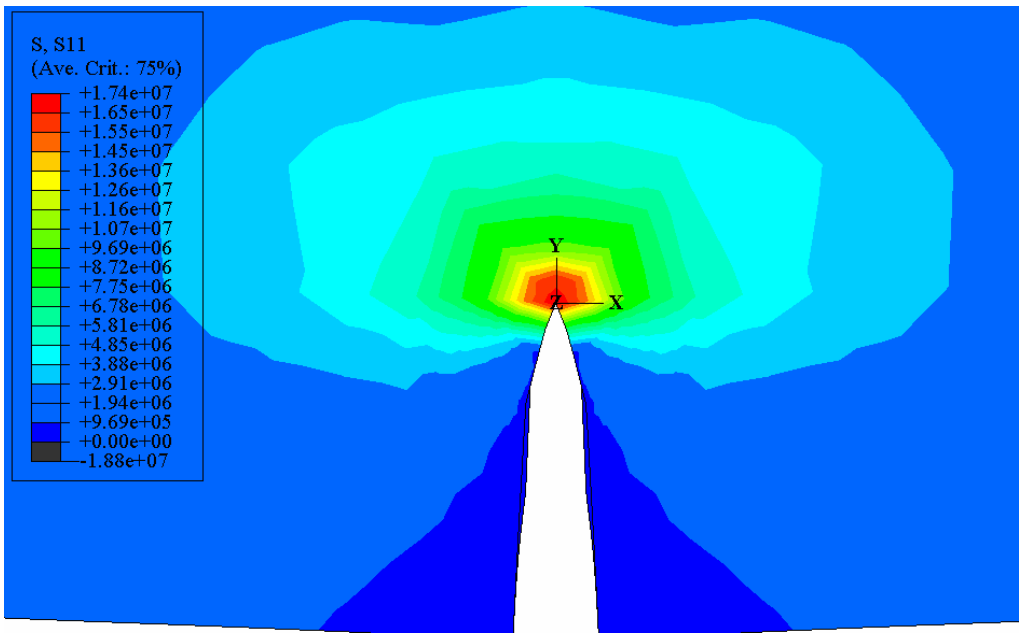

(b) Applied load was 14.76 kN for SNDB specimen

Figure 4.26 Horizontal stress contours around the notch front

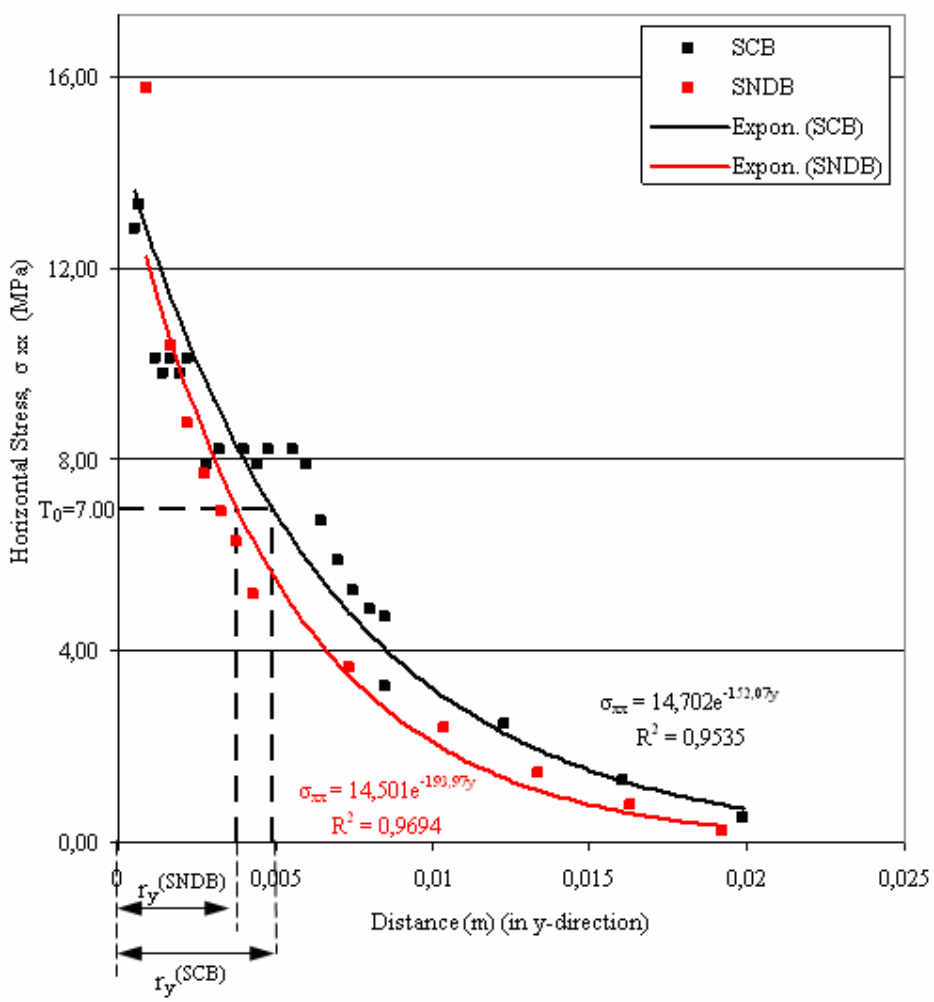

Figure 4.27 Variation of the notch front horizontal stresses ahead of the notch front

In Figure 4.27, crack tip horizontal stress curves are seen to tend infinity as the crack tip is approached. These curves were intersected with the tensile strength value T_0 = 7.00 MPa as found in the laboratory experiments presented in the next section. This way an estimate of the extent of a possible plastic or yield zone around the crack tip was believed to be achieved. According to these estimates the extent for SNDB model ($r_y^{(SNDB)}$ = 3.75 mm) was about 23% lower than the extent for SCB model ($r_y^{(SCB)}$ = 4.88 mm) for a 10 mm notch (a/R = 0.2) and a span of 70 mm (S/R = 0.7).

As seen from the Figure 4.26 and Figure 4.27, stress intensities around the notch front were higher for SCB specimen model therefore there was more extensive yield zone. As mentioned before (in Chapter 2), LEFM assumption is valid only when the inelastic deformation is smaller than the size of the crack. If large zones of plastic deformation develop before the crack propagations, Elastic Plastic Fracture Mechanics (EPFM) should be used and LEFM assumptions become invalid. That is why the new testing method with SNDB specimens is expected to produce more accurate results being less affected by the crack tip plasticity.

Out of plane stress (i.e. confining pressure (σ_{zz})) contours in the models were plotted as seen in the Figure 4.28 for SCB specimen model and Figure 4.29 for SNDB specimen model. Confining pressure data was obtained from the nodal points on the paths which were located on the notch fronts for both models. Confining pressure distributions on the notch fronts were plotted and the nodal point data were fitted to obtain the smooth stress distribution curves in Figure 4.30. After fitting the curves the Equation 4.8 for SCB model and Equation 4.9 for SNDB model were obtained.

$$\sigma_{zz} = -2885.4z^2 + 0.1115z + 4.0937 \quad \text{with } R^2 = 0.9418 \tag{4.8}$$

$$\sigma_{zz} = -614.28z^2 + 0.0009z + 3.2958 \quad \text{with } R^2 = 0.9498 \tag{4.9}$$

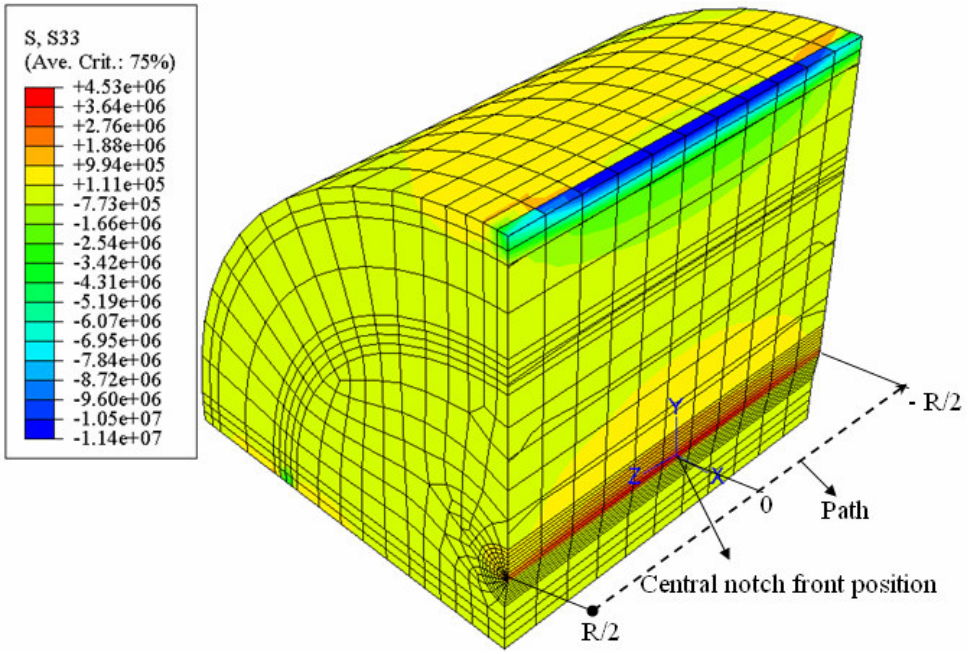

Figure 4.28 Confining pressure (σ_{zz}) distribution on SCB specimen

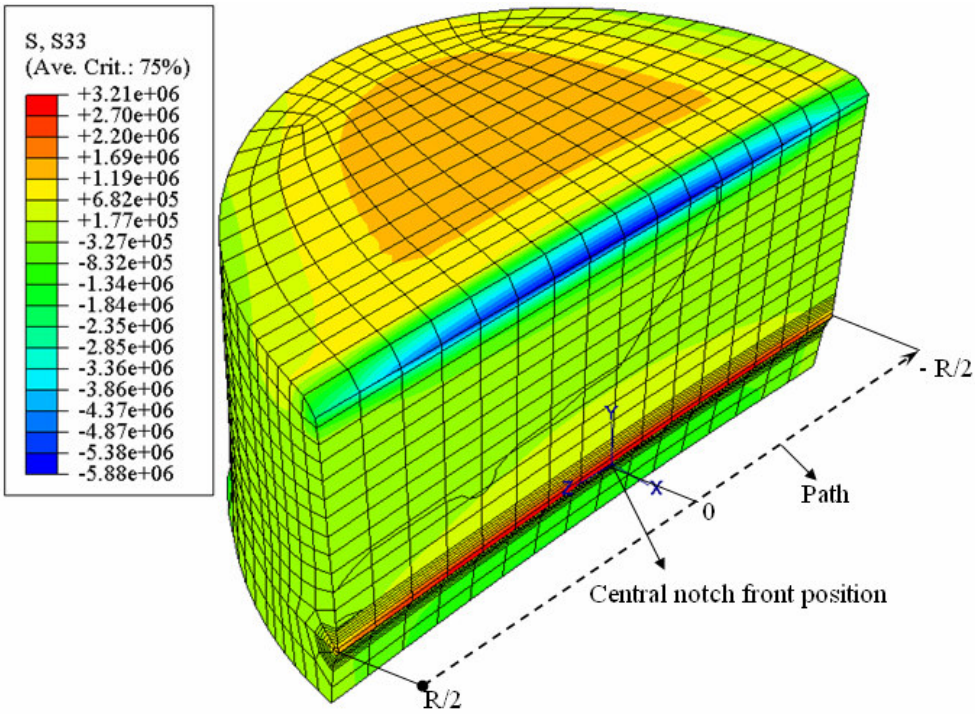

Figure 4.29 Confining pressure (σ_{zz}) distribution on SNDB specimen

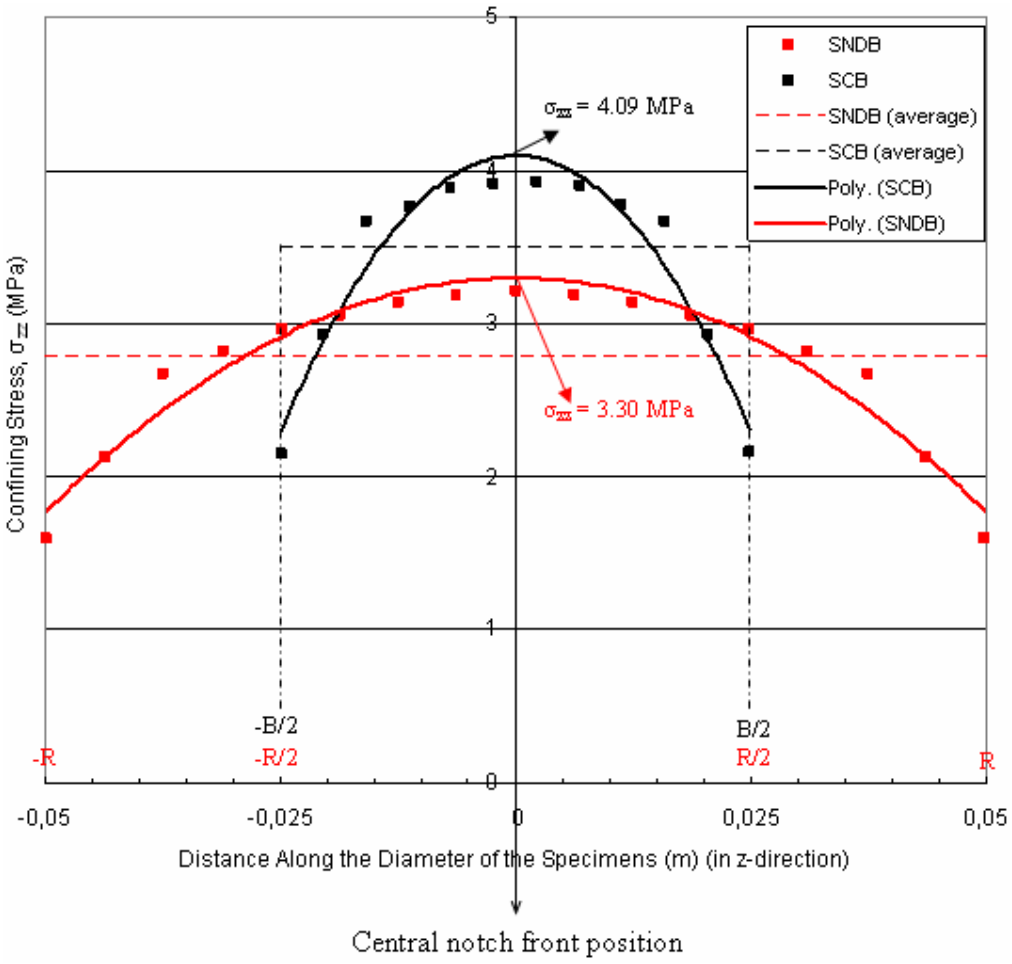

Figure 4.30 Variation of the confining stresses (σ_{zz}) along the notch front (in z-direction)

As seen from the Figure 4.30, corresponding to the central position along the notch, peak confining stress was 4.09 MPa for SCB specimen and 3.30 MPa for SNDB specimen. They were both tensile stresses, and peak confining stress was 24% higher for SCB model.

To determine average values of confining pressures, areas of the regions below the curves in Figure 4.30 were computed by integrating the equations above over the thickness (B = 50 mm) for SCB specimen and over the diameter (D = 2R = 100 mm) for SNDB specimen. These integrations for the averaging purposes are presented in Equation 4.10.

$$\sigma_{zz(avg.)} = \frac{\int_{-B/2}^{B/2} \sigma_{zz}(z)dz}{B} \quad \text{for SCB specimen model}$$
$$\sigma_{zz(avg.)} = \frac{\int_{-R}^{R} \sigma_{zz}(z)dz}{2R} \quad \text{for SNDB specimen model} \tag{4.10}$$

For the SCB and SNDB model examples here, average confining pressure values were computed as in the equations below.

$$\sigma_{zz(avg.)} = \frac{\int_{-0.025}^{0.025} \left(-2885.4z^2 + 0.1115z + 4.0937\right)dz}{0.05} = 3.49MPa \text{ for SCB model} \tag{4.11}$$

$$\sigma_{zz(avg.)} = \frac{\int_{-0.05}^{0.05} \left(-614.28z^2 + 0.0009z + 3.2958\right)dz}{0.10} = 2.78MPa \text{ for SNDB model} \tag{4.12}$$

Again the average confining pressure value 3.49 MPa for SCB model was about 26% higher than 2.78 MPa for SNDB model.

Ideally notch front is supposed to have no confining stress for this unconfined test, confining pressure was found to affect the fracture toughness before by other researchers (Backers et. al., 2002 and 2004; Yoon and Jeon, 2004; Al-Shayea et al., 2000; and Al- Shayea, 2002). Having a smaller confining pressure at the notch front, SNDB specimen conditions were closer to the desired conditions for the unconfined fracture toughness tests. Furthermore, having a larger tensile out of plane stress at the notch front was expected to contribute to the undesired crack tip plasticity by possibly extending the size of the yield zone.

Comparing the stress intensity factors, for the same S/R ratios and the same notch front-upper loading point distance (i.e., a/R for SCB model and a/B for SNDB model) stress intensity factor values for SCB specimen models were about 37% higher than for SNDB specimen models (Figure 4.31). Again this indicated a possible more intensive crack tip plasticity. In general, stress intensity factors increased with increasing notch and span length in numerical models.

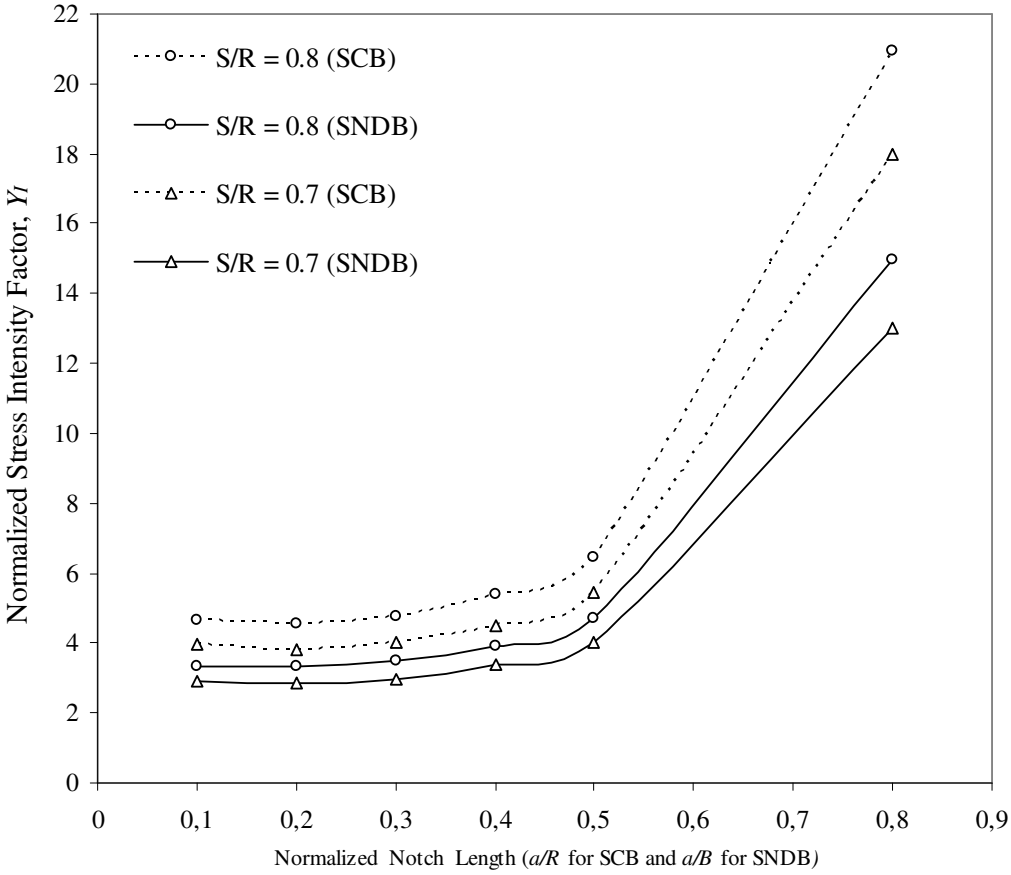

Figure 4.31 Stress intensity factor comparison for SCB and SNDB techniques

For the same normalized notch length and normalized span length data points, fitting a linear relationship to the Y_I results of two techniques (Figure 4.32) the following regression Equation 4.13.

$$Y_{I(SNDB)} = 0.7273 Y_{I(SCB)} \text{ with } R^2 = 0.9991 \quad (4.13)$$

If the normalized stress intensity factor one method is known, the other can be calculated by using Equation 4.13.

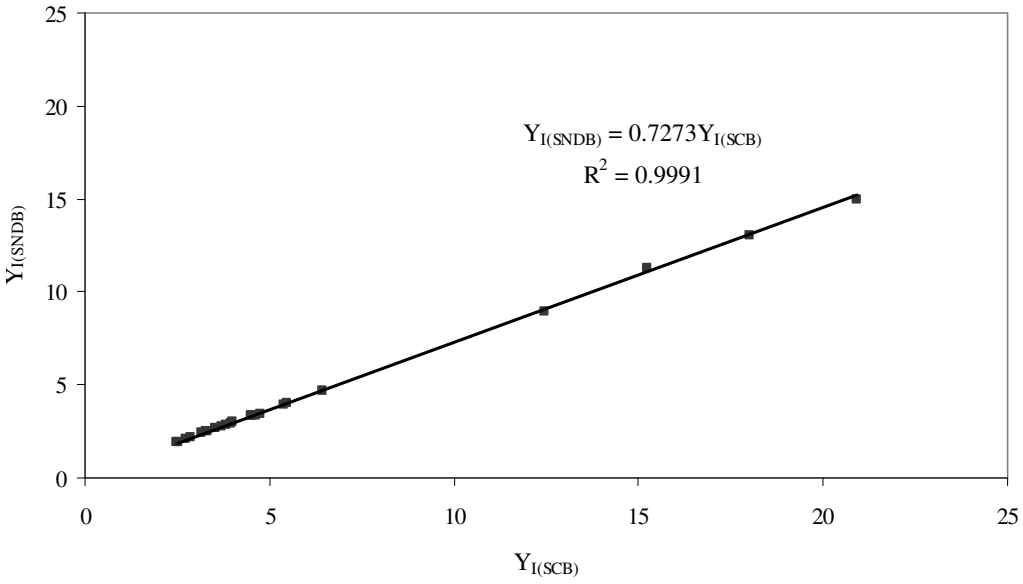

Figure 4.32 Y_I relation between SCB and SNDB methods

CHAPTER 5

EXPERIMENTAL STUDIES

In laboratory studies, pink colored Ankara Gölbaşı andesite blocks were used. Rock blocks were taken from a quarry near Gölbaşı region in Ankara. In order to perform fracture tests, two different specimen shapes were used with three point bending configuration in experiments. One of them was Semi-Circular specimen under three-point Bending (SCB), which was used before by other researchers. This sample geometry was used for comparison purposes; the reason for this choice is that the simplicity of specimen preparation, laboratory setup and test procedure (Lim et. al., 1994). The other specimen type was the new disc type specimen introduced here. Disc samples have not been tested with three point bending configuration by other researchers, yet. This method was called as Straight Notched Disc specimen under three-point Bending (SNDB).

Before fracture tests, in order to determine physical and mechanical properties of the pink andesite, uniaxial compressive strength (UCS) tests and indirect tensile (Brazilian) strength tests were done.

5.1 Physical and Mechanical Properties of Pink Ankara Andesite

5.1.1 UCS Tests

By considering ISRM's (1979) suggested methods, UCS tests were performed to determine uniaxial compressive strength, Young's modulus and Poisson's ratio. Three samples were used in UCS tests and all of them were NX size specimens ($\approx$ 54 mm) and $L/D \geq 2$. The MTS 815 Material Testing System was used in tests. Two external LVDT transducers were used to measure vertical displacement and circumferential extensometer was used to measure circumferential displacement.

Figure 5. 1 UCS test specimen with circumferential extensometer before test

Figure 5. 2 UCS test specimen with circumferential extensometer after test

After experiments, load and displacement data was converted to stress and strain to achieve stress-strain curves (Figure 5.3). By considering these curves, UCS, Young's modulus and Poisson's ratio were calculated (Table 5.1).

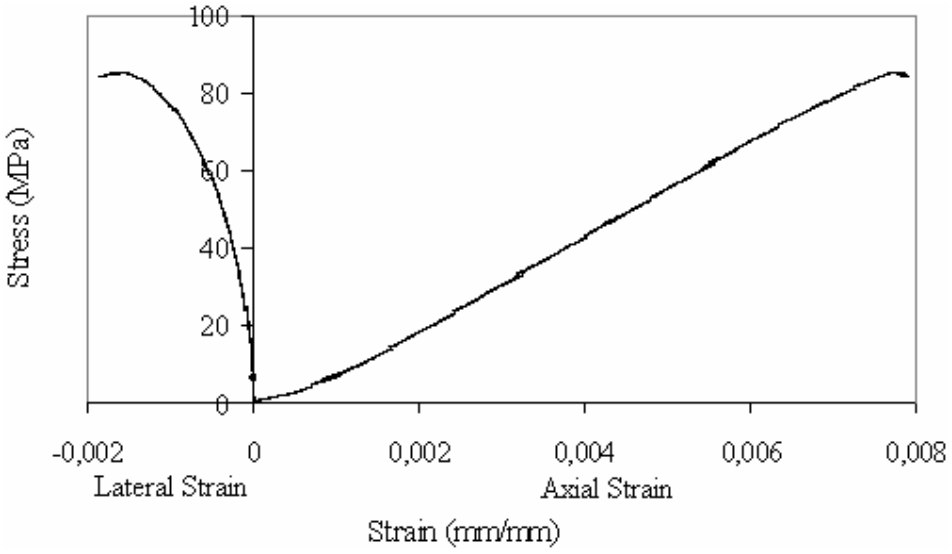

Figure 5.3 Stress-Strain curve of a UCS test

Table 5.1 UCS test data and results

Name	Diameter (mm)	Length (mm)	L/D	UCS (MPa)	E (MPa)	υ
UCS-1	54.09	129.10	2.4	85.11	12365	0.156
UCS-2	54.04	126.76	2.3	75.96	12126	0.140
UCS-3	54.11	129.07	2.4	86.52	12530	0.158
			Average	82.53±5.73	12340	0.151

5.1.2 Indirect Tensile Strength (Brazilian) Test

Indirect tensile tests were done to measure tensile strength of the pink Ankara andesite in accordance with ISRM (1978). Six specimens were used in Brazilian tests and all of them were NX size samples (≈ 54 mm) and L/D = 0.5-1. The MTS 815 Material Testing System was used in tests. Two external LVDT transducers were used to measure vertical displacement.

Figure 5. 4 Brazilian test specimen before test

Figure 5. 5 Brazilian test specimen after test

After experiments, load-displacement curves were plotted (Figure 5.6). According to these curves, tensile load at failure was achieved and tensile strength was calculated (Table 5.2).

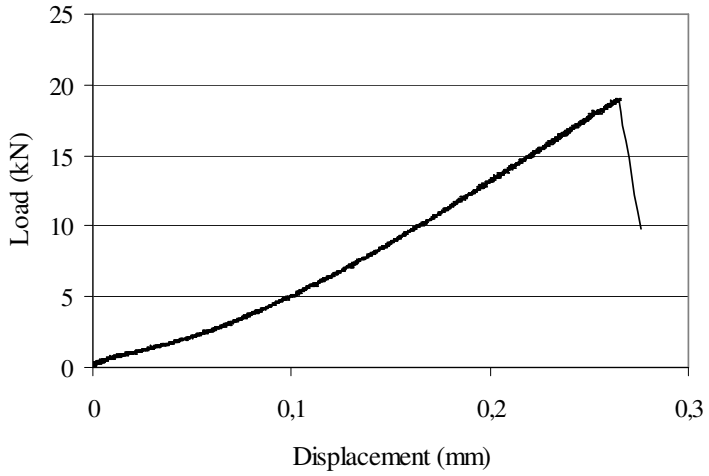

Figure 5.6 Load-Displacement graph of a Brazilian test

Table 5.2 Indirect tensile strength test data and results

Name	D	L	L/D	T_0
	mm	mm		MPa
Braz-1	53.45	29.35	0.55	6.60
Braz-2	53.43	27.86	0.52	5.94
Braz-3	53.30	27.32	0.51	7.15
Braz-4	53.40	28.06	0.53	7.86
Braz-5	53.47	30.23	0.57	7.45
Braz-6	53.40	32.00	0.60	7.03
			Average	7.00±0.67

5.2 Specimen Preparation

5.2.1 SCB Specimen

Firstly large blocks were brought to the cutting saw lathe by the help of crane and cut into carriable blocks (Figure 5.7 and Figure 5.8).

Figure 5.7 Crane and lathe

Figure 5.8 Block cutting

After that, those blocks were cored with boring machine ($\phi = 102$ mm), the cores have diameter of about 100 mm (Figure 5.9). In sample cuttings, rotary saw was used to cut discs in to about 55 mm thicknesses. Since the diameter of the saw was so large, deflection occurred. To remove that deviation, cutting discs were polished with grinding machine to 50 mm thickness (Figure 5.10).

Figure 5.9 Boring machine

Figure 5.10 Polishing machine

By the help of goniometer, center of the disc was marked and a line passing through the disc diameter was drawn (Figure 5.11).

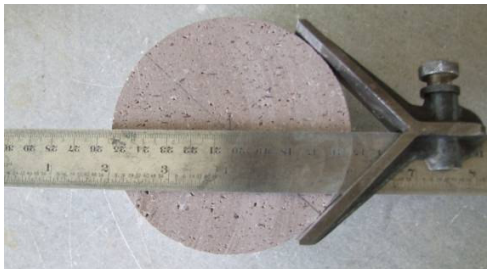

Figure 5.11 Goniometer on disc sample

The disc was cut into halves following this line by using Smartcut 1004 precision diamond saw apparatus. It was so difficult to hold the disc with hand during cutting thus a holding fixture was attached to the Smartcut 1004 (Figure 5.12).

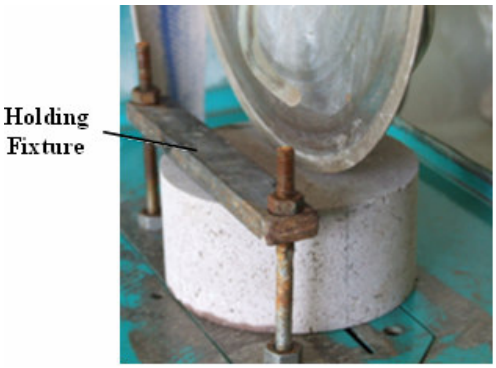

Figure 5.12 Smartcut with holding fixture apparatus

In order to cut the notch properly according to the desired dimensions an apparatus was designed by using ABAQUS program (Figure 5.13). Notch length was adjusted with the help of a digital caliper (Figure 5.14). During the travel of the holding fixture on the tracks, a notch with the desired length was cut through the specimen. After notch was cut, load application points were marked on the sample.

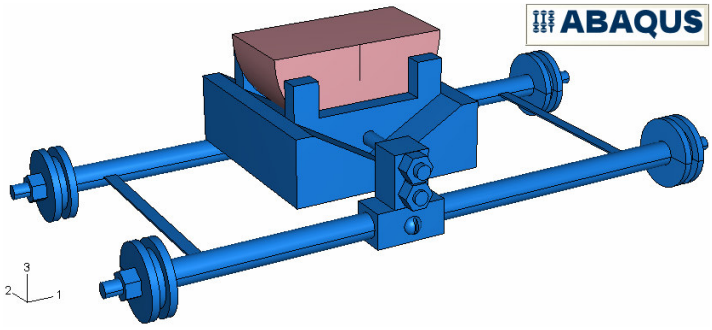

Figure 5.13 An apparatus model to open a straight notch to the semi-circular specimen by using ABAQUS Program

Figure 5.14 Cutting platform for half disc specimens

Before loading the specimen, each specimen was coded considering its testing method, notch thickness-specimen radius ratio (i.e., a/R), span length-specimen radius ratio (i.e., S/R) and specimen number (Figure 5.15).

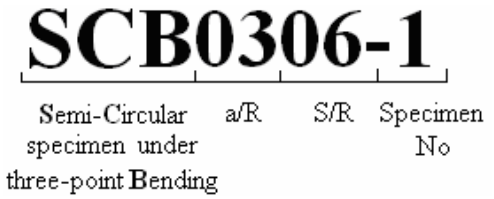

Figure 5.15 An example to show SCB code

5.2.2 SNDB Specimen

To prepare SNDB, the same initial steps were followed. After polishing, load application lines where the roller supports would contact were marked on the discs. By using ABAQUS program, another apparatus to precisely cut the notches through the SNDB specimens, was designed (Figure 5.16). Notch length was measured with

a digital caliper (Figure 5.17). Before loading, load application lines were marked on the sample.

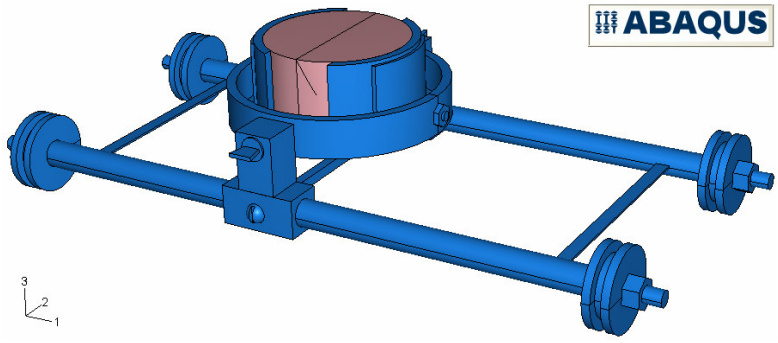

Figure 5.16 An apparatus model to open a straight notch to the disc specimen by using ABAQUS Program

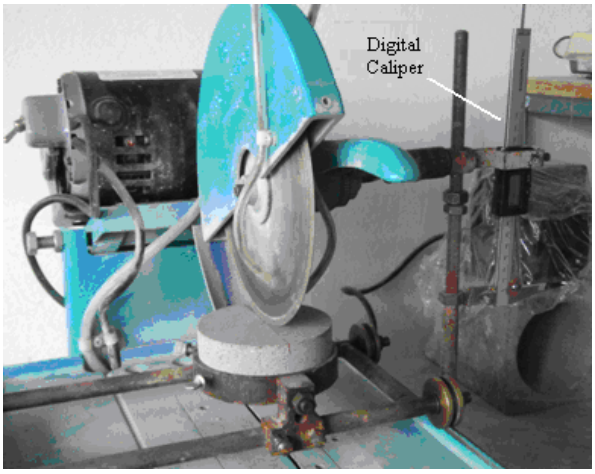

Figure 5.17 Cutting platform for disc specimens

Sample coding was a bit different than the SCB. The SNDB code included testing method, notch thickness-specimen thickness ratio (i.e., a/B), span length-specimen radius ratio (i.e., S/R) and specimen number (Figure 5.18).

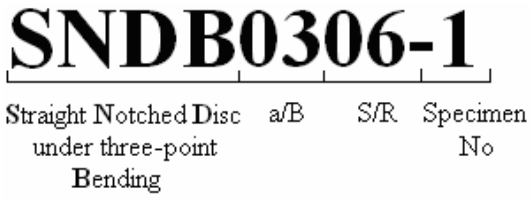

Figure 5.18 An example to show SNDB code

5.3 Specimen Geometries

5.3.1 SCB Specimen

In SCB method, radiuses and thicknesses were almost the same and about 50 mm for each sample. Notch lengths were 5, 10, 15 and 20 mm. Figure 5.19-22 and Table 5.3 show the dimensions of the SCB used in experiments (For some of the detailed figures see Appendix B, Figure B.1). In experiments, to perform three- point bending steel roller supports with 10 mm diameter and 100 mm length were used.

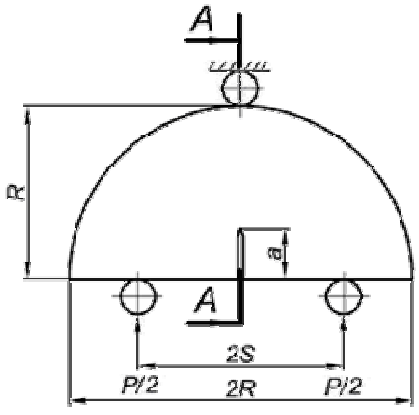

Figure 5.19 Front view of the SCB

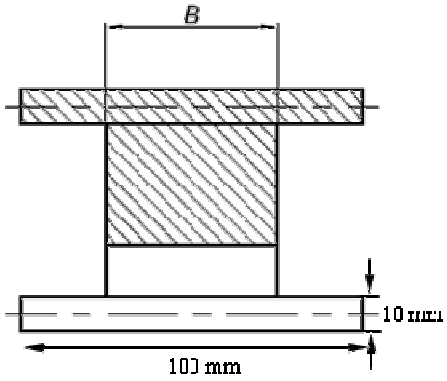

Figure 5.20 AA-Cross Section of the SCB

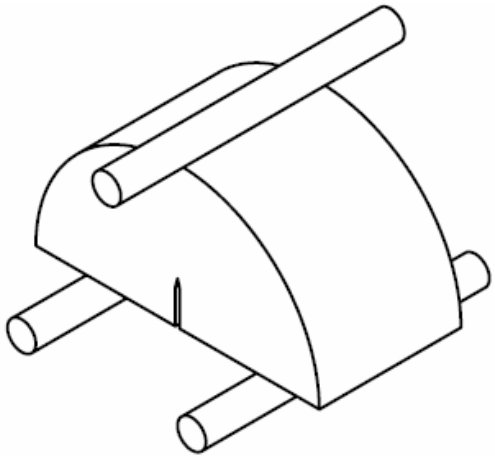

Figure 5.21 3-D view of the SCB

Figure 5.22 Semi-circular specimens

Table 5.3 Dimensions of the SCB used in the laboratory work

Name		a	R	B	S	a/R	S/R
		mm	mm	mm	mm		
SCB0106	1	5.75	49.06	50.30	30.75	0.1	0.6
SCB0106	2	4.75	49.13	50.22	30.75	0.1	0.6
SCB0106	3	5.13	50.00	50.05	30.56	0.1	0.6
SCB0107	1	5.00	50.00	49.91	35.50	0.1	0.7
SCB0107	2	5.50	50.00	50.08	35.75	0.1	0.7
SCB0107	3	5.50	50.00	50.58	35.88	0.1	0.7
SCB0206	1	11.00	49.75	51.03	30.88	0.2	0.6
SCB0206	2	10.25	50.00	49.52	30.75	0.2	0.6
SCB0206	3	10.38	49.50	49.80	30.88	0.2	0.6
SCB0207	1	10.50	50.00	50.55	35.75	0.2	0.7
SCB0207	2	10.00	50.00	50.11	35.88	0.2	0.7
SCB0207	3	10.25	49.50	50.75	35.75	0.2	0.7
SCB0306	1	15.25	50.00	49.89	30.75	0.3	0.6
SCB0306	2	15.50	50.00	49.27	30.75	0.3	0.6
SCB0306	3	15.38	50.00	50.67	30.75	0.3	0.6
SCB0307	1	14.63	49.50	49.81	35.75	0.3	0.7
SCB0307	2	14.50	49.75	50.75	35.75	0.3	0.7
SCB0307	3	17.00	50.25	51.26	35.88	0.3	0.7
SCB0406	1	20.50	50.00	49.84	30.88	0.4	0.6
SCB0406	2	19.88	50.25	49.43	30.75	0.4	0.6
SCB0406	3	20.13	50.25	50.96	30.75	0.4	0.6
SCB0407	1	21.13	50.19	50.32	36.00	0.4	0.7
SCB0407	2	20.50	50.00	50.64	35.75	0.4	0.7
SCB0407	3	20.00	50.00	50.39	35.88	0.4	0.7

5.3.2 SNDB Specimen

In disc specimens, diameters were almost the same and they were equal to approximately 100 mm. Thickness of the discs was almost 50 mm. Moreover, span length was changed between 35 and 40 mm. Notch thicknesses were chosen 5, 10, 15, 20 mm. The geometry of the disc samples was illustrated in Figure 5.23-27 and the dimensions of the SNDB samples are listed in Table 5.4 (For some of the detailed figures see Appendix B, Figure B.2). The same steel support rollers with 10 mm diameter and 100 mm length were used.

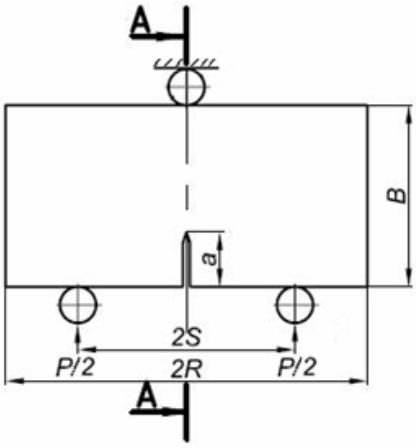

Figure 5.23 Front view of SNDB

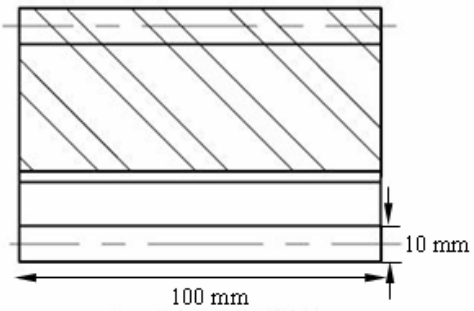

Figure 5.24 AA-Cross Section of SNDB

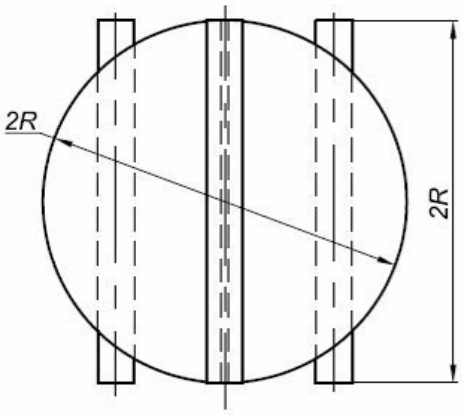

Figure 5.25 Top view of the SNDB

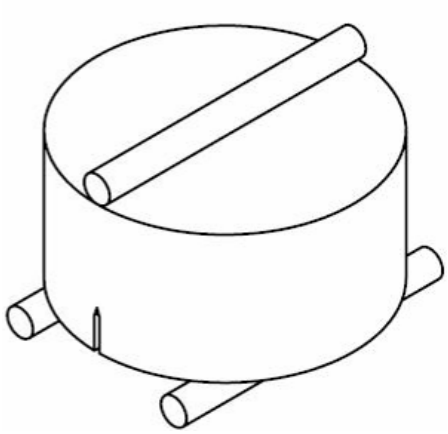

Figure 5.26 3-D view of the SNDB

Figure 5.27 Disc specimens

Table 5.4 Dimensions of the disc specimens used in the laboratory work

Name		a	D	R	B	S	a/B	S/R
		mm	mm	mm	mm	mm		
SNDB0106	1	6,50	101,74	50,9	50,1	30,88	0,1	0,6
SNDB0106	2	5,50	101,02	50,3	49,6	30,31	0,1	0,6
SNDB0106	3	5,00	100,98	50,5	50,1	30,51	0,1	0,6
SNDB0107	1	5,50	101,85	50,9	50,4	35,92	0,1	0,7
SNDB0107	2	5,50	101,48	50,8	50,2	35,76	0,1	0,7
SNDB0206	1	10,00	101,83	50,9	48,0	30,91	0,2	0,6
SNDB0206	2	9,75	101,80	50,9	48,1	30,89	0,2	0,6
SNDB0206	3	9,75	101,71	50,8	47,8	30,85	0,2	0,6
SNDB0207	1	10,50	101,67	50,8	49,7	35,84	0,2	0,7
SNDB0207	2	10,75	101,81	50,9	50,2	35,90	0,2	0,7
SNDB0207	3	9,75	101,80	50,9	50,4	35,90	0,2	0,7
SNDB0306	1	15,63	101,68	50,9	50,1	30,86	0,3	0,6
SNDB0306	2	15,25	101,68	50,8	50,0	30,85	0,3	0,6
SNDB0307	2	15,38	101,77	50,9	51,1	35,89	0,3	0,7
SNDB0307	3	15,50	101,68	50,8	50,0	35,83	0,3	0,7
SNDB0406	1	20,50	101,65	50,8	50,5	30,80	0,4	0,6
SNDB0406	2	20,25	101,68	50,8	50,9	30,85	0,4	0,6
SNDB0406	3	20,00	101,43	50,7	50,0	30,66	0,4	0,6
SNDB0407	2	20,00	101,70	50,9	51,3	35,87	0,4	0,7
SNDB0407	3	21,00	101,76	50,9	51,2	35,88	0,4	0,7

5.4 Loading System

MTS 815, servo-controlled hydraulic testing machine, was used as loading system in the experiments. The testing machine contains two main parts, which are Electronic Components and Servohydraulic Devices and Mechanical Components.

5.4.1 Electronic Components

5.4.1.1 458.20 MicroConsole

The MTS 815 Material Testing System has been configured with a 458.20 MicroConsole. 458.20 MicroConsole supplies closed-loop control of the test system. In particular, it contains controls and indicators required for system operation, such as cycle counter, digital display, hydraulic pressure, program run/stop, emergency stop and interlock controls.

The 458.20 MicroConsole has been configured with a 458.13 AC Controller and a 458.11 DC Controller (Figure 5.28).

Figure 5.28 458.20 MicroConsole

5.4.1.2 458.13 AC Controller

458.13 AC Controller (Figure 5.29) is used for controlling and measuring displacement. Zero control is used to adjust transducer conditioner output for zero volts when mechanical input to the transducer is at a desired zero condition. Set Point control is used to position of the Lower platen of the Load frame. ± 50 mm linear variable differential transformer (LVDT) transducers signals are picked through the 458.13 AC Controller and output data is seen from the 458.20 MicroConsole's digital indicator and recorded to computer.

5.4.1.3 458.11 DC Controller

A 458.11 DC Controller (Figure 5.29) is used for controlling and measuring load. In this laboratory work, since loading condition was displacement controlled, DC Controller was used only for measuring. Zero control is used to regulate transducer conditioner output for zero volts when mechanical input to the transducer is at a desired zero condition. As LVDT transducers signals, load signals are from the DC Controller are sent to MicroConsole's digital display and recorded to computer.

Figure 5.29 458.13 AC and 458.11 DC Controllers

5.4.1.4 418.91 Micro Profiler

418.91 Micro Profiler (Figure 5.30) is configured with MTS 815 to provide command programs for tests in force, strain, displacement, temperature and other test control parameters. The Micro Profiler generates waveforms to satisfy command programs.

The Micro Profiler has three operating modes, which are the “Programmed” mode, the “Direct” mode and the “Remote” mode. “Programmed” mode is used in order to create segments and grouping them together to form a block or a waveform program. Up to 99 programs and 99 blocks can be stored under “Programmed” mode. The “Direct” mode is preferred for immediate execution. Up to 9 programs can be stored under “Direct” mode. The “Remote” mode allows the Micro Profiler to be controlled by a computer. In this study, “Direct” mode was used with program 4 for displacement controlled loading. For loading period, rate was adjusted to 0.005. Namely, 0.005 means that 0.005% full-scale in one second (i.e. since the 100% full-scale equals to 100 mm, rate was 0.005 mm/sec).

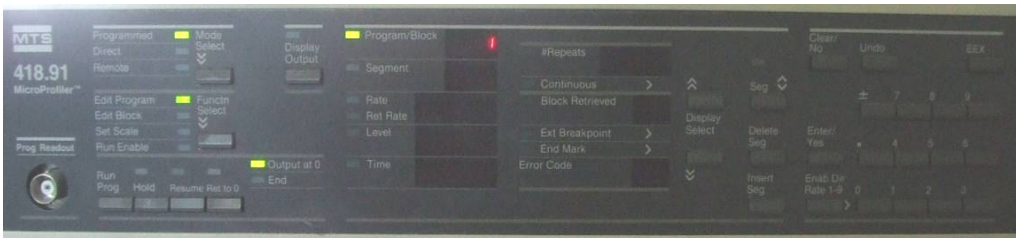

Figure 5.30 418.91 Micro Profiler

5.4.2 Servo-hydraulic Devices and Mechanical Components

Some of the basic servo-hydraulic devices and mechanical components of the MTS Material Testing machine are briefly described in paragraphs below.

5.4.2.1 The MTS Series 315 Load Frame

The MTS Series 315 Load Frame (Figure 5.31 and Figure 5.32) consists of a movable crosshead to accommodate various sized specimens and load cell mounting, columns on which the crosshead travels, and a base that provides actuator mounting. This actuator has a heavy, one piece, U-shaped upper frame bolted directly to the base plate. This set-up provides very high loading capacity in a compact frame.

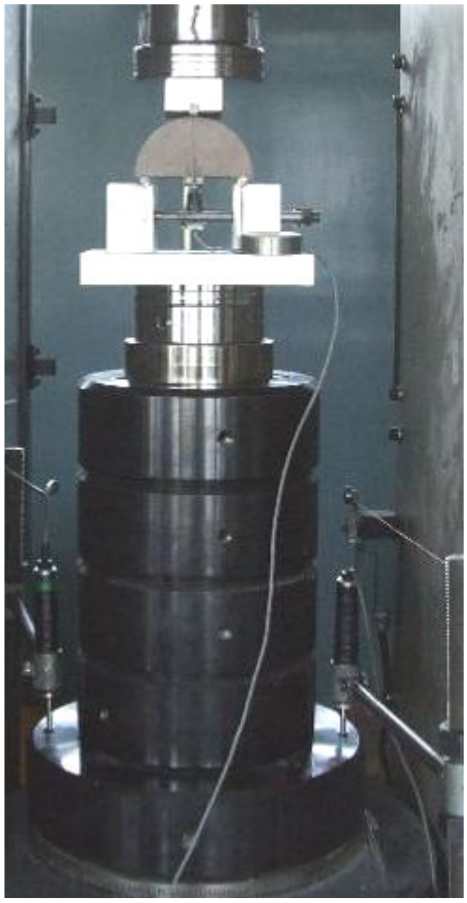

Figure 5.31 SCB Configuration

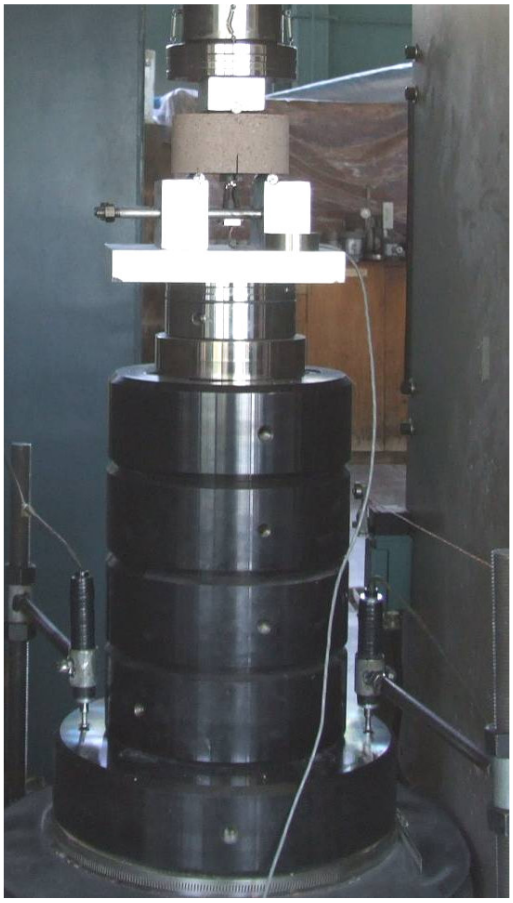

Figure 5.32 SNDB Configuration

Two feedback transducers are included in the frame structure. One is differential pressure (ΔP) cell which monitors the difference in pressure on each side of the actuator piston. Output signals from this transducer are calibrated to represent the force output of the actuator. The other is an internal linear variable differential transformer (LVDT) which provides stroke control of the actuator during specimen handling (MTS System Catalog, 1992).

In the system, the internal ΔP based load cell is rated 2800kN. In order to increase the accuracy, an external 500 kN force sensor (load cell) with ± 0.25 kN accuracy is added to the system to measure load.

In the system, to measure displacement an internal LVDT transducer is used. The LVDT capacity is ± 50 mm with ± 0.01 mm accuracy. For this study, in addition to internal LVDT, in fracture tests two external LVDT transducers were used to measure vertical displacement (Figure 5.31 and Figure 5.32). The capacity of the external LVDT transducers is ± 10 mm with ± 0.005 mm accuracy.

For these fracture tests, to measure the Crack Mouth Opening Displacement (CMOD), crack opening displacement gage was used. The capacity of the gage is ± 4 mm with ± 0.0001 mm accuracy.

5.4.2.2 Hydraulic Power Supply

The Model 506.01E Hydraulic Power Supply (HPS) provides pressurized hydraulic fluid to the servovalve, which converts a control signal (from AC, DC, or Valve Controller) to control the direction and amount of fluid flow to the actuator, or hydraulic service manifold, which filters and distributes fluid to the servovalves. An HPS typically contains a reservoir for hydraulic fluid, a pump to pressurize the hydraulic fluid, a motor to run the pump, a heat exchanger to cool the hydraulic fluid, and sensors to monitor the level and temperature of the hydraulic fluid.

5.5 Data Acquisition Devices

5.5.1 DBK80 Analog Multiplexor

The DBK80 is a low-noise, high-speed, unity-gain multiplexer card that provides 16 channels of differential voltage input. Maximum voltage range is ±10 V with typical ±[0.025% +150 μV] and maximum ±[0.1% +250 μV] accuracy.

In this study, the external load cell (for all experiments in the study), the circumferential and axial displacement (for stress-strain analysis) data were acquired with DBK80 device from Channel P10-1, Channel P10-3 and Channel P10-4, respectively. All these data obtained in terms of volts therefore conversion was required. For external load cell 1 V equals to 50 kN, for circumferential displacement 1 V equals to 0.4 mm, for axial displacement 1 V equals to 10 mε.

5.5.2 DBK43 and DBK43A Strain-Gage Cards

DBK80 connects to the primary data acquisition devices, which are DBK43 and DBK43A strain-gage cards (Figure 5.33). They are designated as P1 – Analog I/O as DBK80 Analog Multiplexor.

In these tests, the COD was achieved with DBK43 Strain-gage card from Channel P11-0. For COD 1V equals to 0.25 mm. the external LVDT transducers' data was acquired with DBK43A Strain-gage card from Channel P12-0-0 and Channel P12-0-1. For the transducers, 1V equals to 1mm.

Figure 5.33 DBK80 Analog Multiplexor, DBK43 and DBK43A strain-gage cards

5.6 Data Acquisition Program

As a data acquisition program DaqView, which is a 32-bit Windows-based software, is used. DaqView can be used to operate DBK cards and modules.

In these experiments, after starting the program, firstly, the required channels by considering experiment type were turned on in channel setup (Figure 5.34). In Acquisition Setup Tab (Figure 5.35) trigger and stop events were selected as manual. Scan rate was chosen as 20 scan per second and averaging was equal to scan rate. Therefore at the final data the scan rate was equal to 1 scan per second. Then by using Data Destination Tab (Figure 5.36), file formats and directories for acquired data was selected. After controlling channels working or not, "Acquire" item was selected under "Data Menu" to start data acquisition. After data acquisition started, the "Run Button" was turned on the MicroConsole and "Direct Module", "Run Enable" and "Program 4" were selected on Micro Profiler. After output data acquisition finished, the data exported to an Excel file and required graphs were plotted.

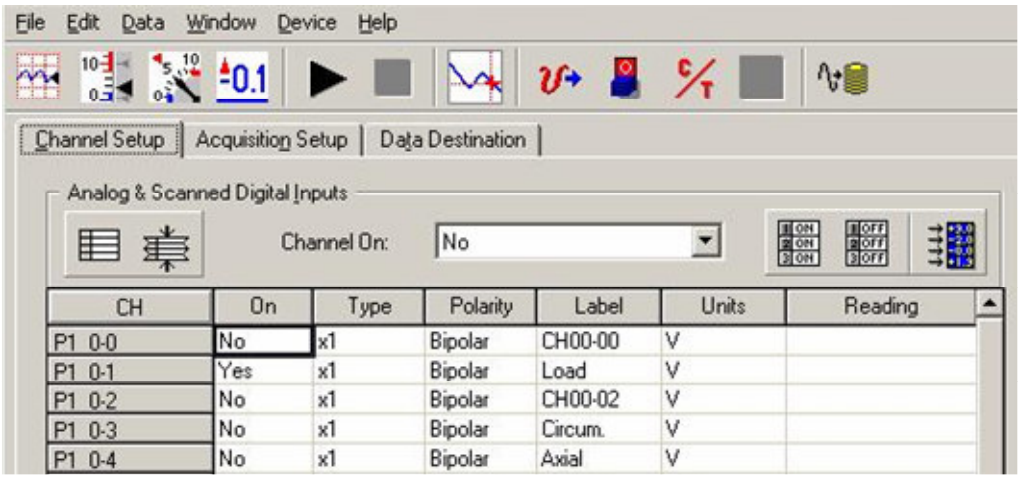

Figure 5.34 DaqView Main Window

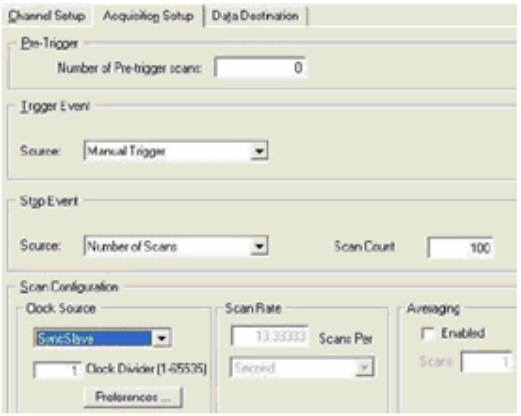

Figure 5.35 Acqusition Setup Tab

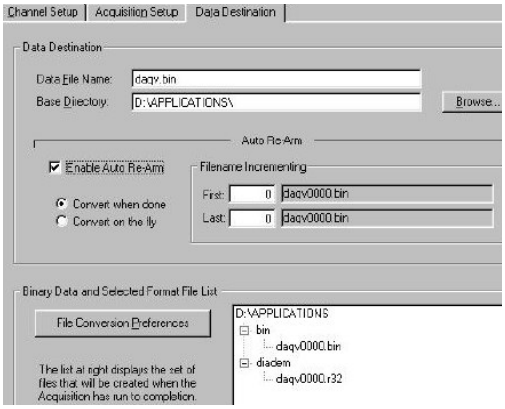

Figure 5.36 Data Destination Tab

5.7 Result of Three-Point Bending Tests

5.7.1 SCB Results

While SCB tests were performed, the data was recorded and by using this data Load-Displacement and Load-CMOD curves were plotted (in Appendix A, Figure A.1). Considering these graphs and error bands of these graphs, the maximum load, maximum vertical displacement and maximum CMOD ($CMOD_f$) were determined as in Table 5.5. By using maximum loads (i.e. critical load), fracture toughness (K_{IC}) of the Ankara andesite was calculated. K_{IC} is calculated from the Equation 5.1.

$$K_{IC} = Y_I \sigma_{cr} \sqrt{\pi a} \tag{5.1}$$

where

Y_I = normalized stress intensity factor

$$\sigma_{cr} = \frac{P_{cr}}{2RB}$$

P_{cr} = load at fracture

R = specimen radius

B = specimen thickness

According to Equation 5.1, K_{IC} values for each SCB were calculated (Table 5.5).

Table 5.5 Fracture data for each SCB

Name		P_{cr}	Disp.	$CMOD_f$	K_{IC}
		kN	mm	mm	MPa$\sqrt{\text{m}}$
SCB0106	1	12.0971	0.2443	0.0334	1.0963
SCB0106	2	12.4716	0.1991	0.0354	1.0277
SCB0106	3	10.0775	0.1947	0.0276	0.8503
SCB0107	1	8.3371	0.1622	0.0310	0.8311
SCB0107	3	8.1073	0.1795	0.0290	0.8365
SCB0206	1	9.0401	0.2032	0.0200	1.0437
SCB0206	2	7.5400	0.1666	0.0456	0.8616
SCB0207	1	6.6518	0.1814	0.0391	0.9158
SCB0207	2	6.9520	0.1849	0.0414	0.9421
SCB0207	3	6.9519	0.2174	0.0327	0.9514
SCB0306	1	5.6300	0.1599	0.0430	0.8074
SCB0306	2	6.2028	0.1379	0.0439	0.9081
SCB0306	3	5.8404	0.1337	0.0416	0.8281
SCB0307	1	4.4179	0.1403	0.0471	0.7686
SCB0307	3	5.3761	0.1079	0.0527	0.9652
SCB0406	1	5.1942	0.1614	0.0465	0.9754
SCB0406	2	5.8923	0.1433	0.0488	1.0931
SCB0406	3	6.8518	0.1748	0.0569	1.2406
SCB0407	1	3.6205	0.1171	0.0540	0.8312
SCB0407	2	4.8035	0.1364	0.0586	1.0837
SCB0407	3	3.8264	0.0912	0.0468	0.8569

According to the Table 5.5, maximum load decreases with increasing notch and span length (Figure 5.37). Failure load values with increasing vertical displacement values at peak loads are plotted in Figure 5.38.

To see the effect of crack mouth opening at failure ($CMOD_f$) on a/R and S/R, normalized $CMOD_f$ (i.e., $P_{cr}/CMOD_f = k_f$) versus a/R graphs were plotted for each S/R ratio. From the plot, it is seen that k_f which is a kind of measure of specimen stiffness decreases with increasing notch and span length (Figure 5.39).

Fracture toughness of the Ankara andesite using SCB technique was found as $0.93 \pm 0.11\ MPa\sqrt{m}$ (Figure 5.40).

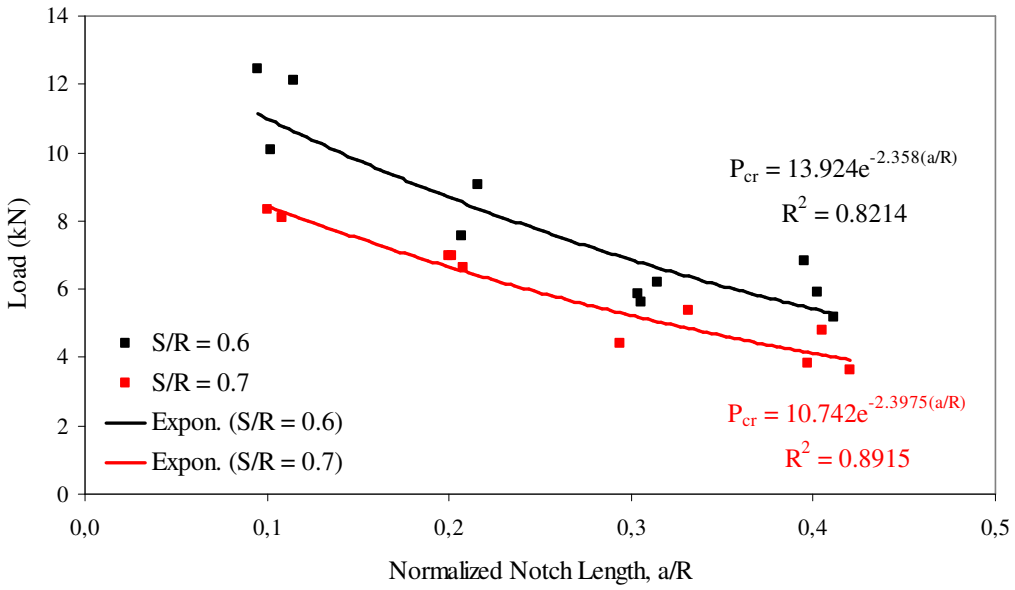

Figure 5.37 Load-Normalized Notch Length Curve of SCB

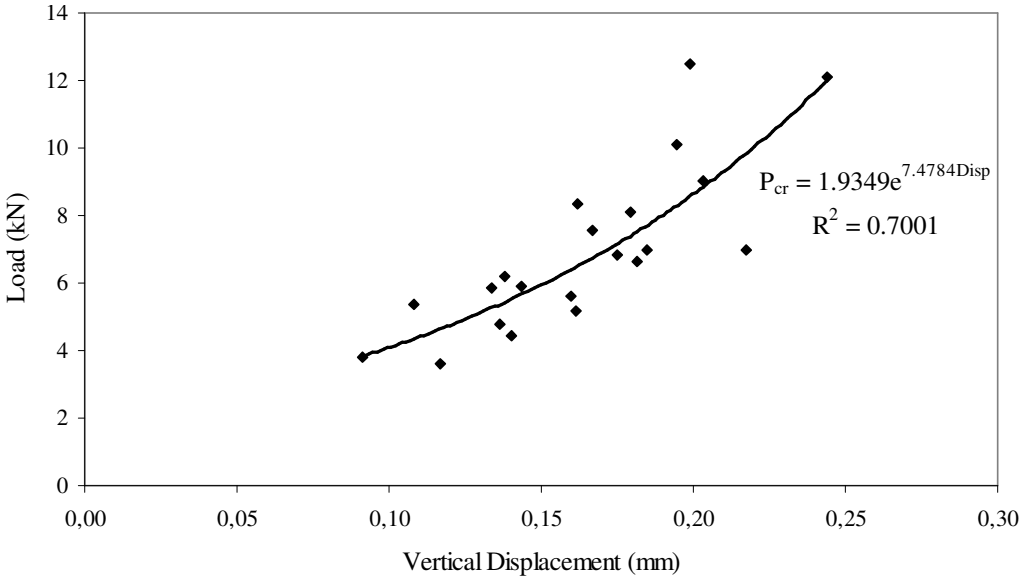

Figure 5.38 Load-Vertical Displacement values for each SCB specimen

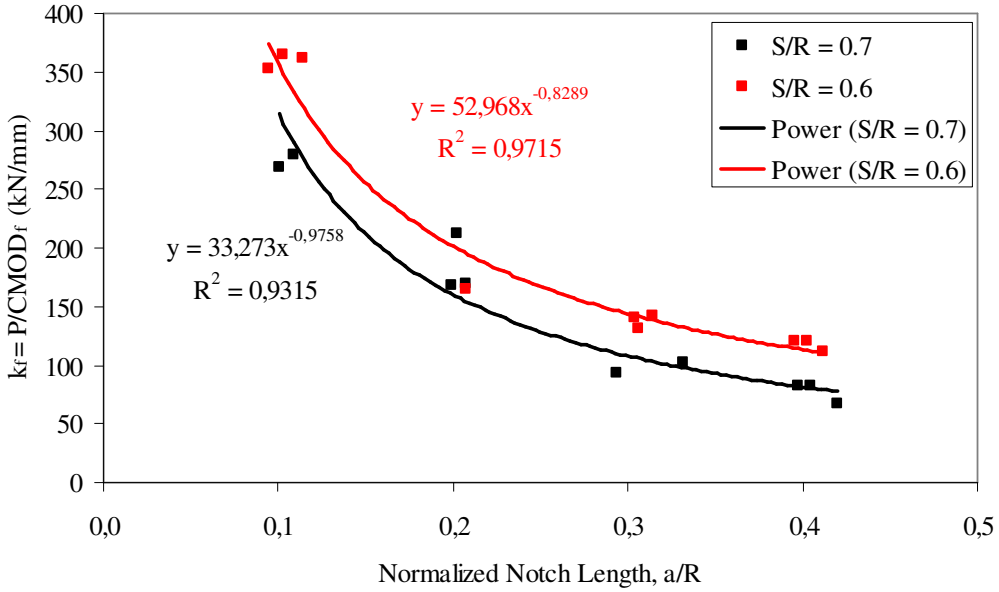

Figure 5.39 k_f versus a/R plot for each SCB specimen

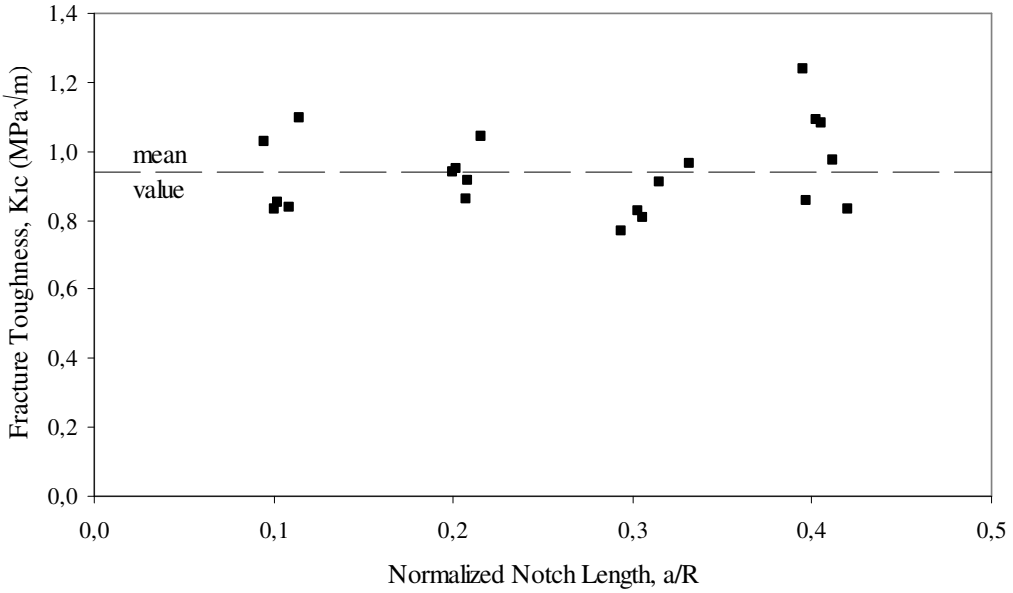

Figure 5.40 Fracture Toughness-Normalized Notch Length values for each SCB specimen

5.7.2 SNDB Results

Data about load, vertical displacement and CMOD were recorded during SNDB tests. As a result of this data, Load-Displacement and Load-CMOD curves were plotted (in Appendix A, Figure A.2). Considering these graphs and error bands of these graphs, the maximum load, maximum vertical displacement and $CMOD_f$ were achieved (Table 5.6). By using maximum loads (i.e. critical load), fracture toughness (K_{IC}) of the Ankara andesite was calculated. K_{IC} is calculated from the Equation 5.2.

$$K_{IC} = Y_I \sigma_{cr} \sqrt{\pi a} \tag{5.2}$$

where

Y_I = normalized stress intensity factor

$$\sigma_{cr} = \frac{P_{cr}}{\pi R^2}$$

P_{cr} = load at fracture

R = specimen radius

Table 5.6 Fracture data for each SNDB

Name		P_{cr} kN	Disp. mm	$CMOD_f$ mm	K_{IC} $MPa\sqrt{m}$
SNDB0106	1	26.0200	0.2247	0.0347	1.1423
SNDB0106	2	24.5487	0.2064	0.0299	1.0140
SNDB0106	3	21.7122	0.2597	0.0334	0.8481
SNDB0107	1	18.3374	0.2336	0.0341	0.8600
SNDB0107	2	20.3098	0.2057	0.0352	0.9585
SNDB0206	1	15.8817	0.2013	0.0350	0.8409
SNDB0206	2	16.3458	0.2075	0.0380	0.8553
SNDB0206	3	16.5352	0.1799	0.0414	0.8665
SNDB0207	1	13.6487	0.1761	0.0419	0.8727
SNDB0207	2	15.0582	0.1626	0.0450	0.9717
SNDB0207	3	15.5684	0.1789	0.0398	0.9567
SNDB0306	1	15.7280	0.2029	0.0471	1.0682
SNDB0306	2	14.4561	0.1770	0.0443	0.9706
SNDB0307	2	12.9169	0.1927	0.0488	1.0380
SNDB0307	3	12.1495	0.1748	0.0548	0.9824
SNDB0406	1	10.3262	0.1318	0.0488	0.9007
SNDB0406	2	12.2497	0.2098	0.0532	1.0601
SNDB0406	3	12.4307	0.1419	0.0513	1.0772
SNDB0407	2	9.5955	0.1479	0.0480	0.9947
SNDB0407	3	10.3772	0.1762	0.0573	1.1019

By using data in Table 5.6, maximum load decreases with increasing notch and span length (Figure 5.41). Failure load values with increasing vertical displacement values at peak loads are plotted in Figure 5.42.

k_f versus a/R graphs were plotted as in SCB studies, the k_f value decreases with increasing notch and span length (Figure 5.43). Fracture toughness of the SNDB technique for Ankara andesite equals to $0.96\pm0.09\ MPa\sqrt{m}$ (Figure 5.44).

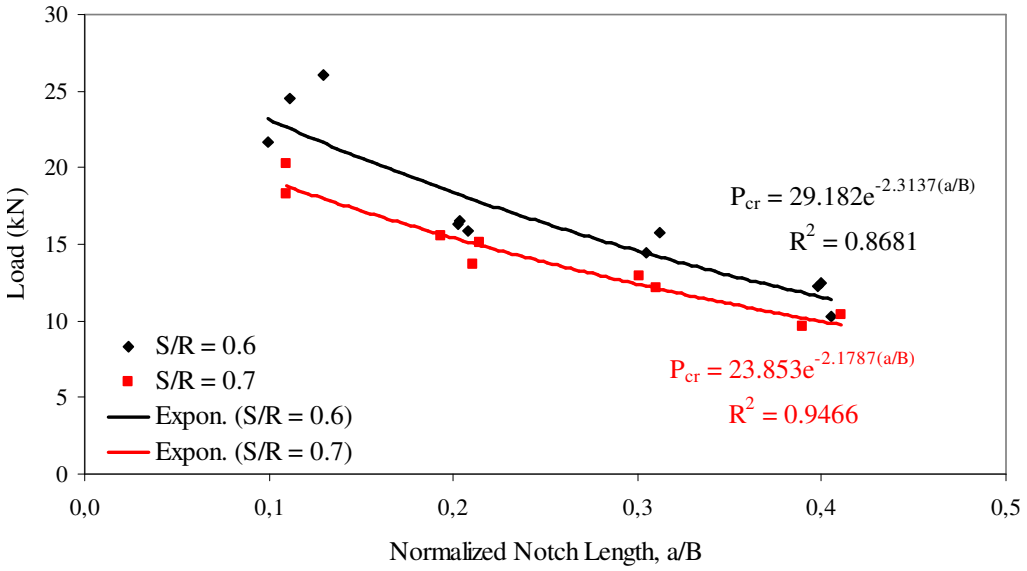

Figure 5.41 Load-Normalized Notch Length Curve of SNDB

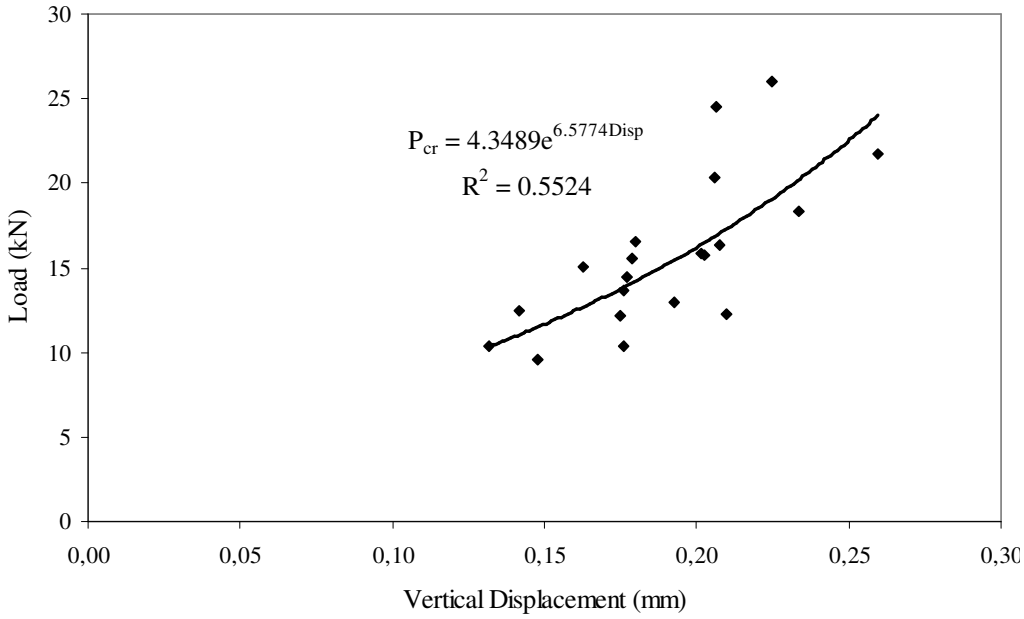

Figure 5.42 Load-Vertical Displacement values for each SNDB specimen

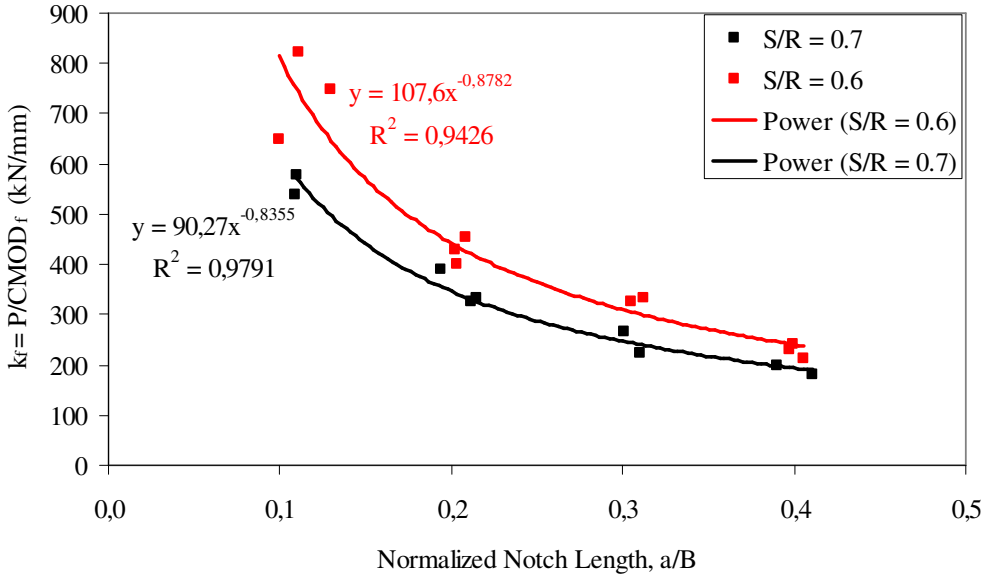

Figure 5.43 k_f versus a/R plot for each SNDB specimen

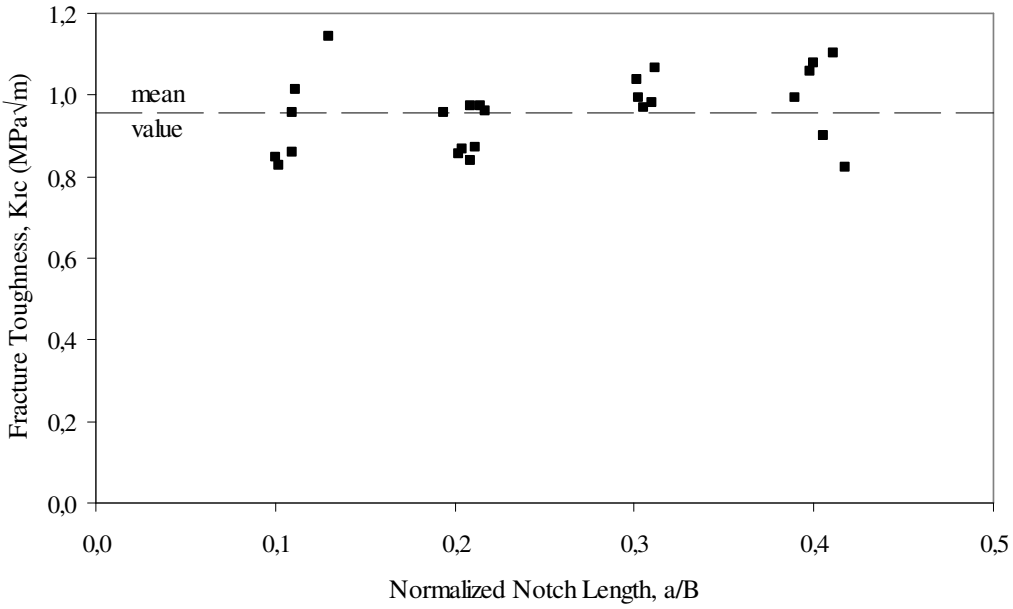

Figure 5.44 Fracture Toughness-Normalized Notch Length values for each SNDB specimen

5.7.3 Comparison of the SCB Test with the SNDB Test

In experiments, specimen preparation of the SNDB was easier than SCB specimen. Notch cutting of SCB specimen was difficult process owing to the curved surface of the specimens. Moreover, this curved surface caused problems in attaching upper roller support loading arrangement on it because of the curvature of the top surface of the specimen.

The stiffness k_f values of both specimen types were plotted in Figure 5.45 for S/R = 0.7. The stiffness values for SNDB are seen to be approximately 120% higher. This means that with the same notch and span length, maximum load values achieved with SNDB method are higher than SCB method load values. Higher failure load levels will be an advantage considering the accuracy of the load measuring system. With our load measuring and data acquisition system, error band of the load-displacement curves of SNDB test was observed to be less than the error band of the load-displacement plots of SCB tests.

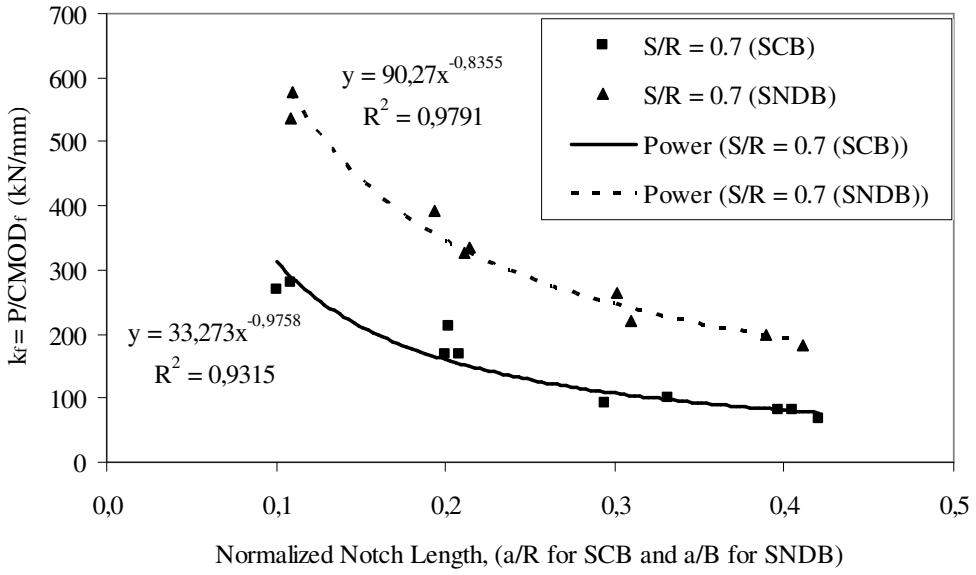

Figure 5.45 Comparison of both methods for k_f versus notch length

The error band difference is seen clearly in the Figure 5.46 (more figures about Load-Displacement and Load CMOD curves are in Appendix A, Figure A.1 and A.2).

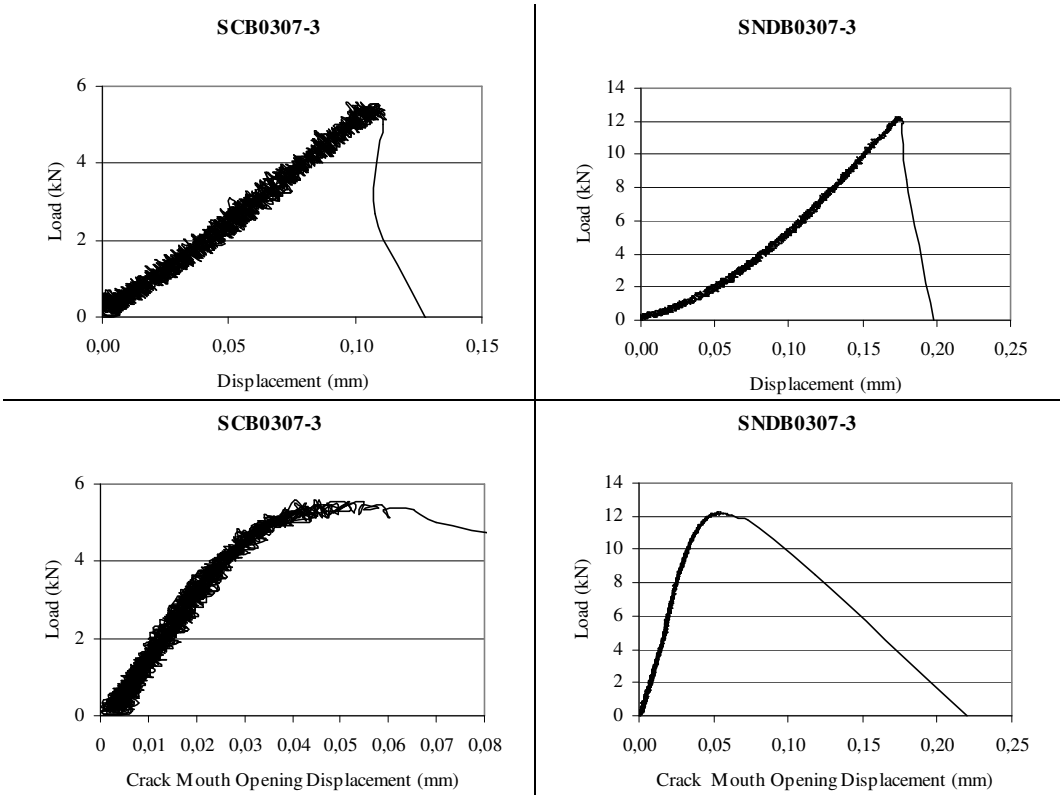

Figure 5.46 Comparison of Load-Displacement and Load-CMOD plots of SCB and SNDB tests

Fracture toughness values of pink colored Ankara Gölbaşı andesite were $0.93\pm0.11\,\mathrm{MPa}\sqrt{\mathrm{m}}$ and $0.96\pm0.09\,\mathrm{MPa}\sqrt{\mathrm{m}}$ for SCB technique and for SNDB technique, respectively. Results show that the standard deviation calculated for fracture toughness of SNDB method is less than the SCB method, possibly indicating that SNDB method produces more accurate results.

CHAPTER 6

CONCLUSIONS

A new testing method was introduced to determine Mode I fracture toughness of rock core specimens. The new method named as SNDB uses Straight Notched Disc specimen under three-point Bending. 3D Numerical modeling was carried out with FE program ABAQUS to find and develop relationships for the stress intensity factors with varying disc specimen geometries. Models were also developed for well-known specimen type SCB for verification and in order to compare the results of this work to the previous results of other investigators.

In the numerical models, for both SCB and SNDB specimen type stress intensity factors increased with increasing notch length and increasing span length. Stress intensity factor in general were higher for SCB specimen models than SNDB specimen models. For both methods stress intensity factors slowly increase for crack fronts far from the upper roller support loading point, that is small a/R ratios for SCB specimens and small a/B ratios for SNDB specimens between 0.1-0.5. Then a rapid increase is observed as crack front approaches to the upper boundary load application point. Variation in stress intensity factors for varying span distance (S/R ratios) is not as much as for crack front-upper loading point distance.

For the same S/R ratios and the same crack front-upper loading point distances (a/R for SCB and a/B for SNDB) stress intensity factors values for SCB specimen models are a little bit higher than for SNDB specimen models. Also crack tip tensile yield zone and tensile crack front confining pressure were higher for SCB specimen models. This means that a more intensive stress field with higher values of crack tip stresses exists at the crack tip for SCB specimens. This might cause more extensive yield zone and higher crack tip plasticity leading to deviations from the assumptions

of LEFM. That is why the new testing method with SNDB specimens is expected to produce more accurate results being less affected than crack tip plasticity.

In the experimental work, higher loads were observed for SNDB method tests than for SCB method tests. Failure load decreased with increasing notch length for both techniques. From fracture tests, fracture toughness of SCB technique is equal to $0.93\pm0.11\,\mathrm{MPa}\sqrt{\mathrm{m}}$ and fracture toughness of SNDB technique is equal to $0.96\pm0.09\,\mathrm{MPa}\sqrt{\mathrm{m}}$. As seen from the values, there is a little difference between SCB and SNDB tests.

Recommendations

The effects of the notch angle and thickness, specimen diameter and thickness can be examined by numerical methods. The type of the notch can be changed to see the variation in normalized stress intensity factor.

The newly developed testing method, SNDB can be tried with other types of rock which have different characteristics.

In experiments different notch angles and thicknesses and various specimen diameters and thicknesses can be tested in order to observe their effects on fracture toughness.

Besides the Mode I normalized stress intensity factor, pure Mode II normalized stress intensity factor should be studied by numerical modeling. Moreover, by considering numerical results pure Mode II fracture toughness should be investigated by changing notch angle in experiments.

Number of experiments could be increased to satisfy the accuracy. Various span and notch lengths should be studied to extend the application of the test.

REFERENCES

ABAQUS Analysis User's Manual, Version 6.5 Documentation.

ABAQUS/CAE User's Manual, Version 6.5 Documentation.

ABAQUS, Inc., "Modeling Fracture and Failure with ABAQUS", 2006.

ABAQUS Technology Brief, "Fracture Mechanics Study of a Compact Tension Specimen Using ABAQUS/CAE", 2004.

Abrahamsson, S., Niklasson, B., and Ouchterlony, F., "Fragmentation monitoring of production blasts at Mrica" SveDeFo Report DS 1987: 6, Swedish Detonic Research Foundation, Stockholm, 1987.

Alber, M., "Factors influencing fracture toughness K_{IC} from simple screening tests", Int. J. of Rock Mech. Min. Sciences, Technical Note, Vol. 40, pp. 779-784, 2003.

Almeida, L.C.R., et al., "Mechanical characterization of rock splitting planes in granitic rocks", Int. J. of Rock Mech. Min. Sci., Technical Note, Article in Press, 2006.

Al-Shayea, N., "Comparing Reservoir and Outcrop Specimens for Mixed Mode I–II Fracture Toughness of a Limestone Rock Formation at Various Conditions", Rock Mech. Rock Engng., Vol. 35, Issue 4, pp. 271-297, 2002.

Anderson, T.L., "Fracture mechanics: Fundamentals and Applications", CRC Press, Inc., Florida, 1991.

Atkinson, B.K., "Fracture Mechanics of Rock", Academic Press, London, 1987.

Ayatollahi, M.R and Aliha, M.R.M., "On determination of mode II fracture toughness using semi-circular bend specimen",International Journal of Solids and Structures, Volume 43, Issue 17 , pp. 5217-5227, August 2006.

Ayatollahi, M.R and Aliha, M.R.M., "Wide range data for crack tip parameters in two disc-type specimens under mixed mode loading", Computational Materials Science, Artical in Press, 2006.

Ayatollahi, M.R, Aliha, M.R.M., and Hassani, M.M., "Mixed mode brittle fracture in PMMA- An experimental study using SCB specimens", Materials Science and Engineering A, Vol. 417, pp. 348-356, 2006.

Backers, T., et al, “Effect of loading rate on Mode I fracture toughness, roughness and micromechanics of sandstone”, Int. J. of Rock Mech. Min. Sci., Technical Note, Vol. 40, pp. 425–433, 2003.

Backers, T., et al. ,” New data on mode II fracture toughness of rock from the punch-through shear test”, Int. J. of Rock Mech. Min. Sci., Vol. 41, Paper 1A 01, 2004.

Backers, T., et al. , “Rock fracture toughness testing in Mode II punch-through shear test”, Int. J. of Rock Mech. Min. Sci., Vol. 39, pp. 755-769, 2002.

Balme, M.R., “Fracture toughness measurements on igneous rocks using a high-pressure, high- temperature rock fracture mechanics cell”, Journal of Volcanology and Geothermal Research, Vol. 132, pp.159-172,2004.

Barker, L.M., “A simplified method for measuring plane strain fracture toughness”, Engng. Fracture Mech., Vol. 9, 361-369, 1977.

Başbay, O., “Investigation of Mixed Mode Crack Propagation from Preexisting Notches in Brazilian Discs of Ankara Andesite”, M.S. Thesis, METU, Ankara, 168 p., 2002.

Bearman, R.A., “The use of the point load test for the rapid estimation of Mode I fracture toughness”, Int. J. Rock Mech. Min. Sci., Vol. 36, pp. 257-263, 1999.

Ceriolo, L. and Tommaso A. D., “Fracture Mechanics of Brittle Materials: A Historical Point of View”, 2nd Int. PhD Symposium in Civil Engineering, Budapest, 1998.

Chan, S.K., Tuba, I.S. and Wilson, W.K., “On the finite element method in linear fracture mechanics”, Engng. Fract. Mech., Vol 2, pp. 1-17, 1970.

Chang, J., “A General Mixed-Mode Brittle Fracture Criterion for Cracked Materials”, Engineering Fracture Mechanics, Vol. 73, 1249-1263, 2006.

Chang, S. H., Chung-In Lee, Jeon, S., “Measurement of rock fracture toughness under modes I and II and mixed-mode conditions by using disc-type specimens”, Engineering Geology, Vol. 66, pp. 79–97, 2002.

Chen M., Zhang, G., “Laboratory measurement and interpretation of the fracture toughness of formation rocks at great depth”, Journal of Petroleum Science and Engineering, Vol. 41, pp. 221-231, 2004.

Chen, Z.X., Chen, M., “Study on measurement of Rock Fracture toughness”, The Third National Rock Mechanics and Engineering Academy Symposium, University of Xinan Traffic Press, Chengdu, pp. 368-372, 1995.

Chong, K.P, and Kuruppu, M.D., "New specimen for fracture toughness determination for rock and other materials", Int. J. Fract., Vol. 26, R59-R62, 1984.

Chong, K.P, Kuruppu, M.D. and Kuszmaul, J.S., "Fracture toughness determination of layered materials", Engng. Fract. Mech., Vol. 28, pp. 55-65, 1987.

Cook, R.B., "Non-Invasively Assessed Skeletal Bone Status and its Relationship to the Biomechanical Properties and Condition of Cancellous Bone", Ph.D. Thesis, Cranfield University, England, 401 p., 2005.

Cornell Fracture Group, "FRANC3D & BES Benchmarking", Version 2.6, 2003.

Cornell Fracture Group, "FRANC3D Menu & Dialog Reference", Version 2.6, 2003.

Cornell Fracture Group, "FRANC3D & OSM 3D Tutorial", Version 2.6, 2003.

DaqView and DaqViewXL Documents.

DBK Option Cards & Modules User's Manual, 2003.

Denyse de Araújo, T., Bittencourt, T.N., Roehl, D., and Martha, L.F., "Numerical Estimation of Fracture Parameters in Elastic and Elastic-Plastic Analysis", European Congress on Computational Methods in Applied Sciences and Engineering, Barcelona, 2000.

Division of Engineering, Brown University, Advanced Mechanics of Solids, ABAQUS tutorial, 2001.

EFunda Engineers, Fracture Mechanics. EFunda Engineering Fundamentals. http://www.efunda.com/formulae/solid_mechanics/fracture_mechanics/fm_intro.cfm

Erdoğan, F., and Sih, G.H., "On the Crack Extension in Plates Under Plane Loading and Transverse Shear", J. Basic Engng. Am. Soc. Mech. Engrs., Vol 85, pp. 519-527, 1963.

Fowell, R. J. and Chen, J. F., "The third chevron-notch rock fracture specimen-the cracked chevron-notched Brazilian disk". Proc. 31st U.S. Symp. on Rock Mechanics, pp. 295-302, 1990.

FRANC2D, "A Two Dimensional Crack Propagation Simulator", User's Guide, Version 3.1, 1993.

Getting Started with ABAQUS, Version 6.5 Documentation.

Griffith, A.A., "The Phenomena of Rapture and Flow in Solids", Phil. Trans. Roy. Soc. Of London, A221, pp. 163-197, 1921.

Griffith, A.A., "The Theory of Rupture", Proc. 1st Int. Congress Appl. Mech., pp. 55-63, 1924.

Gunsallus, K.L. and Kulhawy, F.H., "A comparative evaluation of rock strength measures", Int. J. Rock Mech. Min. Sci. Geomech. Abstr., 21(5); pp. 233-48, 1984.

Haberfield, C.M. and Johnston 1.W., "Determination of the fracture toughness of a saturated soft rock", Can. Geotech. J., Vol. 27, pp. 276-284, 1990.

Iesulauro, E.,"FRANC2D/L: A Crack Propagation Simulator for Plane Layered Structures", User's Guide, Version 1.5,Cornell University, Ithaca, New York.

Ingraffea, A.R. and Schmidt, R.A., "Experimental verification of a fracture mechanics model for tensile strength prediction of Indiana limestone". Proc. 19th U.S. Symp. On Rock Mechanics, pp. 247-253, 1979.

ISRM Commission on Standardization of Laboratory and Field Tests, "Suggested Methods for Determining Tensile Strength of Rock Materials", Int. J. Rock Mech. Min. Sci. & Geomech. Abstr., Vol. 15, pp. 99-103, 1978.

ISRM Commission on Standardization of Laboratory and Field Tests, "Suggested Methods for Determining the Uniaxial Compressive Strength and Deformability of Rock Materials", Int. J. Rock Mech. Min. Sci. & Geomech. Abstr., Vol. 16, pp. 135-140, 1979.

ISRM Commission on Testing Methods, "Suggested Method for Determining Fracture Toughness of Rocks", Int. J. Rock Mech. Min. Sci. & Geomech. Abstr., Vol. 25, pp. 71-96, 1988.

ISRM Commission on Testing Methods, "Suggested Method for Determining Mode I Fracture Toughness Using Cracked Chevron Notched Brazilian Disc (CCNBD) Specimens", Int. J. Rock Mech. Min. Sci. & Geomech. Abstr., Vol. 32, pp. 57-64, 1995.

Kahraman, S. and Altindag, R., "A brittleness index to estimate fracture toughness", Int. J. of Rock Mech. Min. Sci., Technical Note, Vol. 41, pp. 343-348, 2004.

Key to Metals Task Force & INI International, Fracture Mechanics, http://www.key-to-steel.com/articles/art45.htm (2006, 30 May).

Khan, K. and Al-Shayea, N. A., "Effect of Specimen Geometry and Testing Method on Mixed Mode I-II Fracture Toughness of a Limestone Rock from Saudi Arabia", Rock Mech. Rock Engng., Vol. 33, pp. 179-206, 2000.

Köksal, N., “Stable Crack Propagation Studies in Ankara Andesite”, Ph.D. Thesis, METU, Ankara, 1989.

Krishnan, G.R., et al, “Fracture Toughness of a Soft Sandstone”, Int. J. of Rock Mech. Min. Sci., Vol. 35, pp. 695-710, 1998.

Li, X., et.al., “Low Temperature Cracking Study at Mn/ROAD”, 2004.

Lim, I.L., Johnston, I.W. and Choi, S.K. “Assesment of mixed-mode fracture toughness testing methods for rock”, nt. J. Rock Mech. Min. Sci. & Geomech. Abstr., Vol. 31, pp. 265-272, 1994.

Lim, I.L., Johnston, I.W., Choi, S.K. and Boland, J.N., “Fracture Testing of a Soft Rock with Semi-circular Specimens Under Three-point Bending. Part I-Mode I”, Int. J. Rock Mech. Min. Sci. & Geomech. Abstr., Vol. 31, No. 3, pp. 185-197, 1994.

Lim, I.L., Johnston, I.W., Choi, S.K. and Boland, J.N., “Fracture Testing of a Soft Rock with Semi-circular Specimens Under Three-point Bending. Part II- Mixed Mode”, Int. J. Rock Mech. Min. Sci. & Geomech. Abstr., Vol. 31, No. 3, pp. 199-212, 1994.

Lim, I.L., et.al, “Stress intensity factors for semi-circular specimens under three-point bending”, Engineering Fracture Mechanics, Vol. 44, No. 3, pp. 363-382, 1993.

Marji, M.F., et al., “On the uses of special crack tip elements in numerical rock fracture mechanics”, International Journal of Solids and Structures, Vol. 43, 1669-1692, 2006.

Matsuki, K., Nozuyama, Y. and Takahashi, H., “Size effect in the fracture toughness testing of rocks using a boring core”, Proc. Spring Meeting Min. Metall. Inst, Japan, pp. 193-194, 1987.

Meredith, P.G.A., “Fracture mechanics study of experimentally deformed crustal rocks”, Unpublished Ph. D. Thesis, University of London, 1983.

Momber, A.W., “A transition index for rock failure due to liquid impact”, Wear, Vol. 260, pp. 996-1002, 2006.

MTS System Catalog, 1992.

Müller, W., and Rummel, F., Bruchzahigkeitsmessungen an Gesteinen. Bericht zu den BMFT-FE-Vorhaben 03e-3068-B. Ruhr University, Bochum, F. R. G., 1984.

Nordlund, E., Li, C., Carlsson, B., “Mechanical properties of the diorite in the prototype repository at Äspö HRL—laboratory tests”, International Progress Report, IPR-99-25, SKB, June 1999.

Othman, A.M., "Fracture Resistance of Rubber-modified Asphaltic Mixtures Exposed to High-Temperature Cyclic Aging", Journal of Elastomers and Plastics, Vol 38, pp. 19-30, 2006.

Ouchterlony, F., "A presentation of the ISRM Suggested Methods for determining fracture toughness of rock material", Proc. 6th Int. Congr. Rock Mechanics, Balkema, Rotterdam, Vol. 2, pp. 1181-1186, 1987.

Ouchterlony, F., "Suggested methods for determining the fracture toughness of rock", Int. J. Rock Mech Min. Sci., ISRM Working Group Report, Vol. 25, pp 71-96, 1988.

Ouchterlony, F., "Unreported data", Swedish Detonic Research Foundation, Stockholm, Sweden, 1987.

Phan, A.V., "ANSYS TUTORIAL - 2-D Fracture Analysis", ANSYS Release 7.0, University of South Alabama.

Pilkey, W.D., "Formulas for Stress, Strain, and Structural Matrices". New York, Wiley, 1994.

Rice, J.R., "A path independent integral and the approximate analysis of strain concentration by notches and cracks", J. App. Mech., Vol. 35, pp. 379-386, 1968.

Roylance, D., "Introduction to Fracture Mechanics", Department of Materials Science and Engineering, Massachusetts Institute of Technology, Cambridge, 2001.

Schmidt, R.A. and Lutz, T.J., "K_{IC} and J_{IC} of Westerly granite effects of thickness and in-plane dimensions", ASTM STP 678, pp.166-182, 1979.

Sean Grealis, "The History and Brief Introduction of Fracture". Virginia Tech Materials Science and Engineering. http://www.sv.vt.edu/classes/MSE2094_NoteBook/97ClassProj/anal/grealis/history.html (1997, May 4).

Seher, C., and Smith, C., "Managing the Aging Aircraft Problem, the AVT Symposium on Aging Mechanisms and Control and the Specialists Meeting on Life Management Techniques for Aging Air Vehicles", Manchester, England, 2001.

Shi, X.Q., "Determination of interface fracture toughness of adhesive joint subjected to mixed-mode loading using finite element method", International Journal of Adhesion & Adhesives, Vol. 26, pp. 249-260, 2006.

Singh R.N. and Sun G.X., "An investigation into factors affecting fracture toughness of coal measures sandstone", J. Mines, Metals & Fuels, pp. 11I-118, 1990.

Sousa, J.L.A.O. and Bittencourt, T.N., "Experimental Analysis of Fracture Processes in Concrete", Journal of the Brazilian Society of Mechanical Sciences, Vol. 23, No. 4, 2001.

Sun, Z. and Ouchterlony, F., "Fracture toughness of Stripa granite cores", Int. J. Rock Mech. Min. Sci. & Geomech. Abstr., Vol. 23, pp. 399-409,1986.

Şantay, A.Ö., "Critical Analysis of Short Rod Fracture Toughness Testing Method", M.S. Thesis, METU, Ankara, 83 p., 1990.

Şener, S., "Fracture Toughness Tests on Brazilian Discs of Ankara Andesite", M.S. Thesis, METU, Ankara, 122 p., 2002.

Takahashi, H., Hashida, T., and Fukazawa, T., "Fracture toughness tests by use of core based specimens", GEEE Research Report, No. T-002-86, Faculty of Engineering, Tohoku University, Sendai, Japan, 1986.

Wang, Q.Z., "Stress Intensity Factors of the ISRM Suggested CCNBD Specimen Used for Mode-I Fracture Toughness Determination", Int. J. of Rock Mech. Min. Sci., Vol. 35, No. 7, pp. 977-982, 1998.

Wells, A.A., "Unstable crack propagation in metals: cleavage and fast fracture", Proceedings of the Crack Propagation Symposium, Cranfield, UK, Vol. 1, Paper 84, 1961.

Whittaker, B.N., Singh, R.N., Sun, G., "Rock Fracture Mechanics-Principles, Design and Applications", Elsevier, Amsterdam, 1992.

Yi, X., "Fracture toughness and crack growth in short rod specimens of rock", Licentiate Thesis, Lulea Univ. Techn., Lulea, Sweden, 1987.

Yoon, J. and Jeon, S., "Experimental verification of a PTS mode II test for rock", Int. J. of Rock Mech. Min. Sci., Vol. 41, Paper 1A 02, 2004.

Yu Y., "Measuring properties of rock from the site of permanent shiplock in three Gorges project", Test Report, Yangtze River Scientific Research Institute, June 2001.

Zafošnik, B., "Evaluation of stress intensity factors using finite elements", Laboratory for Computer Aided Engineering, Faculty of Mechanical Engineering, University of Maribor, Maribor, Slovenija, 2000.

Zhang, Z.X., "An empirical relation between mode I fracture toughness and the tensile strength of rock", Int. J. of Rock Mech. Min. Sci., Technical Note, Vol. 39, pp. 401-406, 2002.

APPENDIX A

LOAD-DISPLACEMENT AND LOAD-CRACK MOUTH OPENING DISPLACEMENT CURVES OF TESTS

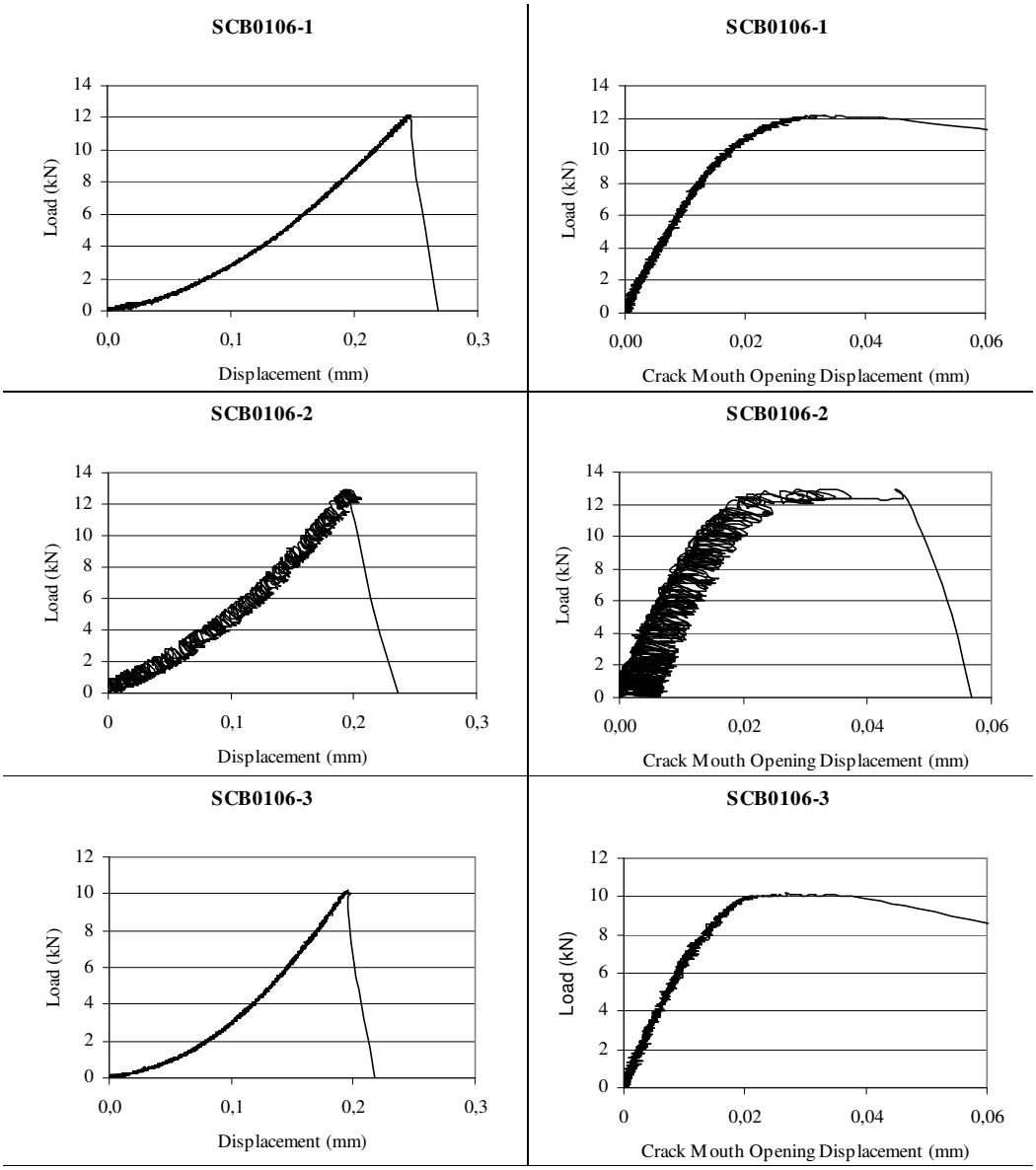

Figure A.1 Load-Displacement and Load-CMOD curves of SCB tests

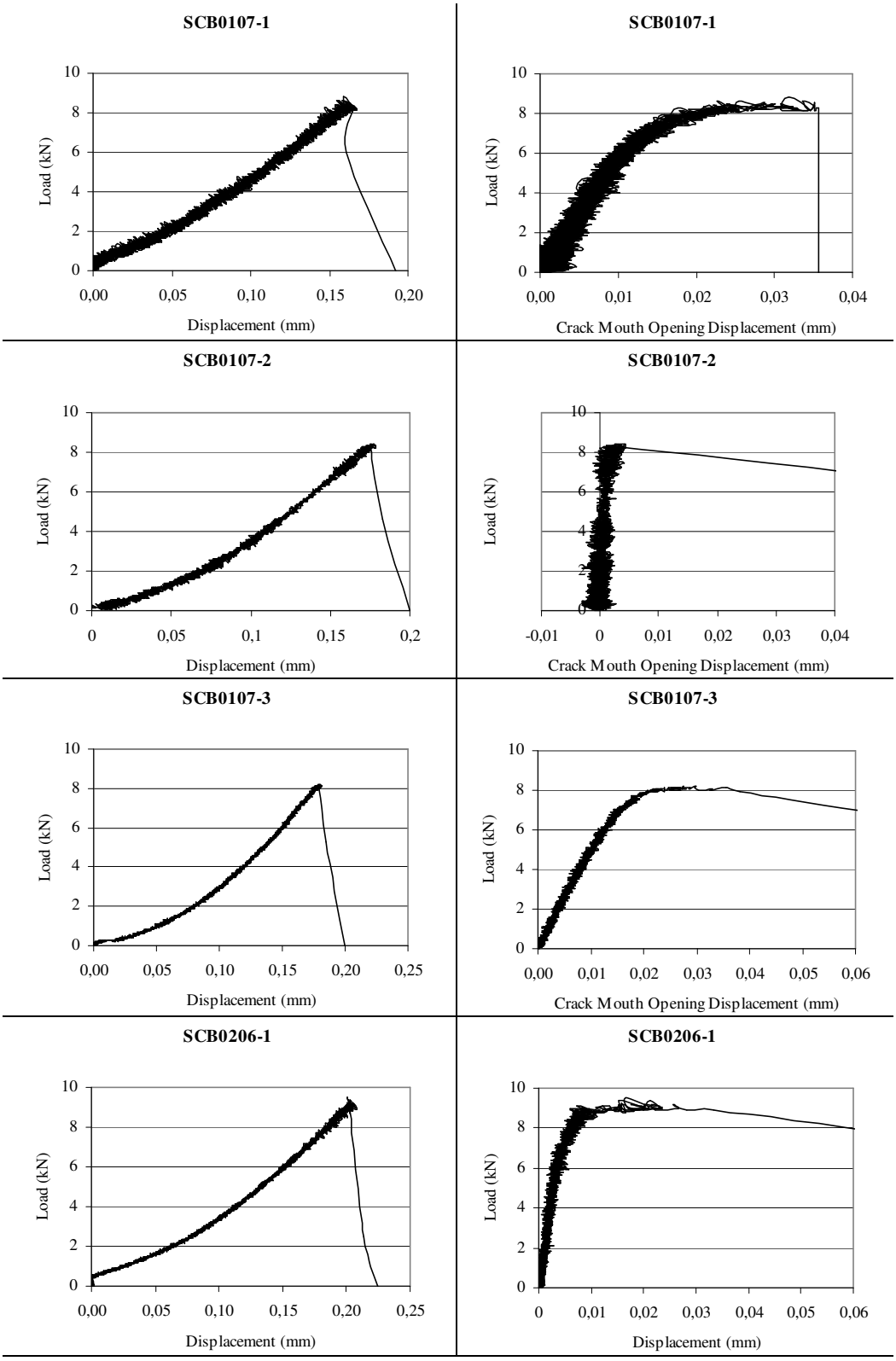

Figure A.1 (Continued) Load-Displacement and Load-CMOD curves of SCB tests

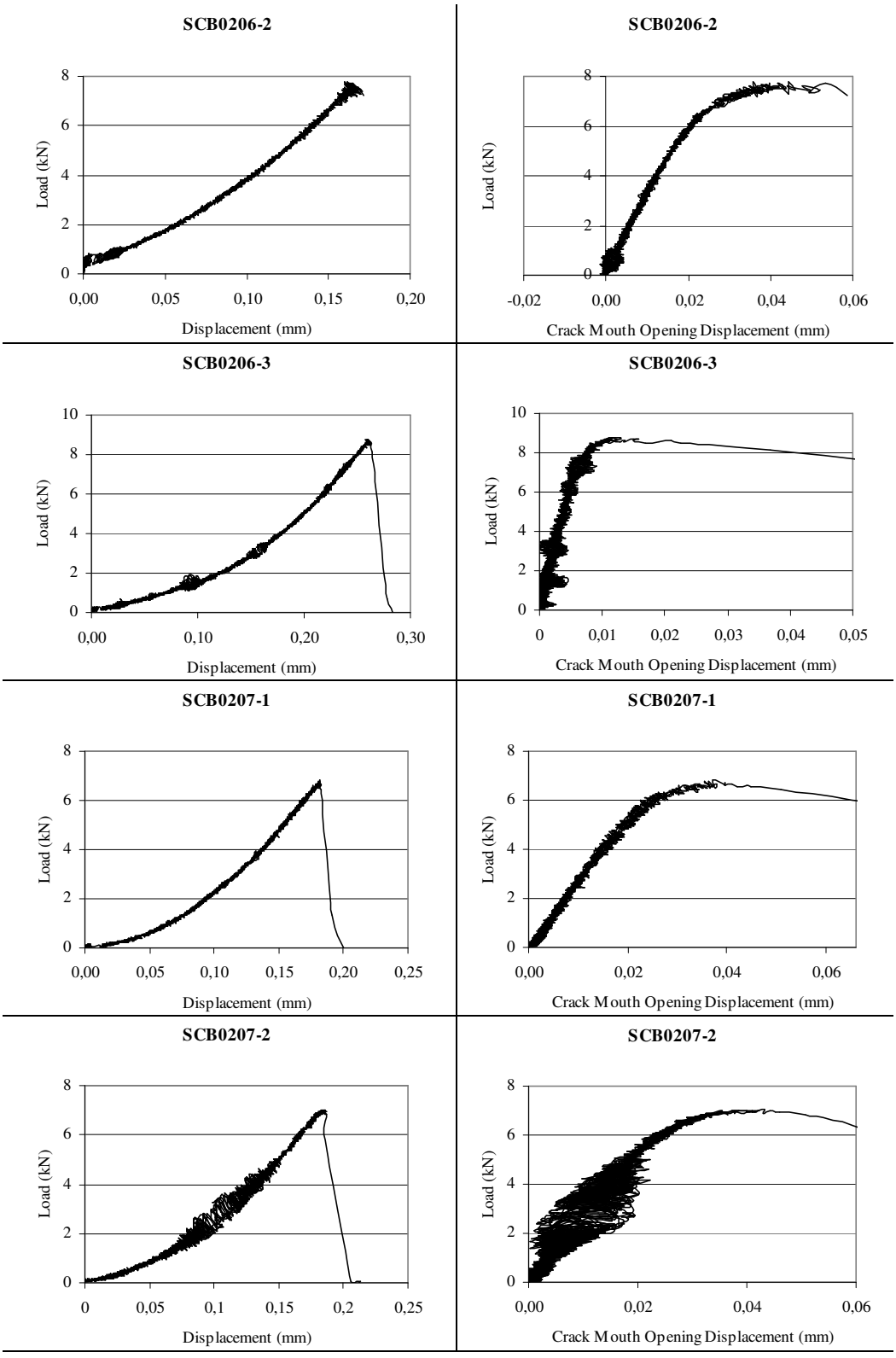

Figure A.1 (Continued) Load-Displacement and Load-CMOD curves of SCB tests

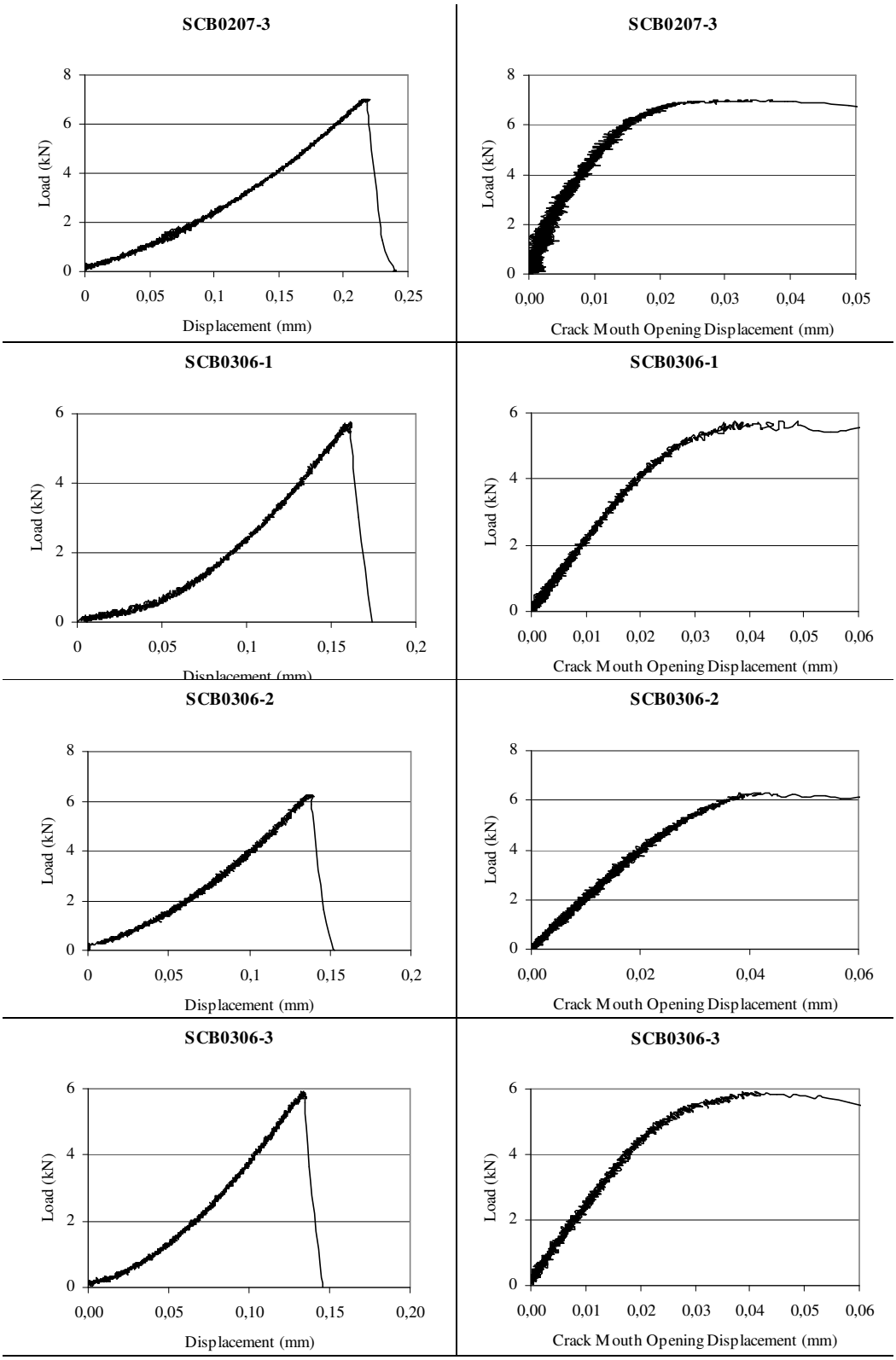

Figure A.1 (Continued) Load-Displacement and Load-CMOD curves of SCB tests

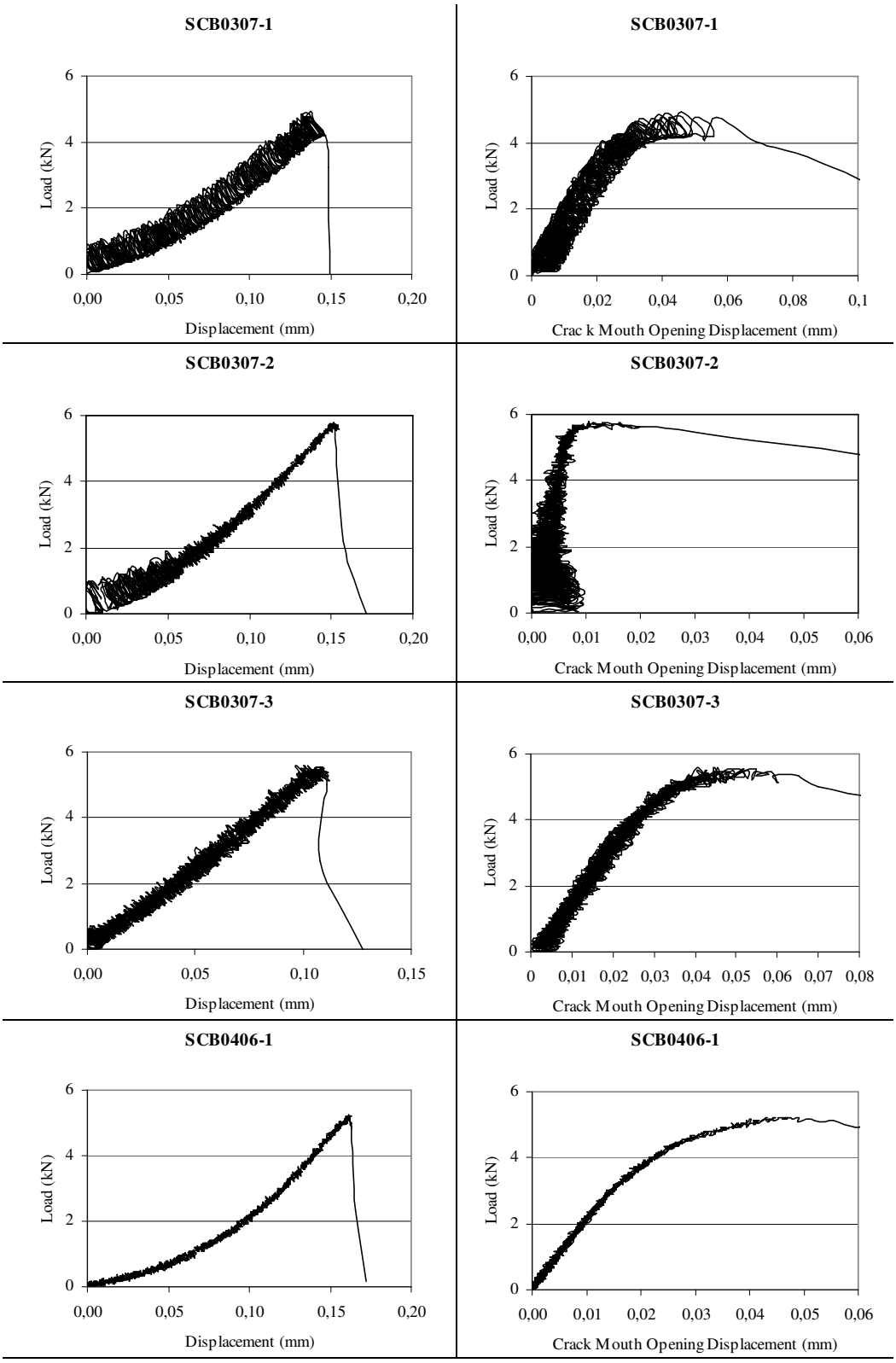

Figure A.1 (Continued) Load-Displacement and Load-CMOD curves of SCB tests

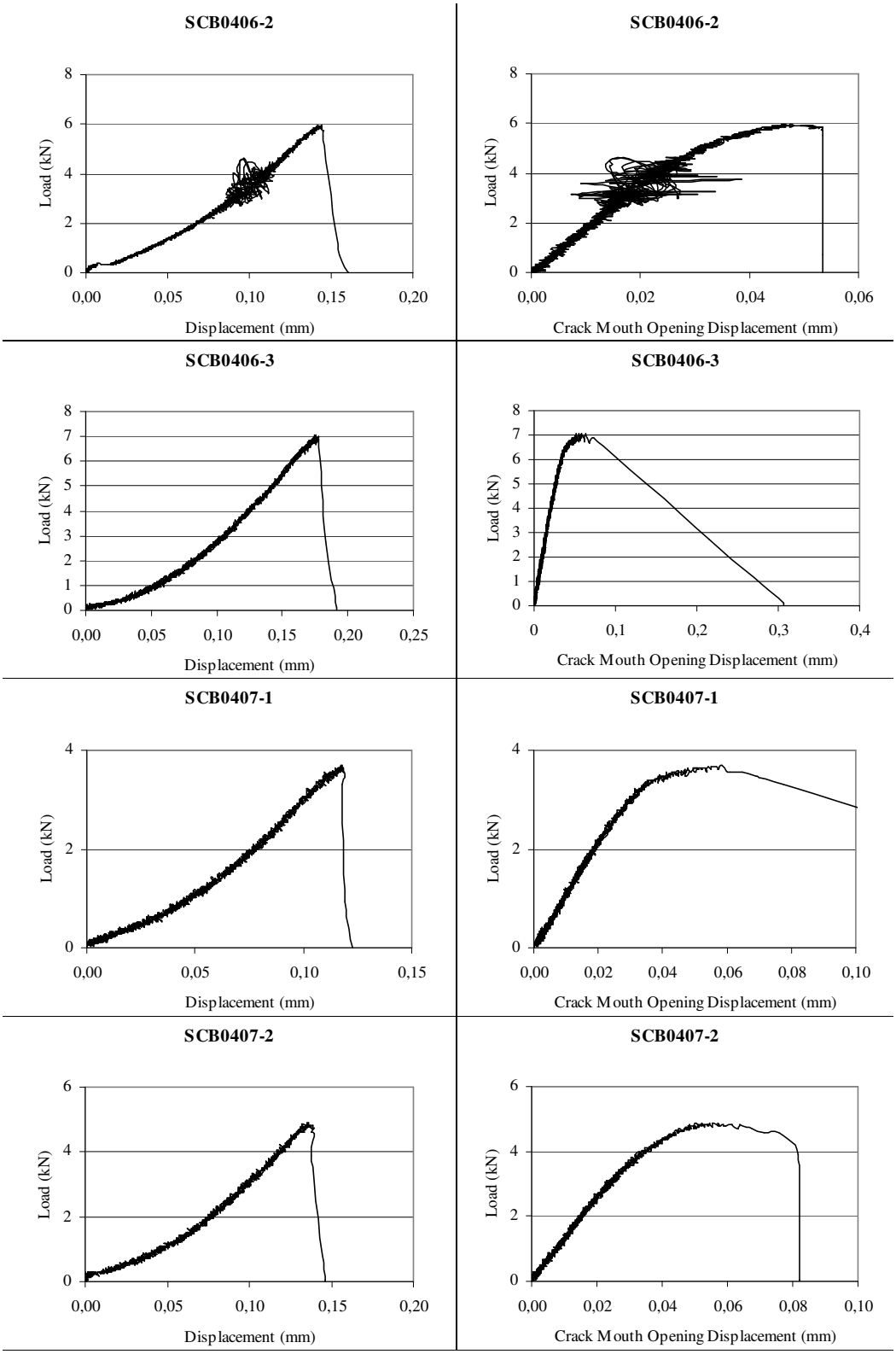

Figure A.1(Continued) Load-Displacement and Load-CMOD curves of SCB tests

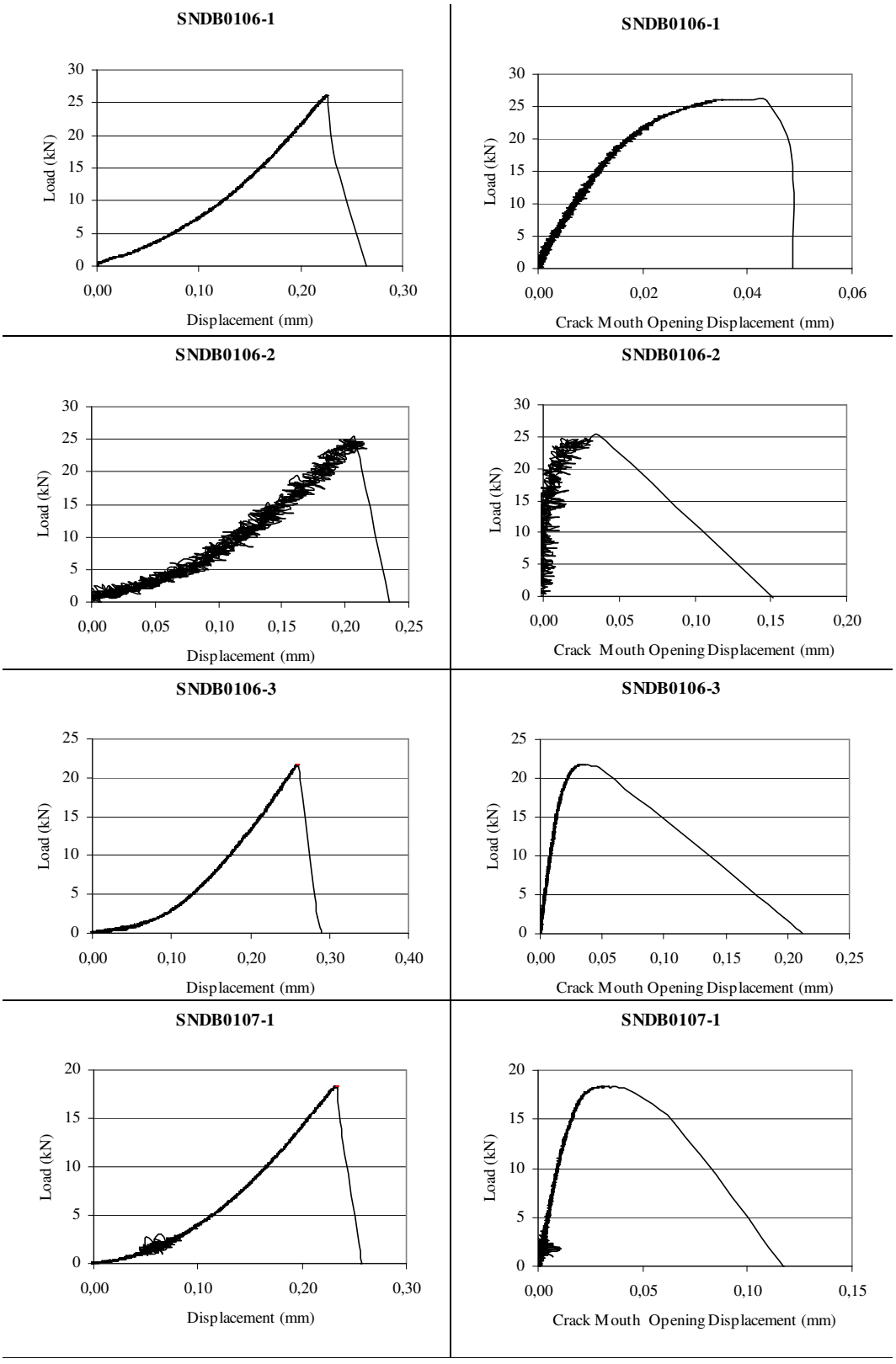

Figure A.2 Load-Displacement and Load-CMOD curves of SNDB tests

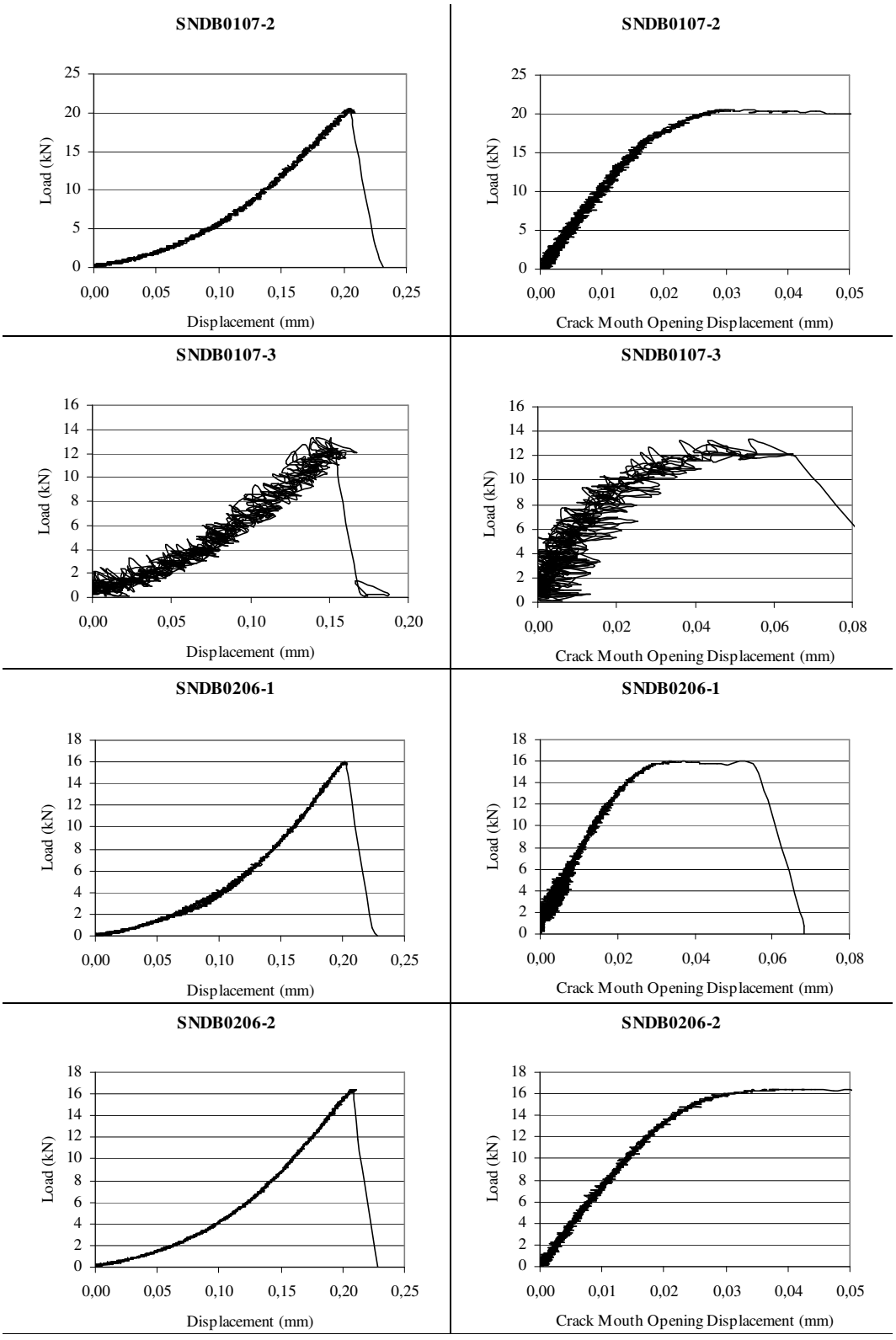

Figure A.2 (Continued) Load-Displacement and Load-CMOD curves of SNDB tests

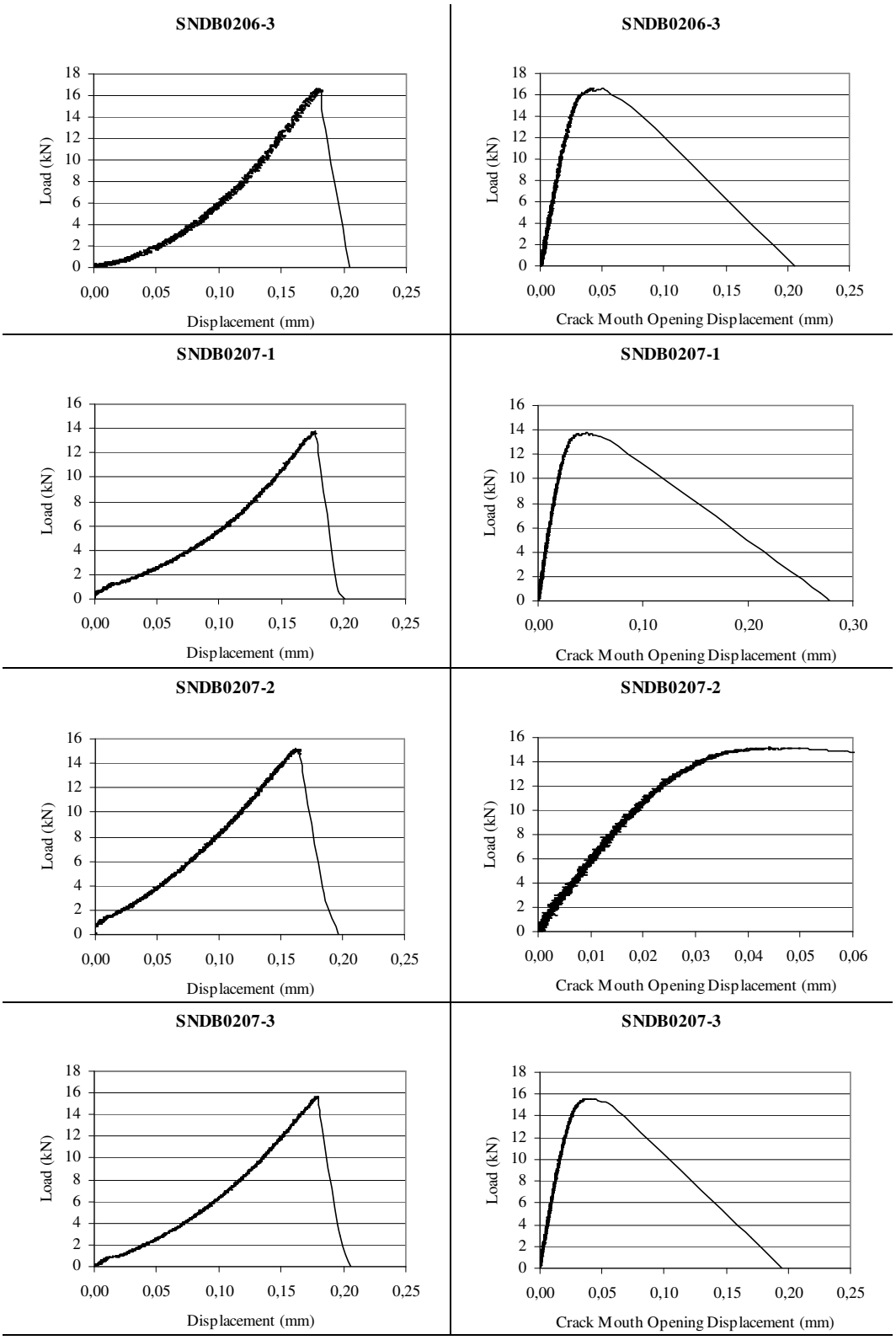

Figure A.2 (Continued) Load-Displacement and Load-CMOD curves of SNDB tests

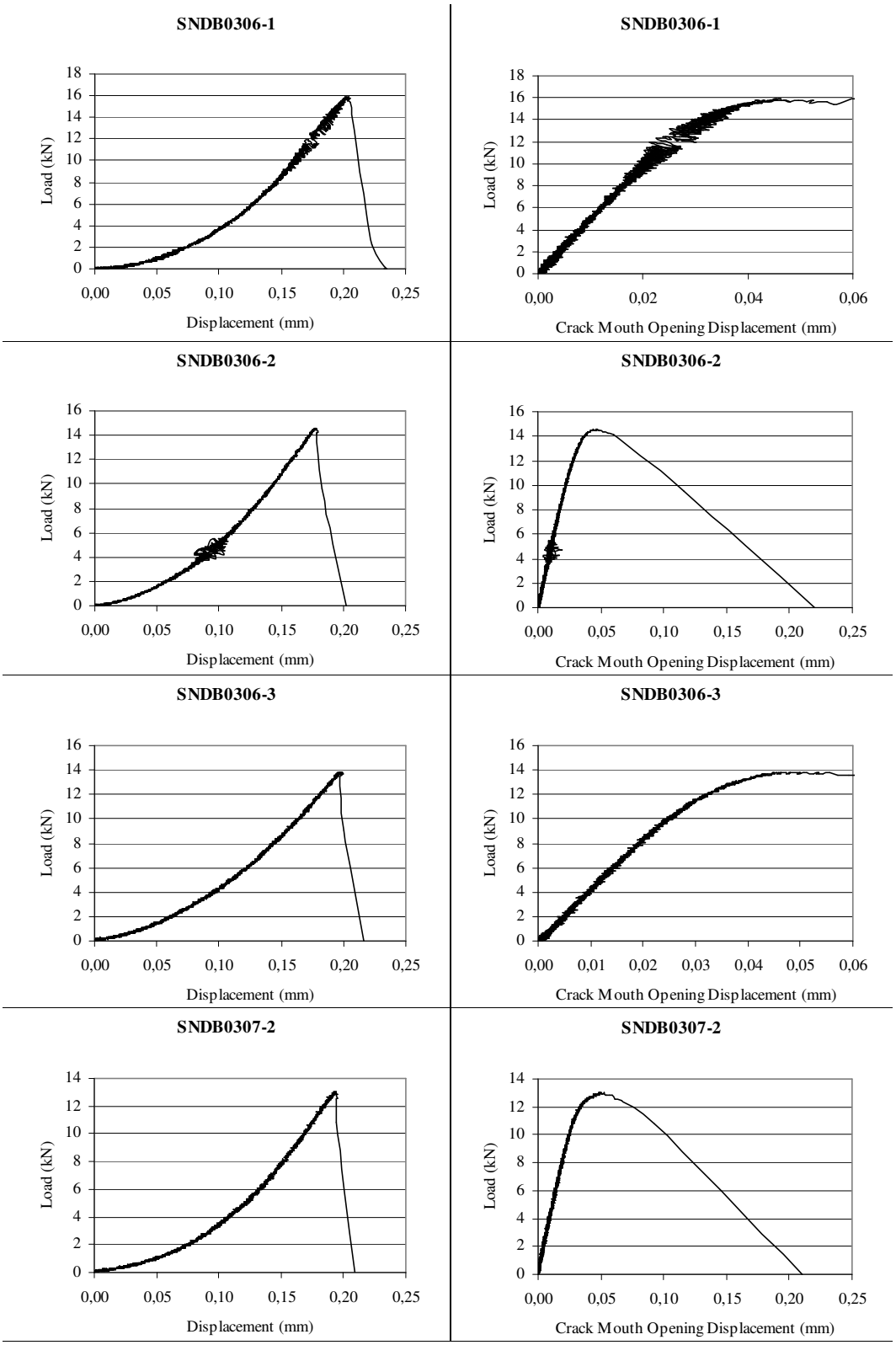

Figure A.2 (Continued) Load-Displacement and Load-CMOD curves of SNDB tests

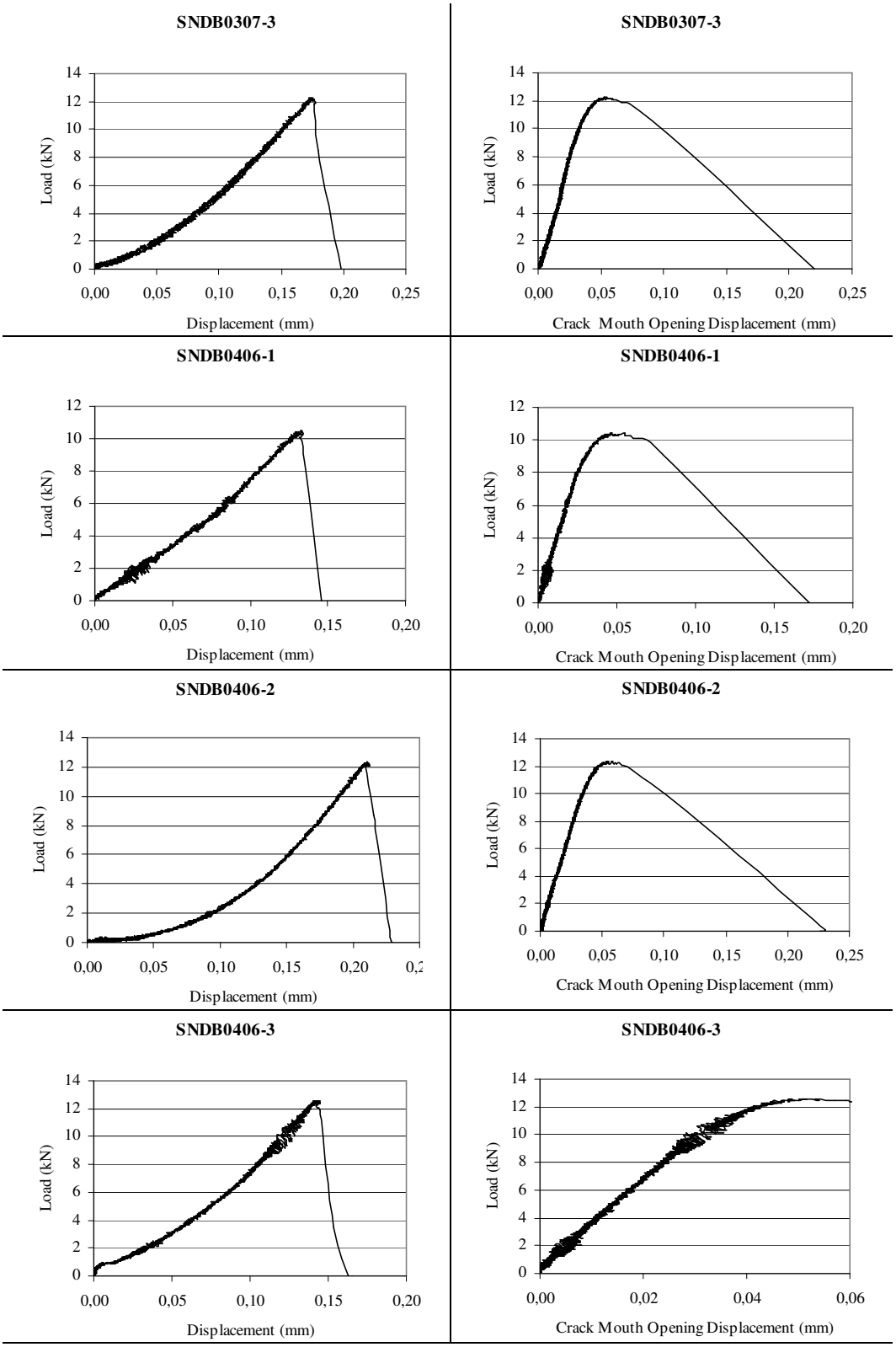

Figure A.2 (Continued) Load-Displacement and Load-CMOD curves of SNDB tests

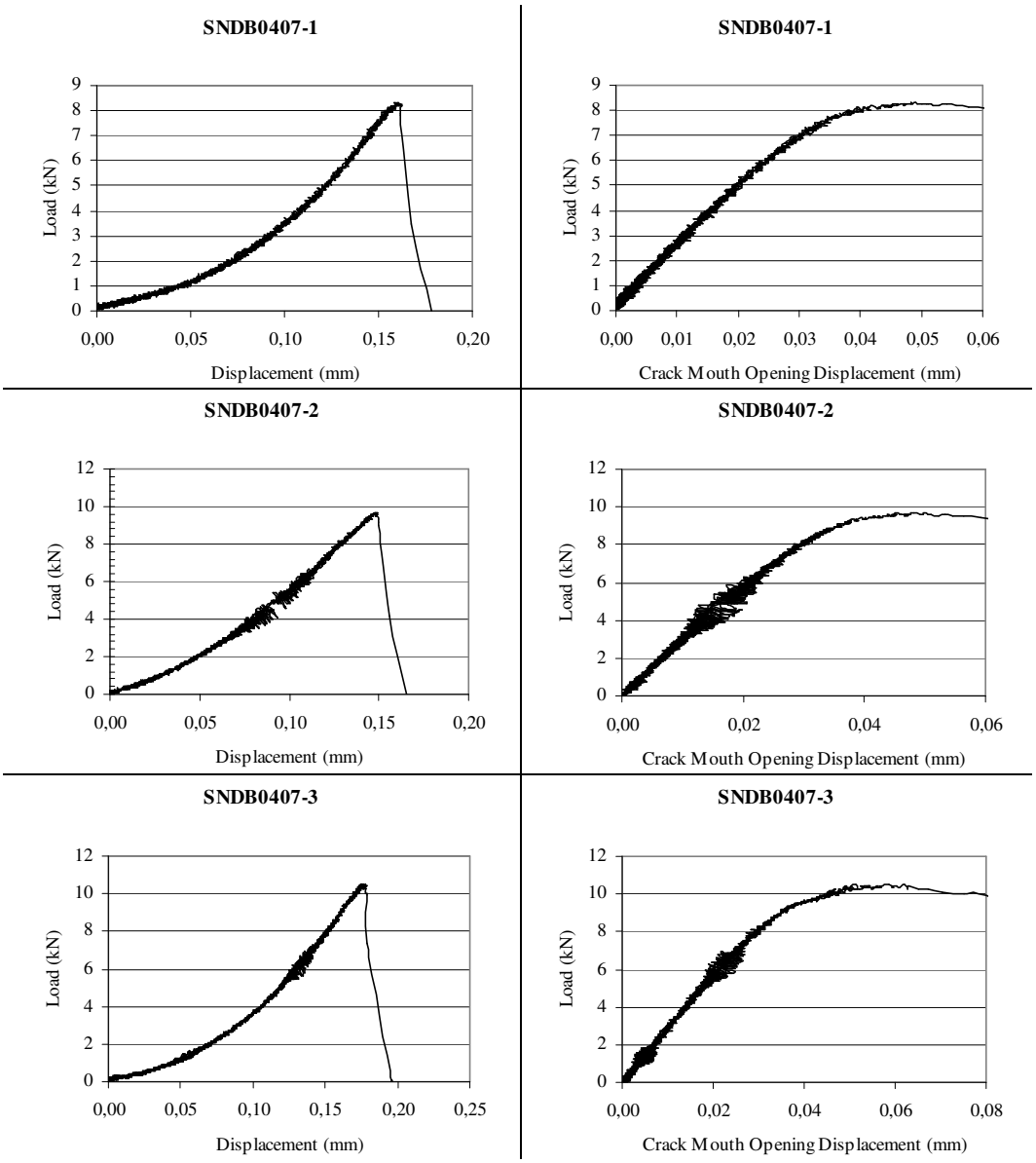

Figure A.2 (Continued) Load-Displacement and Load-CMOD curves of SNDB tests

APPENDIX B

SPECIMEN PHOTOS AFTER EXPERIMENTS

Figure B.1 Some of the SCB specimen photos after experiments

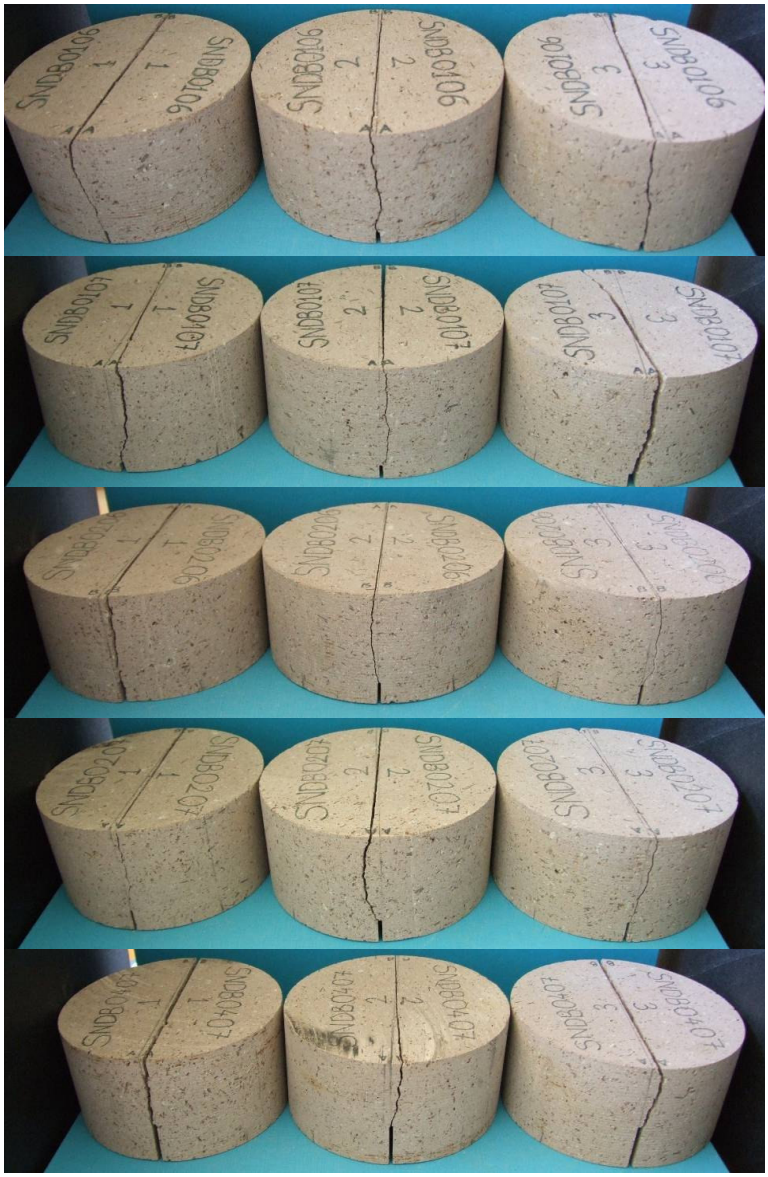

Figure B.2 Some of the SNDB specimen photos after experiments